AD-A042 342 NAVAL SURFACE WEAPONS CENTER DAHLGREN LAB VA F/G 6/4
MATHEMATICAL MODEL OF THE VESTIBULOOCULAR REFLEX.(U)
JUN 77 K S CHUN
UNCLASSIFIED NSWC/DL-TR-3669 NL

1 OF 3
AD A042342

NSWC/DL TR-3669

MATHEMATICAL MODEL OF THE VESTIBULOOCULAR REFLEX

by
KEE SOON CHUN
Warfare Analysis Department

JUNE 1977

NAVAL SURFACE WEAPONS CENTER
DAHLGREN LABORATORY
Dahlgren, Virginia 22448
WHITE OAK LABORATORY
Silver Spring, Maryland 20910

NAVAL SURFACE WEAPONS CENTER
DAHLGREN LABORATORY
Dahlgren, Virginia
22448

UNCLASSIFIED

SECURITY CLASSIFICATION OF THIS PAGE (When Data Entered)

REPORT DOCUMENTATION PAGE

READ INSTRUCTIONS BEFORE COMPLETING FORM

(14) 1. REPORT NUMBER: NSWC/DL-TR-3669	2. GOVT ACCESSION NO. / 3. RECIPIENT'S CATALOG NUMBER
(6) 4. TITLE (and Subtitle): MATHEMATICAL MODEL OF THE VESTIBULOOCULAR REFLEX.	(9) 5. TYPE OF REPORT & PERIOD COVERED: Final Rept. / 6. PERFORMING ORG. REPORT NUMBER
(10) 7. AUTHOR(s): Kee Soon Chun	8. CONTRACT OR GRANT NUMBER(s)
9. PERFORMING ORGANIZATION NAME AND ADDRESS: Naval Surface Weapons Center (Code DK-55), Dahlgren Laboratory, Dahlgren, VA 22448	10. PROGRAM ELEMENT, PROJECT, TASK AREA & WORK UNIT NUMBERS: NSWC Overhead
11. CONTROLLING OFFICE NAME AND ADDRESS: Naval Surface Weapons Center, Dahlgren Laboratory, Dahlgren, VA 22448	(11) 12. REPORT DATE: June 1977 / 13. NUMBER OF PAGES: 231
14. MONITORING AGENCY NAME & ADDRESS (if different from Controlling Office): (12) 249p.	15. SECURITY CLASS. (of this report): UNCLASSIFIED / 15a. DECLASSIFICATION/DOWNGRADING SCHEDULE

16. DISTRIBUTION STATEMENT (of this Report)

Approved for public release; distribution unlimited.

17. DISTRIBUTION STATEMENT (of the abstract entered in Block 20, if different from Report)

18. SUPPLEMENTARY NOTES

19. KEY WORDS (Continue on reverse side if necessary and identify by block number)

Vestibuloocular reflex, semi-circular canal, cybernetics, neurophysiology, central nervous system

20. ABSTRACT (Continue on reverse side if necessary and identify by block number)

A mathematical model of the vestibuloocular reflex based on experimental data obtained from an alert cat was constructed and tested. This model includes quick-phases and also deals with the stochastic behavior of quick-phase timing and amplitude. The structure of the model is consistent with recent findings of neurophysiology.

The slow-phase portion of the reflex is generated by integrating the output signal from the semi-circular canals. A common neural integrator is →

(Continued on back)

DD FORM 1 JAN 73 1473 EDITION OF 1 NOV 65 IS OBSOLETE

S/N 0102-LF-014-6601

UNCLASSIFIED

SECURITY CLASSIFICATION OF THIS PAGE (When Data Entered)

391 598

B

used for both quick-phase and slow-phase velocity signals. The quick-phase portion of the reflex is generated by a neural pulse generator which utilizes a closed-loop bang-bang type of control system (instead of an open-loop pulse generator operated by a sampler). This quick-phase model is based on the theory that rapid eye movements are caused by a mechanism which drives the eye to a commanded position in the orbit instead of using ballistic pre-programming.

The positions to which and from which quick-phases move the eye are considered as continuous noisy signals which are sampled by the occurrence of each quick-phase. The noises are injected into the model at neurophysiologically appropriate locations in such a way that the variances of these signals, and correlation between them computed from the model, are similar to those obtained from the cat.

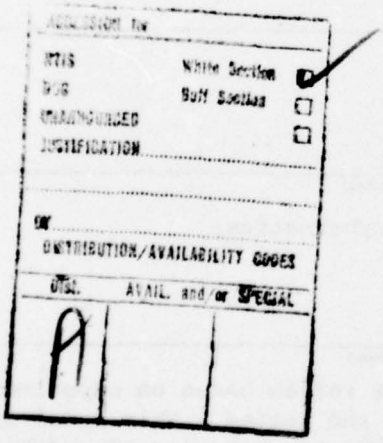

FOREWORD

The base-motion isolation in navigation, guidance, and gunfire control systems is a relatively new practice in the history of technology.

In nature, however, all vertebrates, which include Homo sapiens, possess built-in base-motion isolation systems in the form of vestibuloocular reflexes to stabilize the visual axis despite head rotations. This reflex was developed early in evolution, literally millions of years ago, as a means of survival to obtain food and to protect against danger by allowing enough time for the visual observation of a stationary environment during rotatory head motion.

This report presents the mathematical model of the vestibuloocular reflex which is formulated from the viewpoint of cybernetics. It also presents the model's simulation results and discusses the comparison with physiological data. The model is constructed in such a way that the signals from it are compatible with the physiological data at the system output level. Moreover, the model's internal signals are similar to the neural discharge patterns observed at the corresponding locations of the central nervous system.

The mathematical tools and the approaches used in the formulation of the model are similar to those used in the modeling of the weapon systems. Particularly, the way the noise problem is treated in the model may be useful in simulations of certain weapon systems.

This report comprises the author's Ph.D. dissertation in the area of Systems Control given by the Department of Electrical Engineering at the Johns Hopkins University. The research for the model was conducted at the University's School of Medicine under Professor David A. Robinson.

The research activity was supported by the Naval Surface Weapons Center under its training program. This report was reviewed by R. W. Carson of the Guidance and Re-entry Analysis Branch and R. H. Hughey, Jr., Head, FBM Geoballistics Division.

Released by:

Ralph A. Niemann

RALPH A. NIEMANN, Head,
Warfare Analysis Department

ACKNOWLEDGEMENTS

I express my sincere appreciation to Dr. David Robinson, my primary thesis advisor, for his excellent guidance and numerous discussions which instilled in me a deeper insight into modeling and systems control. I am grateful for the use of the facilities and the cooperation of the personnel in Dr. Robinson's research laboratory in the Department of Ophthalmology of the School of Medicine of the Johns Hopkins University.

I thank Dr. David VandeLinde, my second thesis advisor, for bringing me into the graduate program at the Johns Hopkins University and also for valuable comments and discussions particularly on stochastic systems during my research.

I thank Dr. David Zee for his friendly comments and discussions on neurophysiology and also for criticisms of a preliminary version of the manuscript of my thesis. I thank my fellow researcher, Mr. Lance Optican, for various stimulating discussions on linear systems analysis.

This research was supported by the training program of the Naval Surface Weapons Center in Dahlgren, Virginia. I express my appreciation to Mr. James Colvard, the technical director of the center, and also to the supervisors, Mr. Ralph Niemann, Mr. Raymond Hughey, and Mr. Roger Carson, in my department for their support. I thank my colleague, Mr. Tom Alexander, for many discussions on various technical topics. Finally, I thank Ms. Christine Garza for her cooperation in typing, and Mrs. Danielle Dodd for her proofreading.

TABLE OF CONTENTS

I. INTRODUCTION

1.1 An Elementary Description of the Vestibuloocular Reflex 1

1.2 A Brief Sketch of Vestibuloocular Physiology 5

1.3 The Statement of the Problem 13

II. METHODS

2.1 Experimental Data 18

2.2 Experimental Setup 19

2.3 Theoretical Calculation 20

III. THE COMPENSATORY SLOW-PHASE

3.1 The General Description 22

3.2 The Semicircular Canal 22

3.3 The Oculomotor Plant 27

3.4 The Central Pathways 28

3.5 The Compensatory Slow-Phase Model 30

IV. THE MODELS OF SACCADES AND QUICK-PHASES

4.1 General Description of Saccades and Quick-Phases 36

4.2 Processing of Information 42

4.3 Control Scheme for the Pulse Generator 49

4.4 The Description of the Quick-Phase Generation Mechanism 53

V. THE INTEGRATED MODEL OF THE SLOW-PHASE AND THE QUICK-PHASE

5.1 The Outline of the Integrated Model 64

5.2 The Contours of the Deterministic WHEN Curve and WHERE Curve 82

5.3 The Model of the Deterministic WHERE Curve 84

5.4 The WHEN Curve 98

5.5 The Threshold Device 107

5.6 The Total Integrated Deterministic VOR Model 108

VI. STOCHASTIC MODEL

6.1 Introduction 111

6.2 The Stochastic Model 114

6.3 Noise Generation 120

6.4 Statistical Analysis in the Model 140

6.5 Summary 147

VII. RESULTS

7.1 General Approach 149

7.2 The Adjustment of the Threshold Value Q 150

7.3 The Adjustment of the Time Constant T_L in the WHERE Function 153

7.4 The Variance of the Noise Input to the Model 161

7.5 Results 174

7.6 Discussion of Results 196

7.7 Comments 201

VIII. DISCUSSIONS AND COMMENTS

8.1 Modification of the VOR Model for Saccades 211

8.2 Discussion on Head Velocity Around Zero Value 216

8.3 Comments on Other VOR Models 218

BIBLIOGRAPHY

DISTRIBUTION

TABLE OF ILLUSTRATIONS

Figure 1.1	Rotatory Nystagmus	4
Figure 1.2	The Semicircular Canal (Diagramatic) (adapted from Melvill Jones and Milsum, 1965)	8
Figure 1.3	Neural Signal Flow Diagram (bilateral push-pull arrangement)	11
Figure 1.4	Neural Signal Flow Diagram (equivalent single channel arrangement)	15
Figure 3.1	Compensatory Slow-Phase Model	35
Figure 4.1	Saccade Generation	41
Figure 4.2	The Outline of the Control Scheme for Retinotopic Organization	45
Figure 4.3	The Outline of the Control Scheme for Spatial Organization	47
Figure 4.4	*Modified Bang-Bang Control System*	51
Figure 4.5	Outline of the Quick-Phase Generation Mechanism	55
Figure 4.6	The High-Gain Amplifier (used in Figure 4.5)	57
Figure 4.7	Model Used to Determine the Equation for the Bang-Bang Amplifier (for $\Delta\theta > 0$)	62
Figure 5.1	The Hypothesis that Integration of SP and QP Commands Linearly Summate (To be rejected)	66
Figure 5.2	The Hypothesis that the Canal Signal is Suppressed by Quick-Phases (This scheme is used in this study)	69
Figure 5.3	Outline of the Integrated Model (s_1 and s_2 in in QP Mode)	71
Figure 5.4A	A Typical VOR Response from Our Cat for $\dot{H} \simeq 60$ deg/sec	74

Figure 5.4B VOR Response from Our Cat for Step Head Input Velocity of About 60 deg/sec (for Left Turn Head Motion) 77

Figure 5.4C VOR Response from Our Cat for Step Head Input Velocity of About 60 deg/sec (for Right Turn Head Motion) 78

Figure 5.4D VOR Response from Our Cat for Step Head Input Velocity of About 60 deg/sec (for Right Turn Head Motion) 79

Figure 5.4E VOR Response from Our Cat for Step Head Input Velocity of About 60 deg/sec (for Left Turn Head Motion) 80

Figure 5.4F VOR Response from Our Cat for Step Head Input Velocity of About 60 deg/sec (for Right Turn Head Motion) 81

Figure 5.5 Deterministic WHERE Curve, $\bar{C}(t)$, and WHEN Curve, $\bar{C}(t) - Q$ (for Right Turn Head Motion) 87

Figure 5.6 Deterministic WHERE Curve, $\bar{C}(t)$, and WHEN Curve, $\bar{C}(t) + Q$ (for Left Turn Head Motion) 88

Figure 5.7 Plot of f_0, g_0, C_0, and T_L vs $\dot{\theta}_s$ 92

Figure 5.8 The Model for Generation of the Deterministic WHERE Curve 97

Figure 5.9 The Threshold Value Q vs the SCC Signal ϕ 102

Figure 5.10 $\bar{D}_0$ vs $|\phi|$ for Step Input Head Velocity 104

Figure 5.11 The Threshold Device for Quick-Phases 106

Figure 5.12 The Total Integrated Deterministic VOR Model 110

Figure 6.1 Introduction of Noises on the Deterministic WHEN and WHERE Curves 116

Figure 6.2 The Stochastic VOR Model 122

Figure 6.3 Noise Generation 142

Figure 7.1 The Components of the Deterministic WHERE Curve for Sinusoidal Input (1.2 Hz) 156

Figure 7.2 Interaction Between Eye Position and WHERE and WHEN Curves (corresponds to the solid curve of f(t) in Figure 7.1) 158

Figure 7.3 Interaction Between Eye Position and WHERE and WHEN Curves (corresponds to the dotted curve of f(t) in Figure 7.1) 160

Figure 7.4 Backward Quick-Phase 164

Figure 7.5 Profiles of the Standard Deviations $\sigma(x_2)$ and $\sigma(z_2)$ 170

Figure 7.6 Shading Effects 172

Figure 7.7 Step Response from Our Cat (with mean slow-phase velocity of 8.9 deg/sec) 177

Figure 7.8 Step Response from Our Cat (with mean slow-phase velocity of 21.0 deg/sec) 178

Figure 7.9 Step Response from Our Cat (with mean slow-phase velocity of 30.8 deg/sec) 179

Figure 7.10 Step Response from Our Cat (with mean slow-phase velocity of 46.5 deg/sec) 180

Figure 7.11 Step Response from Our Stochastic VOR Model (with mean slow-phase velocity of 8.9 deg/sec) 182

Figure 7.12 Step Response from Our Stochastic VOR Model (with mean slow-phase velocity of 21.0 deg/sec) 183

Figure 7.13 Step Response from Our Stochastic VOR Model (with mean slow-phase velocity of 30.8 deg/sec) 184

Figure 7.14 Step Response from Our Stochastic VOR Model (with mean slow-phase velocity of 46.5 deg/sec) 185

Figure 7.15 Sinusoidal Response from Our Cat (with input frequency of 1.2 Hz and amplitude of 30 deg/sec) 188

Figure 7.16 Sinusoidal Response from Our Cat (with input frequency of 0.25 Hz and amplitude of 30 deg/sec) 189

Figure 7.17	Sinusoidal Response from Our Cat (with input frequency of 0.05 Hz and amplitude of 30 deg/sec)	190
Figure 7.18	Sinusoidal Response from Our Stochastic VOR Model (with input frequency of 1.2 Hz and amplitude of 30 deg/sec)	192
Figure 7.19	Sinusoidal Response from Our Stochastic VOR Model (with input frequency of 0.25 Hz and amplitude 30 deg/sec)	193
Figure 7.20	Sinusoidal Response from Our Stochastic VOR Model (with input frequency of 0.05 Hz and amplitude of 30 deg/sec)	194
Figure 7.21	Depiction of t_{TR}, $\|\theta_s\|$ and $\|\theta_Q\|$	198
Figure 7.22	Hysteresis Effect Demonstrated on the VOR Model	203
Figure 7.23	Effects of Initial Eye Position on t_{TR} and $\|\theta_s\|_M$ at f = 0.25	205
Figure 7.24	Effect of τ_1 and τ_2 on the Band-Pass Filter	210
Figure 8.1	Our Modified VOR Model with Arrangement for Saccades	213
Figure 8.2	The Essential Features of the VOR Model by Sugie and Melvill Jones (1971)	220
Figure 8.3	Simplified Version of the VOR Model by Schmid and Lardini (1976)	224
Figure 8.4	The VOR Model by Barnes (1977)	228

LIST OF COMMONLY USED SYMBOLS

$C(t)$	angular position where the eye is driven by quick phases; WHERE signal; WHERE curve
$C^*(t)$	sampled sequence of $C(t)$
$D(t)$	WHEN signal; WHEN curve
$D^*(t)$	sampled sequence of $D(t)$
DIR	direct pathway
EOM	extraocular muscle
f	frequency
f_Q	quick-phase frequency in beats per sec in the step response
f'_Q	quick-phase frequency in beats per cycle in the sinusoidal response
G	gain constant in the transfer function of a first order lag system in the WHERE function
L	left
NI	neural integrator
NPG	neural pulse generator
OMN	oculomotor nuclei
OMP	oculomotor plant
$P(t)$, $P(\Delta\theta)$	signal from pulse generator
PG	pulse generator
$\phi(t)$	signal from semicircular canal; cupula deflection
PPRF	paramedian pontine reticular formation
ψ	power spectral density of white noise
Q	threshold value

QP	quick-phase
R	right
R_{12}	linear correlation coefficient between the sampled WHEN noise and WHERE noise
$r_1(t)$	continuous noise on the WHEN curve
$r_1^*(t)$	sampled sequence of $r_1(t)$
$r_2(t)$	continuous noise on the WHERE curve
$r_2^*(t)$	sampled sequence of $r_2(t)$
ρ	linear correlation coefficient between $r_1^*(t)$ and $r_2^*(t+\Delta t)$
s	Laplace transform variable
SCC	semicircular canal
σ	standard deviation
σ^2	variance
SP	slow-phase
T	computation interval
T_1, T_2, T_c, T_c'	time constants associated with semicircular canal
τ_1, τ_2	time constants of noise filter
T_e	time constant of oculomotor plant
T_L	time constant of a first order lag system in WHERE function
T_n	time constant of neural integrator
t_Q	quick-phase duration
t_{TR}	time span in transition region of sinusoidal response
$\theta(t)$	eye position

$\theta(A/B)$	angular position of A relative to B
θ'	efference copy of eye position; signal from neural integrator
$\lvert\theta_Q\rvert$	quick-phase magnitude
$\dot{\theta}_s$	slow-phase eye velocity
VN	vestibular nuclei
VOR	vestibuloocular reflex

CHAPTER I

INTRODUCTION

1.1 An elementary description of the vestibuloocular reflex

The function of the vestibuloocular reflex (VOR) is to stabilize the visual axis in the environment during a head-rotation by compensating for it. It does this by making an equal and opposite eye-rotation in the orbit with the same time course as the head movement.

One way to demonstrate the speed and accuracy of the VOR is to try to read a book held stationary in one's hands while one's head is oscillating at about one or two Hz. Next, reverse the procedure and try to read a book being oscillated by one's hand at similar angular amplitudes and frequencies while one's head is held stationary. In the latter case, because the eye cannot keep up with the book which causes its image to slip on the retina, visual acuity is so low that reading is virtually impossible. In the former case, visual acuity is good (normal) because the visual axes are being automatically stabilized with respect to the stationary book by the VOR.

The VOR isolates the eyeball from the disturbances of the head's motions by an open-loop reflex action, unlike some mechanical control systems which isolate a so-called stable platform from the disturbances of the base motions

of ships and rockets by closed-loop, or negative feedback, control systems.

The reflex is phylogenetically very old. It developed in the early stages of the evolution of vertebrates as a means of survival by stabilizing vision of the environment in spite of head and body motions. The reflex is anatomically and physiologically similar for widely different species. This allows a fairly direct inference from animal experiments to man.

For most normal head movements, the required eye movement is small (e.g., 20 $\sim$ 30°) and well within the oculomotor range. However, because of mechanical limitations of eye rotation, if head rotation is continued beyond a certain limit, the eye must be reset. This is done by a rapid movement to a new position in the direction of the head motion. If the head is continuously rotated in one direction (say to the left) with a step of constant angular velocity $\dot{H}$ (Figure 1.1a), the eye position θ as a function of time t (Figure 1.1b) will describe a rhythmic saw-tooth motion with alternate periods of low velocity in the direction opposite to the head motion, thus compensating the head motion, and fast velocity in the direction of the head motion, thus catching up with the head by rapid resetting movements. This type of eye motion is called rotatory or vestibular nystagmus. The compensatory slow eye motion is called the slow-phase (SP) and the quick returning motion is called

Figure 1.1

For step input head velocity $\dot{H}$ (a), the eye position $\theta(t)$ describes a rhythmic saw-tooth motion (b), with alternate slow and quick eye velocities $\dot{\theta}$ in opposite directions (c).

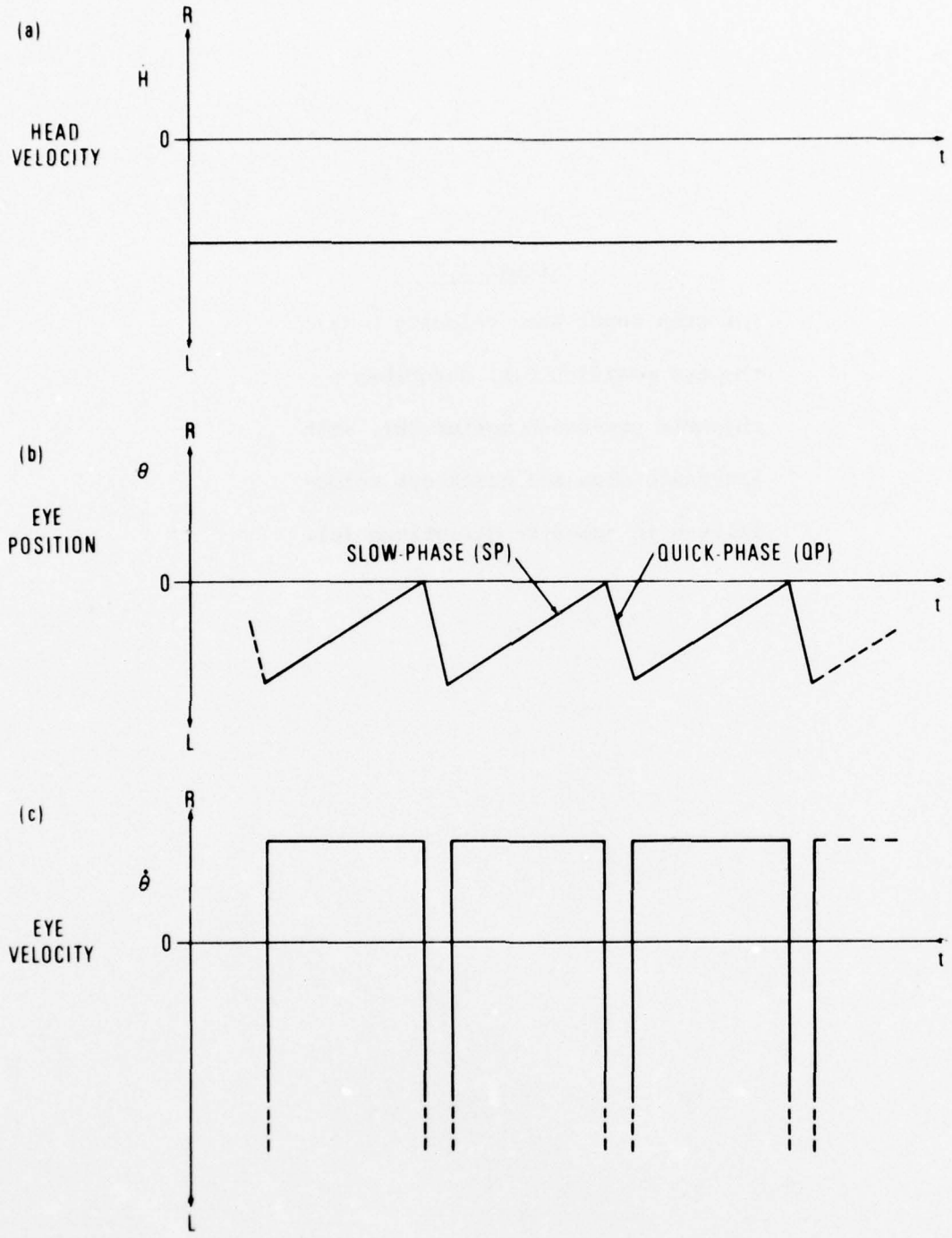

Figure 1.1 Rotatory Nystagmus

the quick-phase (QP) of the nystagmus. The profile of the eye velocity $\dot{\theta}$ during rotatory nystagmus is shown in Figure 1.1c to indicate that during each slow-phase the eye velocity is equal and opposite to head velocity.

The fact that the mean eye position (Figure 1.1b) shifts in the direction of the QP's is one of the major points of investigation in this study and will be discussed in detail subsequently.

This reflex is designed to assist vision but is sufficiently automatic that it works almost as well without it. To eliminate the modifications introduced by vision, the VOR is usually studied in isolation by rotating subjects in the dark. This thesis concerns only the latter situation.

1.2 A brief sketch of vestibuloocular physiology

There are two groups of semicircular canals (SCC) on each side of the skull located within the bony labyrinth of the inner ear. Each group consists of three approximately mutually orthogonal canals. The three canals on each side extend from a common compartment called the utricle which is contained in the egg-shaped "vestibule" of the inner ear. The expression vestibuloocular reflex is derived from the fact that the reflex is created by the action of the vestibular organ upon the oculomotor system.

For horizontal head rotation (yaw) in the normal upright position the lateral semicircular canal pair (one on each side of the head) is primarily stimulated. The experimental data on which this research is based are obtained by rotatory tests in the horizontal plane of subjects in the normal upright position. For this reason, we will consider for simplicity that only the lateral semicircular canals are stimulated in this study. There is no reason to suppose that the data cannot be simply extrapolated to the other canals for rotations in the roll and pitch directions.

The semicircular canal (Figure 1.2) is a circular, closed, membranous tube encased inside rigid bone. The tube's internal radius is about 0.15 mm for man (Melvill Jones and Milsum, 1965). The membranous tube is filled with a fluid called endolymph. The membranous labyrinth is submerged in a clear fluid called perilymph contained in the bony labyrinth in the petrous portion of each temporal bone.

Each semicircular canal completes a hydrodynamic circuit through the utricle to which the three canals on each side of the head are joined. Each canal completes about two-thirds of a circle and is interrupted by an enlarged specialized compartment called the ampulla located adjacent to the utricle. The ampulla contains a transverse

Figure 1.2

The figure shows a schematic representation of the semicircular canal SSC, which is a circular, closed, membranous tube encased inside rigid bone. Head angular acceleration causes the endolymph to flow. This causes a deflection of the cupula, which in turn creates a signal which passes into the central nervous system.

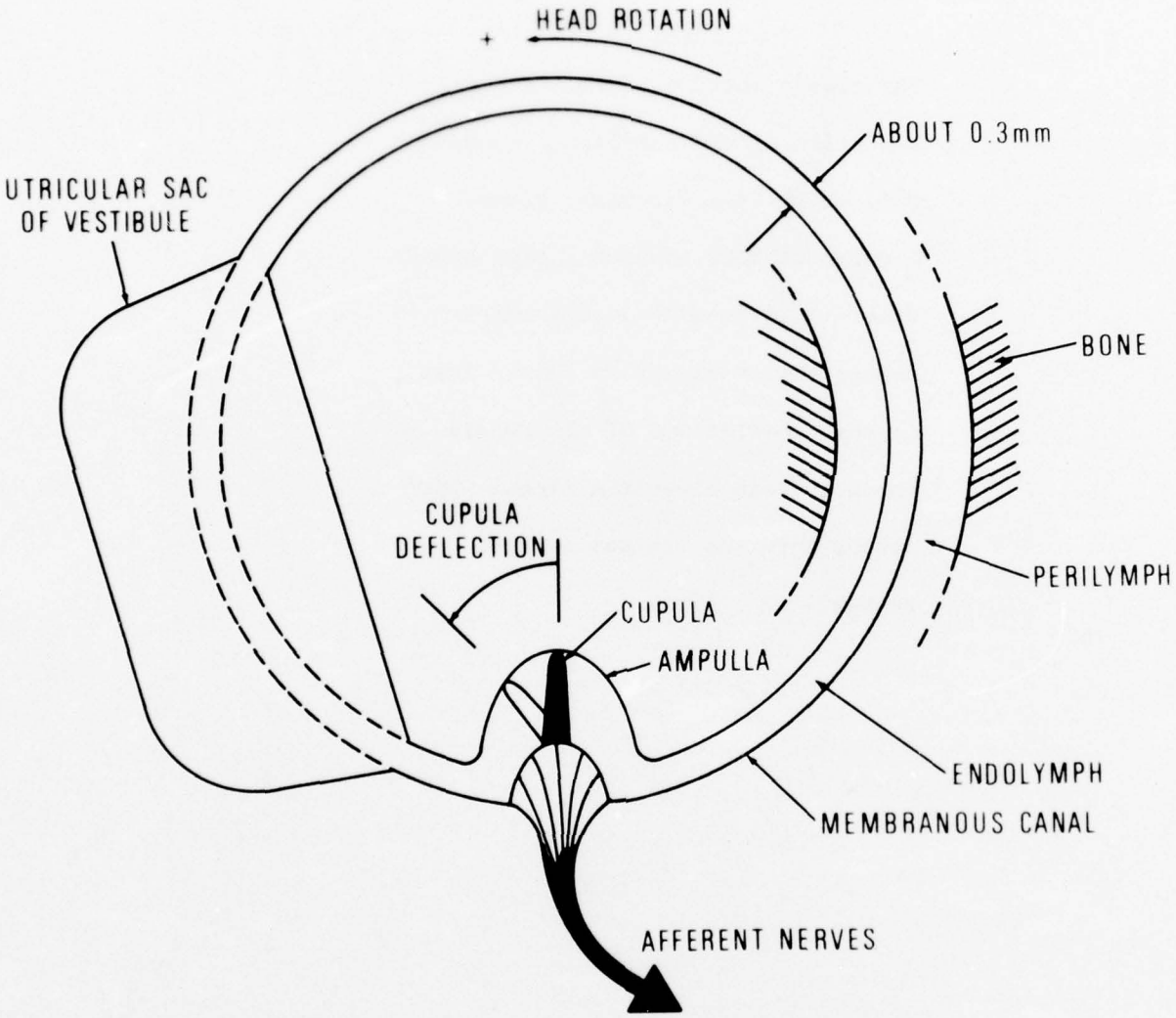

Figure 1.2 The Semicircular Canal (diagramatic) (adapted from Melvill Jones and Milsum, 1965)

crest called the crista ampullaris which contains a sensory epithelium consisting of hair cells. The cupula, a mass of gelatinous material which receives the processes of the hair cells, covers the crista ampullaris and forms a fluid tight, elastic valve across the canal in the ampulla. Head angular acceleration causes the endolymph to flow (in the direction opposite to the head motion) because of its inertial reaction which causes a deflection of the cupula. This, in turn, bends the hairs and depolarizes the sensory hair cells. This modulates the discharge rate of action potentials of first-order vestibular neurons. This signal then passes into the central nervous system.

When the two lateral semicircular canals are stimulated (in push-pull) by head angular acceleration, the signals from them are transmitted to the vestibular nuclei (VN) through the non-auditory (vestibular) portion of the VIIIth cranial nerve (Figure 1.3). From the vestibular nuclei the signal reaches the oculomotor nucleus III and abducens nucleus VI (for simplicity these will often be lumped together and referred to simply as the oculomotor nuclei (OMN)) through two pathways, one, direct (DIR) and another, indirect, through the paramedian pontine reticular formation (PPRF). The signals from the oculomotor nuclei innervate the extraocular muscles (EOM); the medial rectus via the IIIrd nerve and

Figure 1.3

This figure shows schematically the neural signal flow of the vestibuloocular reflex (restricted to the slow-phase, excluding the quick-phase) in the bilateral push-pull arrangement. If we view the VOR as a system, the input to the system is the head acceleration, while the output from the system is the eye position.

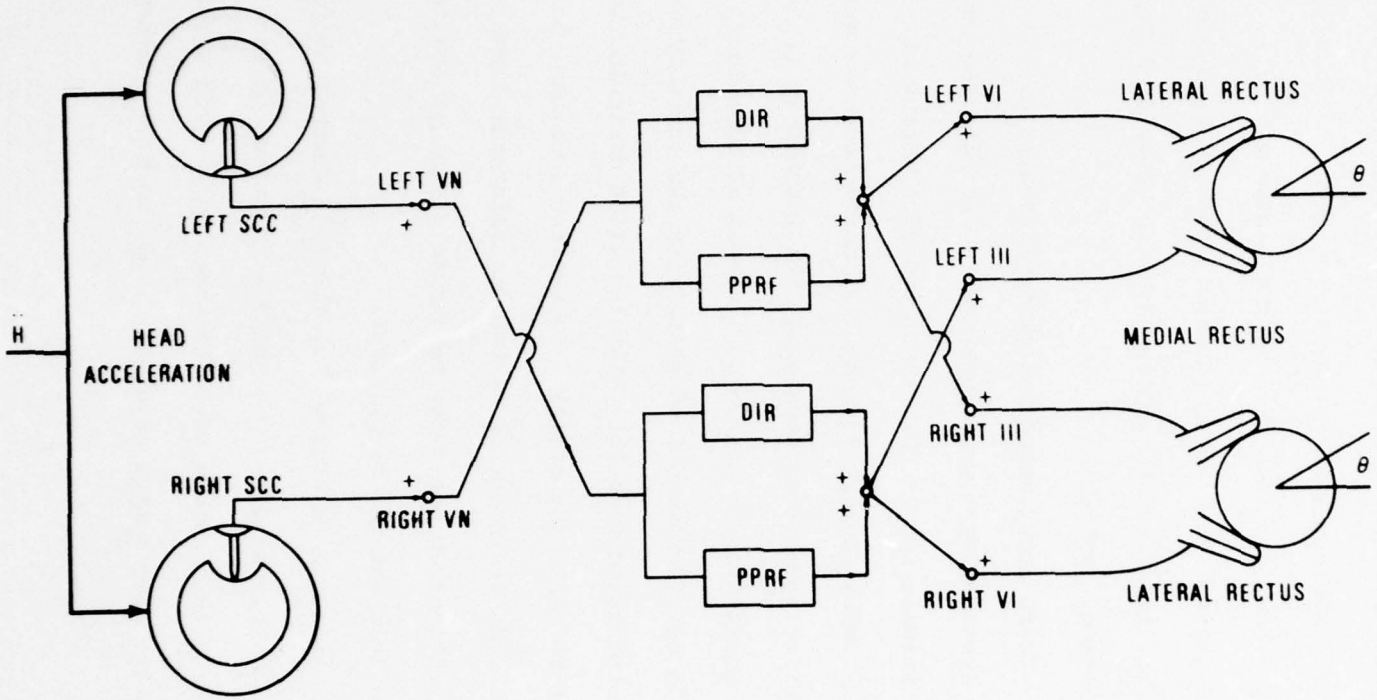

Figure 1.3 Neural Signal Flow Diagram (bilateral push-pull arrangement)

lateral rectus via the VIth nerve. The former pulls the eye medially, the latter laterally; together, in push-pull, they effect horizontal eye movements. There is no stretch reflex in the extraocular muscles and therefore no local feedback around the eye plant (Keller and Robinson, 1971). A simplified diagram with two bilateral push-pull elements (canals, nuclei, fiber tracts and muscles) is shown in Figure 1.3 (Robinson, 1975).

There are crossed inhibitory pathways at, at least, two levels. Each vestibular nerve inhibits the contralateral VN (Shimazu and Precht, 1966) and each output of the brainstem centers inhibits antagonist motoneurons as well as exciting agonist motoneurons. The inhibitory signal reinforces the excitation in a push-pull manner at each level because it is 180 degrees out of phase with the excitory signal and is subtracted from it. This is called disinhibition. Thus each VN cell, for example, is excited from the ipsilateral canal and disinhibited by the contralateral canal. These connections do not alter the basic signal processing and have been left out for simplicity.

As shown in Figure 1.3, the left channel and the right channel of the VOR are exactly symmetrical to each other. Since both channels have the same input (head acceleration) and the same output (eye position), we have constructed an

equivalent single channel diagram (Figure 1.4) to simplify the analysis without loss of generality. In Figure 1.4, the equivalent canal output can go either positive or negative and the equivalent muscle can push as well as pull.

1.3 The statement of the problem

The slow-phase portion of the VOR has been studied by many people, and there is a general consensus of how it works and how it can be represented by a mathematical model. This will be presented in more detail later, but essentially, the canals when stimulated by head angular acceleration, produce a neural signal proportional to head velocity. The velocity signal is integrated in the pontine reticular formation to produce a signal proportional to head angular position. This actuates the eyeball to move in the opposite direction so that eye angular position is equal but opposite to head angular position. The velocity signal is also fed directly to the eye plant to offset the lag generated by the viscoelastic nature of the eye plant. Although a few details remain to be worked out, and there are still problems associated with specific neuroanatomical connections, the general signal processing events are fairly well understood in the modeling of the slow-phase system.

However, the modeling of the quick-phase part is a different story. As of this writing, very little quantitive

Figure 1.4

This figure shows schematically a single channel neural signal flow of the vestibuloocular reflex (restricted to the slow-phase only) equivalent to the bilateral push-pull arrangement of Figure 1.3. This is done to simplify the analysis without loss of generality.

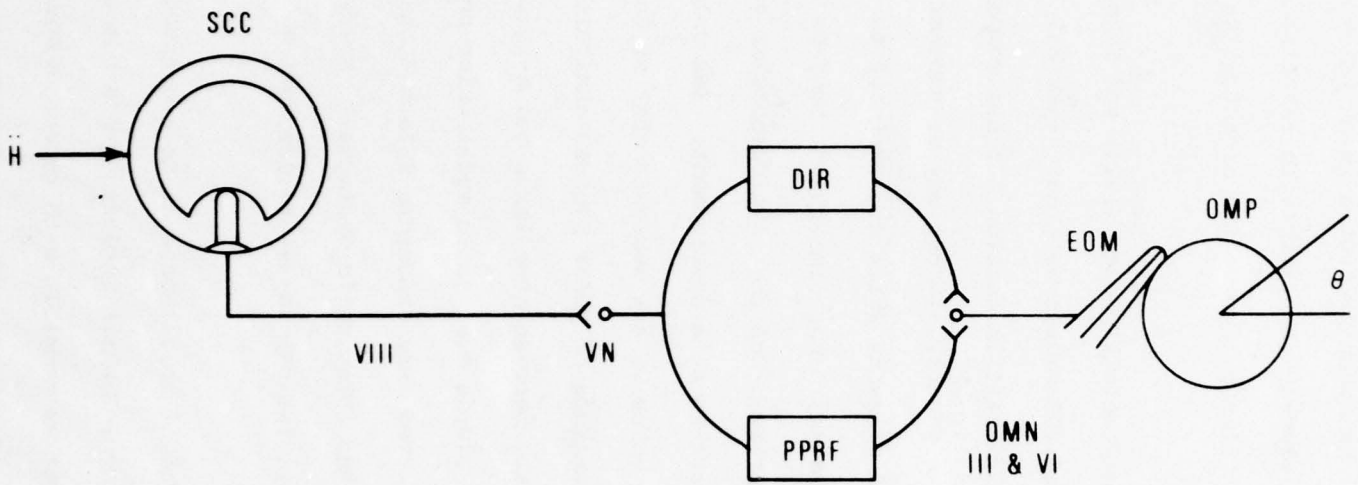

Figure 1.4 Neural Signal Flow Diagram (equivalent single channel arrangement)

descriptions exist as to what determines the time of the quick-phase initiation and the magnitude of a quick-phase, and no model has been presented which tries to tie its elements as closely as possible to establish neurophysiological results and tries to evolve its organization on a teleological basis.

Sugie and Melvill Jones (1971) and Schmid and Lardini (1976) have proposed VOR models with quick-phases. Their models are discussed in detail in section 8.4 and compared to the present model but, in general, in one way or another they have proposed circuits and elements which are contrary to current neurophysiological findings. More important, they do not deal with the stochastic behavior of the vestibuloocular reflex which is a major interest in this development. The only stochastic analysis of which we are aware is that of Cheng (1972) who used the technique of point process analysis to analyze the time intervals between successive quick-phases. He has described a simple stochastic model which could simulate various observed inter-saccadic interval characteristics of vestibular and optokinetic nystagmus. However, his analysis is purely statistical in nature and made no attempt to model the VOR.

The goal of this thesis is to construct a mathematical model for the VOR which includes quick-phases and which is as consistent as possible with recent advances in neurophysiology. First, it must reasonably simulate the

deterministic characteristics of nystagmus and then include the stochastic behavior of the VOR nystagmus by introducing appropriate random signals at neurophysiologically appropriate points in the deterministic model. The final model determines not only when a quick-phase should be triggered, but also determines where it should carry the eye.

Experimental data were obtained from a cat rotated by head velocity steps and sine waves of various amplitudes and frequencies. These results formed the data base for the model. The topology of the model was then set up by inference from a variety of physiological observations and the parameters adjusted to give a best match on a digital computer simulation for the deterministic and stochastic behavior of the reflex that was experimentally observed.

CHAPTER II

METHODS

2.1 Experimental data

All experimental data used in this research were obtained from a single cat. Data from cat were readily available from an ongoing experiment in the laboratory. A fairly direct inference from cat's VOR to man's can be made because the reflex is anatomically and physiologically similar for widely different species.

The fact that the data came from one cat instead of many cats presents no disadvantage in this study because the main interest is in the topology and phenomenology of the VOR in general and not in the quantitative details of the VOR of any particular species. Nevertheless, it was important to show that the model could be adjusted to quantitatively fit actual biological data. The data from one cat formed a self-consistent data base. The data from a large population of cats were simply not of interest.

Two types of inputs (head motions) were used. For step velocity inputs, nominal head velocities of approximately 10, 20, 40, and 60 deg/sec were used. Although some output data from input head velocity of 5 deg/sec were available, they were too limited to be used for any firm conclusions but did indicate some trends. For sinusoidal inputs,

frequencies of 0.05, 0.25, and 1.2 Hz with peak head velocities ranging from 10 to 30 deg/sec were used.

2.2 Experimental setup

Cat's eye movements are measured by techniques originally developed by Robinson (1963) and further refined by Fuchs and Robinson (1966). Briefly, in this method, a coil of fine wire, surgically implanted upon the eyeball beneath the bulbar conjunctiva and recti insertions, is subject to horizontal and vertically alternating magnetic fields 90° out of phase with each other. A voltage is induced in the coil which is a function of the angle between the eye position and magnetic field. This voltage is phase-detected against both horizontal and vertical reference voltages, resulting in two d-c voltages proportional to the horizontal and vertical angles of eye position.

The technique makes it possible to record eye movements conveniently and accurately in the experimental animal in long-term experiments on oculomotor function. The method has a resolution of 1.5 min of arc, is linear within 6% of a full scale of $\pm$ 20 deg, and possesses a system bandwidth of 1,000 Hz.

A platform was attached to the cat's skull by three stainless steel bolts. The cat was restrained in a close-fitting box and its head immobilized by fastening the

platform to a shelf extending from the box. The box was placed in the magnetic field coil frame which could rotate in the horizontal plane. Head (frame) angular velocity was measured by a tachometer generator. Eye velocity was obtained by differentiating eye position over the bandwidth 0-16 Hz. All experiments were done in total darkness. Care was taken to keep the cat alert.

2.3 Theoretical calculation

The mathematical model formulated in this research was programmed in FORTRAN IV language. The simulations of the model were performed by a CDC 6700 digital computer. The output graphs were plotted by a Calcomp plotter. The computation interval was fixed at 0.01 sec which is much smaller than quick-phase durations (which are generally more than 0.1 sec for the cat), the periods of input sinusoids (1.2 Hz, maximum) and any system time constant (which were larger than about 0.1 sec).

For the numerical integration of the differential equations, all with the form of $\dot{x}(t) = a\,x(t) + b\,u(t)$ where a and b are constants, the time domain solutions were directly used. At one point a simple version of the predictor-corrector method for the numerical integration was tried. The two methods were virtually indistinguishable at the accuracy relevant to our investigations which is about 0.1 degrees of eye position.

Gaussian random numbers were generated sequentially by the computer at each computation interval and fed into the model at specified points after passing through appropriate filters to meet the characteristics of randomness shown by the data (for detail, see section 6.3).

CHAPTER III

THE COMPENSATORY SLOW-PHASE

3.1 The general description

From the viewpoint of control systems analysis, the input to the VOR system is the head angular acceleration $\ddot{H}$ with respect to the environment (specifically, an inertial reference frame) and the output from the system is the eye angular position θ with respect to the head. The receptor organs of the VOR, which are stimulated by the head acceleration, are the semicircular canals. The effector organ of the VOR system, which produces the response in the form of eye position, is the oculomotor plant (OMP) which consists of the eyeball, the extraocular muscles and associated suspensory tissues.

The pathway between the receptor and effector organs consists of two branches, one direct from the vestibular nuclei to the eye muscle motoneurons and the other through the paramedian pontine reticular formation (PPRF).

3.2 The semicircular canal*

The semicircular canal (SCC) is considered as a rigid circular tube with a very small uniform cross-section. Each canal completes a hydrodynamic circuit through the utricles (which it shares in common with the other two canals on its

*References: Melvill Jones, and Milsum, 1965; Outerbridge, 1969

side of the head) with negligible coupling with the other canals. The fluid flow within the canal is laminar because of the small, smooth bore of the canal. The canal has high viscous damping as indicated by the small Reynolds number of the flow. It is common to use lumped analysis and ignore the flow distribution within the canal. Thus, the fluid is considered to rotate as a ring relative to head.

The following analysis is based on angular rotation of the canal in a single plane. Consider a counter-clockwise rotation (defined as the positive direction of rotation) of the canal and hence the head as described in Figure 1.2. The damping torque (positive when acting counter-clockwise) M_d on the fluid ring is assumed to be

$$M_d = -b\dot{\theta}(F/H) \tag{3.2.1}$$

where $\dot{\theta}(F/H)$ is the angular velocity of the fluid relative to the head and b is a positive proportionality constant. Note that $\dot{\theta}(F/H)$ is clockwise relative to the head in this case because of inertial reaction. The elastic restoring torque M_e on the fluid ring is assumed to be

$$M_e = -k\theta(F/H) \tag{3.2.2}$$

where $\theta(F/H)$ is the angular displacement of the fluid relative to the head and k is a positive proportionality constant.

By Newton's second law,

$$J\ddot{\theta}(F/I) = M_d + M_e = -b\dot{\theta}(F/H) - k\theta(F/H) \tag{3.2.3}$$

in which J is the fluid ring moment of inertia and $\ddot{\theta}(F/I)$ is the angular acceleration of the fluid relative to inertial space. By denoting the angular acceleration of the head relative to space by $\ddot{\theta}(H/I)$, it follows that

$$\ddot{\theta}(F/I) = \ddot{\theta}(H/I) + \ddot{\theta}(F/H) \tag{3.2.4}$$

Assuming that the cupular deflection relative to the head $\theta(C/H)$ is proportional to the angular displacement of the head relative to fluid $\theta(H/F)$,

$$\theta(C/H) = a\theta(H/F) = -a\theta(F/H) \tag{3.2.5}$$

where a is a positive constant, which reflects the fact that the area of the canal is not equal to the area of the ampulla. Substituting (3.2.4) and (3.2.5) into (3.2.3)

$$J\ddot{\theta}(C/H) + b\dot{\theta}(C/H) + k\theta(C/H) = aJ\ddot{\theta}(H/I) \tag{3.2.6}$$

Replacing cupular deflection $\theta(C/H)$ by ϕ and $\theta(H/I)$ by H in (3.2.6),

$$J\ddot{\phi} + b\dot{\phi} + k\phi = aJ\ddot{H} \tag{3.2.7}$$

which is identical with the equation given by Melvill Jones and Milsum (1965). It is the same form as the differential equation for a torsion pendulum which describes the torsional vibrations of an elastic shaft with a circular rotor rigidly attached to it. The canal system is probably ten times more than critically damped.

Since the system represented by (3.2.7) is very over-damped ($b^2 >> Jk$), the transfer function (in Laplace transform notation) of the SCC may be approximated by

$$\frac{\phi(s)}{\ddot{H}(s)} = \frac{aT_1T_2}{(T_1s + 1)(T_2s + 1)} \tag{3.2.8}$$

where

$$T_1 \simeq \frac{b}{k} \tag{3.2.9}$$

$$T_2 \simeq \frac{J}{b}$$

For man T_1 is thought to be about 10 ~ 16 sec and T_2 about 0.003 sec. For cat T_1 is found to be about 4 sec and T_2 about 0.0015 sec (Melvill Jones and Milsum, 1971). For the frequency range below 5 Hz corresponding to normal daily activities, where $T_2s < 1$, the transfer function may be further approximated as

$$\frac{\phi(s)}{\ddot{H}(s)} \simeq \frac{aT_1T_2}{T_1s + 1} \tag{3.2.10}$$

Further, in the range above about 0.05 Hz, where $sT_1 > 1$ which includes most normal head movements,

$$\frac{\phi(s)}{\ddot{H}(s)} \simeq (aT_2)\frac{1}{s} \tag{3.2.11}$$

which is a pure integrator with gain (aT_2).

It follows that in this frequency range,

$$\phi(t) \propto \int \ddot{H}(t)dt \propto \dot{H}(t) \tag{3.2.12}$$

Thus, the output of the SCC is proportional to head velocity over the range of natural head movements, the role of SCC being that of an integratng accelerometer or velocity transducer. Indeed, the experimentally measured firing rate modulation of primary vestibular afferents is proportional to head velocity over this frequency range (Fernandez and Goldberg, 1971).

The gain constants of the internal neural signal processing elements are all, for practical purposes, indeterminable because the signals all consist of the firing rates of large populations of neurons, only a few of which can be observed at any one time. Only the final overall gain is important and interior gains may be adjusted arbitrarily so long as the total gain is kept correct. Thus, the gain of the transfer function (3.2.10) of the SCC may be arbitrarily adjusted so that (3.2.10) will behave like a pure integrator with a unity scale factor at midband frequencies. That is, T_1 is relabeled the cupula long-time constant T_C and (aT_1T_2) is replaced by T_C. It follows from (3.2.10) that

$$\frac{\phi(s)}{\ddot{H}(s)} = \frac{T_C}{sT_C + 1} \qquad (3.2.13)$$

which reduces to $1/s$ for $sT_C > 1$. The break frequency for $1/(sT_C + 1)$ is about 0.016 Hz with $T_C = 10$ sec (for man). Thus, for all frequencies of normal head rotation above

0.016 Hz, the canals integrate head acceleration and produce a signal proportional to head velocity. For cat for which T_c is about 4 sec, the break frequency is about 0.04 Hz.

3.3 The oculomotor plant

The oculomotor plant consists of the eyeball, the extra-ocular muscles and associated suspensory tissues. The relationship between eye position θ in the head and the discharge rate R_e of the oculomotor neurons has been found by recording these variables simultaneously in alert monkeys (Robinson, 1970; Robinson and Keller, 1972). To a first order approximation,

$$R_e = k(\theta-\theta_T) + r\dot{\theta} \qquad (3.3.1)$$

where θ_T is the threshold eye angle at which the neuron is recruited into activity and k and r are coefficients which relate R_e to θ and $\dot{\theta}$. One can rearrange the above equation by redefining R_e as the change in rate from the baseline value $(-k\theta_T)$ thus dropping this term out.

Factoring out k,

$$R_e = k(\theta + \frac{r}{k}\dot{\theta}) \qquad (3.3.2)$$

This gives the transfer function (arbitrarily making the d.c. gain factor unity)

$$\frac{\theta(s)}{R_e(s)} = \frac{1}{sT_e + 1} \qquad (3.3.3)$$

where the time constant T_e, which is r/k, has a neuron population mean of about 0.2 sec.

There is no stretch reflex in the extraocular muscles (Keller and Robinson, 1971). This means that there is no local feedback around the plant which could conceivably change its transfer function for different eye movement tasks.

3.4 The central pathways

From the viewpoint of control systems analysis, the whole purpose of the VOR is to recover the head angular position signal by integrating the head angular acceleration signal with respect to time twice.

The first integration is performed by the SCC. Another integration is needed somewhere. The oculomotor plant cannot be an integrator in the bandwidth within which the VOR works properly (down to 0.02 Hz) because the plant will not introduce much phase lag below about 0.8 Hz (for $T_e = 0.2$). This has been further verified by rotating monkeys sinusoidally and measuring the phase shift between eye position and the sinusoidally modulated firing rates of ocular motoneurons (Skavenski and Robinson, 1973).

The equation $R_e = k(\theta + 0.2\dot{\theta})$ in the last section suggests two central pathways from the vestibular nuclei VN to the oculomotor nuclei OMN. One, a direct pathway with a pure gain of $T_e = 0.2$, furnishes the $0.2\dot{\theta}$ term (raw

velocity information) in the above equation to the OMN. The other pathway, possibly through the reticular formation, furnishes the θ term in the above equation to the OMN after integrating the velocity signal with respect to time. Thus, this path fulfills the role of the needed second integrator to make the VOR work. The indirect pathway will thus be referred to as the neural integrator NI. The transfer function of the direct pathway is simply its gain T_e. The transfer function of the indirect pathway NI is assumed to be a leaky integrator because it is unlikely to be ideal and there is more direct evidence that it behaves this way. It is given by

$$TF(NI) = \frac{T_n}{sT_n + 1} \tag{3.4.1}$$

which approaches a pure integrator $1/s$ for frequencies greater than about 0.006 Hz because of its rather large time constant of about 25 sec (Becker and Klein, 1973).

Thus for normal head movements whose spectral components lie well above 0.01 Hz, the transfer function for the central pathways between VN and OMN is

$$T_e + \frac{1}{s} = \frac{sT_e + 1}{s} \tag{3.4.2}$$

This conveniently reduces the transfer function between the VN and the eye position to that of a pure integrator as shown below (see Figure 3.1 in the next section):

$$\left(T_e + \frac{T_n}{sT_n + 1}\right)\left(\frac{1}{sT_e + 1}\right) \simeq \left(T_e + \frac{1}{s}\right)\left(\frac{1}{sT_e + 1}\right) = \frac{1}{s} \tag{3.4.3}$$

One may interpret the role of the direct pathway as creating the phase lead needed to offset the phase lag that would otherwise be created by the plant.

3.5 The compensatory slow-phase model

Putting all these elements together, the total transfer function of the compensatory slow-phase model for frequencies above 0.006 Hz (corresponding to $T_n = 25$ sec) is

$$\frac{\theta(s)}{H(s)} \simeq s^2\left(-\frac{T_c}{sT_c + 1}\right)\left(T_e + \frac{1}{s}\right)\left(\frac{1}{sT_e + 1}\right) = -\frac{sT_c}{sT_c + 1} \tag{3.5.1}$$

For frequencies above 0.01 Hz (corresponding to $T_c = 16$ sec), it further simplifies to

$$\frac{\theta(s)}{H(s)} = -1 \tag{3.5.2}$$

Equation (3.5.2) meets the requirement of the slow-phase VOR which is to recover, in the opposite direction, the head angular position signal.

For cat, the cupula time constant of the SCC is experimentally found to be about 4 sec (Melvill Jones and Milsum, 1971). This was determined by directly recording from vestibular neurons. This gives a break-frequency of about 0.04 Hz for the cat, which is about four times as high as that of 0.01 Hz, corresponding to T_c = 16 sec for man. But it turns out that the VOR works properly at a frequency lower than 0.04 Hz for cat. According to a recent investigation (Robinson, 1976) of the Bode diagram of the VOR of about ten cats tested in the dark, the actual transfer function between eye position θ (output) and head position H (input) is given by

$$\frac{\theta(s)}{H(s)} = -(0.9)\left(\frac{sT_c'}{sT_c' + 1}\right)\left(\frac{sT_a}{sT_a + 1}\right) \qquad (3.5.3)$$

in which $T_c' \simeq 12$ sec and $T_a \simeq 50$ sec. The factor $sT_a/(sT_a + 1)$ was noticed by others (e.g., Young, 1969) and appears to reflect adaptation. This factor cannot be the neural integrator (3.4.1) for the following reason. When quick-phase signals are added to the slow-phase signal (see Figure 5.1) they chop up the latter and remove all of its low frequency components. This means that a poor low frequency response of the NI will not be detected. The chopping action of the quick-phase pulses makes even a badly leaky integrator look perfect. Since the effect of $sT_a/(sT_a+1)$ is observable, it must occur before the site of quick-phase injection and adaptation is the most likely cause. The break frequency

of $sT_a/(sT_a + 1)$ is about 0.003 Hz which is well below the lower frequency limit for proper functioning of the reflex and is also below the frequency range of interest in this study. Thus, we may replace $sT_a/(sT_a + 1)$ by unity for our purpose. Equation (3.5.3) now may be approximated as

$$\frac{\theta(s)}{H(s)} = -(0.9)s^2 \left(\frac{T_c'}{sT_c' + 1} \right) \frac{1}{s} \qquad (3.5.4)$$

If we identify s^2 with the conversion of head position to head acceleration and 1/s in (3.5.4) with the neural integrator system described in (3.4.3), it appears that $T_c'/(sT_c' + 1)$ must correspond to some sort of equivalent SCC with an effective time constant of $T_c' \simeq 12$ sec.

It follows that there must exist in the brain a compensation process for the SCC represented by a transfer function $G_c(s)$ such that

$$\frac{T_c}{sT_c + 1} \; G_c(s) = \frac{T_c'}{sT_c' + 1} \qquad (3.5.5)$$

from which we obtain

$$G_c(s) = \frac{T_c'(sT_c + 1)}{T_c(sT_c' + 1)} \qquad (3.5.6)$$

where T_c is the experimentally measured cupula time constant while T_c' is the effective time constant for an equivalent SCC determined from the reflex response.

It is unknown where and how the activity corresponding to $G_c(s)$ as given by (3.5.6) happens neurophysiologically. Our use of $T_c' = 12$ instead of $T_c = 4$ is purely pragmatic.

The complete compensatory slow-phase model is shown in Figure 3.1, in which the reflex gain of 0.9 in the darkness is inserted between the output of the effective SCC and the input of the neural integrator. All animals have a reflex gain less than one in the dark. The reason for this is not known. The reflex gain is brought up to one in the light presumably because of the contribution from the smooth pursuit or optokinetic systems.

Figure 3.1

This figure shows the compensatory slow-phase model. The SCC is replaced by the "effective" SCC which incorporates a compensation process in the brain for the SCC to yield a proper reflex time constant. The reflex gain of 0.9 in the darkness is inserted between the effective SCC and the neural integrator.

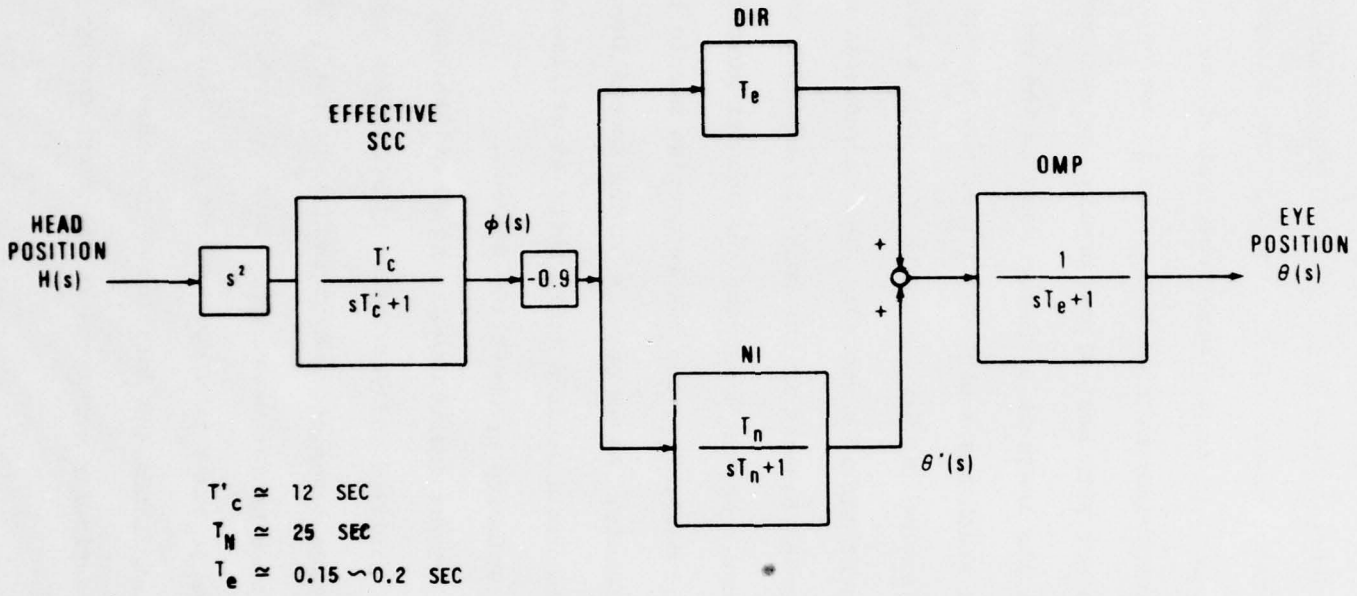

Figure 3.1 Compensatory Slow-Phase Model

CHAPTER IV

THE MODELS OF SACCADES AND QUICK-PHASES

4.1 General description of saccades and quick-phases

Light enters the eye through the lens projecting an image on a photosensitive sheet called the retina. However, the resolving power of the retina is not uniform. To see an object with best visual acuity one must move his eye to place its image on a special area in the retina called the fovea which has a high density of photoreceptors. Target acquisition in this manner is done with a fast discrete eye movement called a saccade. The extraocular muscles are among the fastest in the body and saccades are their fastest product. During a saccade the agonist muscle contracts almost maximally, and the antagonist muscle is inhibited completely. As an example of the speeds involved, a 10 degree human saccade lasts about 45 milliseconds and has a peak velocity of about 400 deg/sec.

It was qualitatively and quantitatively substantiated that saccades and vestibular quick-phases are essentially the same movement, and therefore, probably the product of the same neural mechanism. This was done by comparing the shape of their time courses and the relationship between the amplitude and duration of saccades and the quick-phases of vestibular nystagmus in the alert monkey and showing that

they are almost the same. The differences were so small that it seems unnecessary to hypothesize separate circuits for the two types of rapid eye movements (Ron, Robinson, and Skavensky, 1972). It will be shown subsequently that rapid eye movements are made by cells in the brainstem called bursters. Such cells burst briefly at high discharge rates during saccades and quick-phases. No one has ever reported a cell that burst for one type of movement but not the other. There is no evidence that these movements are different and this idea is generally accepted.

Historically, the term saccade denotes a rapid eye movement to a visual target while the term quick-phase denotes a rapid eye movement made by the VOR even in the dark. There is the tacit assumption that quite different central mechanisms are involved although the final movement machinery is the same. That is, no distinction exists between saccadic and quick-phase signals at the level of the neural pulse generator (the bursters) to effect rapid eye movement, but separate signals, one for the saccade and the other for the quick-phase have been assumed to enter this pre-nuclear pulse generating system. However, vision is not always necessary for saccades. They are stimulated by auditory and tactile stimuli as well. It is more general to think of a saccade as an eye movement to a point in space which may

contain something of interest. If that is the case, why not admit vestibular signals as being able to determine which point in space is of interest? If one is suddenly rotated, say, to the left, what lies to the left is suddenly of great interest because that is where one is going. Is the rapid eye movement to the left, which in fact one always makes, a saccade or a quick-phase? The idea will be proposed that rapid eye movements are designed to bring the eye to a point in space of interest and that point can be determined by any sense modality including vestibular. In that sense, there may not be any distinction between a saccade and a quick-phase even in the higher centers which control the pre-nuclear pulse generator.

The most noticeable event during a rapid eye movement is the burst of high frequency discharges seen to occur in the motoneurons. The discharge rates of the oculomotor neurons during a QP are very high and range from 400 to 600 spikes per sec. This drives the eye at velocities up to 700 deg/sec (in man). Cat's QP eye velocity is much less than that of man. For our cat, it was about 120 deg/sec for saccades of amplitudes of about 13.5 deg.

Neurons that burst with a high frequency discharge time-locked with the motoneuron burst, but which are silent otherwise, are found throughout the pons (Sparks and Travis, 1971). However, a great concentration of so-called bursters

are seen in the PPRF (Cohen and Henn, 1972). They were recently studied in some detail by Keller (1974). Unilateral lesions of the PPRF abolish ipsilateral saccades while lesions elsewhere do not. It is difficult to avoid the conclusion that saccades and quick-phases are generated by the activity of the bursters in the PPRF.

The neural pulse of bursters is very large during a saccade and zero before and after it, just like eye velocity. Therefore, it is assumed that the eye velocity is proportional to the pulse height (by this is meant the firing rate in spikes/sec). That is, the pulse is an eye velocity command. We must transform the neural eye velocity information (pulse height) into eye position. Consequently, the signal must be integrated just like the vestibular signal. So we use the simplest path already existing in the slow-phase model. The consequent arrangement is shown in Figure 4.1. The pathway between the VN and the output of the OMP, that is, the eye position (as shown in Figure 4.1) is defined for our purpose as the extended final common path because it is a common path for both the SP and QP of nystagmus. The neural network that produces the saccadic pulse is termed the pulse generator (PG). A neural pulse generated by the PG enters at the VN and becomes a pulse-step (weighted sum of pulse and step) at the OMN; the pulse being required to move the eye rapidly

Figure 4.1

This figure shows a conceptual arrangement for saccade generation. A neural pulse generated by the pulse generator is injected at the VN level and processed (integrated) through the existing pathway resulting in a saccade.

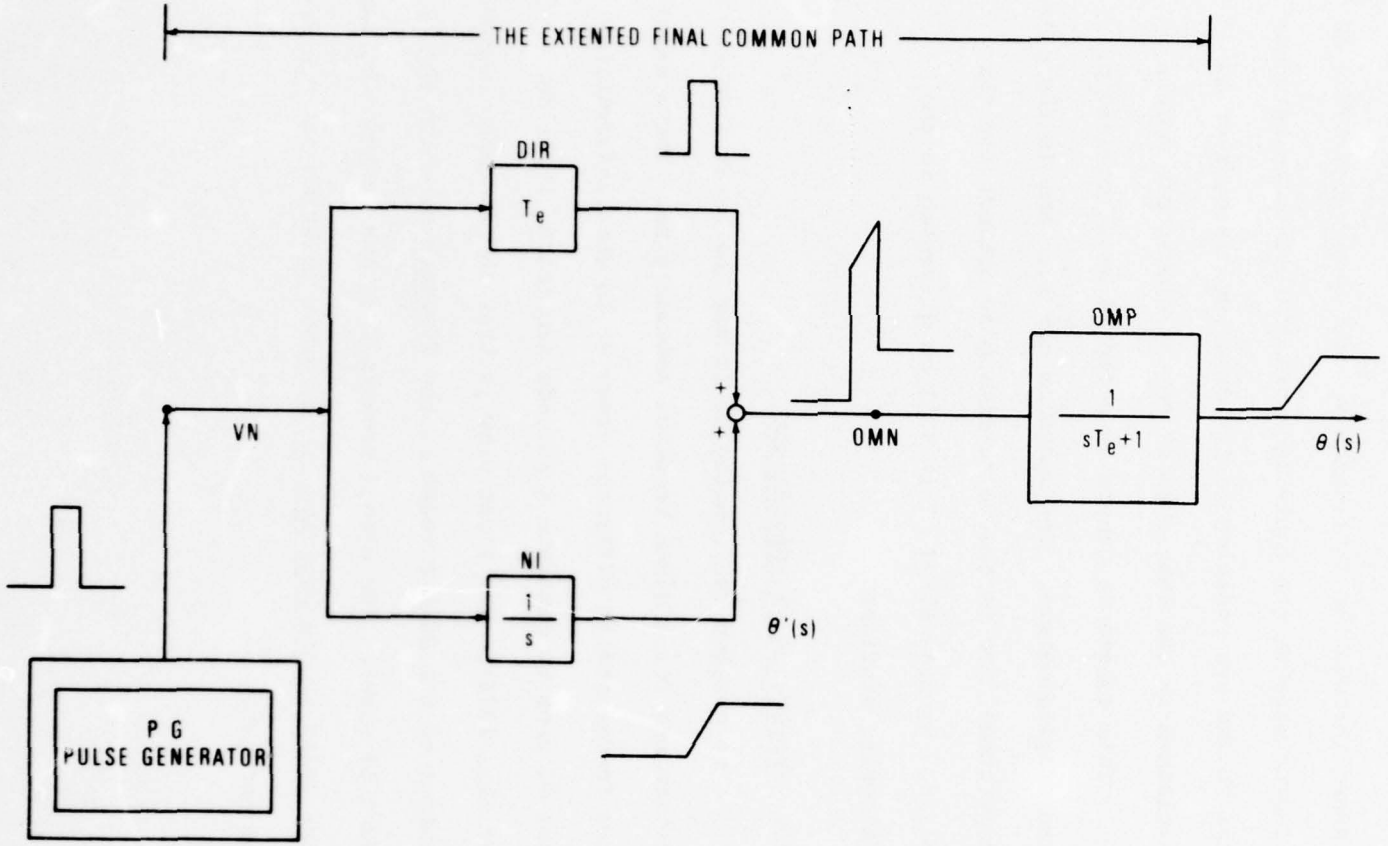

Figure 4.1 Saccade Generation

against orbital viscous forces and the step to hold the new eye position against elastic restoring forces. The relative weight between the pulse and step at the OMN is 0.2 and 1.0 respectively, so that their sum gives the step (after it is passed through the OMP) which we call a saccade. This is assured because the equivalent transfer function between the VN and eye position is 1/s or a pure integrator as explained in the last chapter on the slow-phase model.

This scheme is generally accepted among oculomotor neurophysiologists. The question now is: How is the pulse generated? How is the pulse size made correct for the desired saccade size? This will be discussed in the following sections.

4.2 Processing of information

The problem confronting us is how the burst size is determined for a given required saccade size. There exist two fundamentally different views as to what information the PG uses to generate a saccade (Robinson, 1973; Zee et al., 1976). The first view is that the saccadic commands coming to the PG are coded in the distance by which the eye must be moved. The second view is that the saccadic commands are coded in the position in the orbit to which the eye must be brought.

The former view is illustrated in Figure 4.2. The PG does not have to know the initial and the final coordinates of the eye but rather it has to recognize only the difference between two points on the retina and then drives the eye with a high velocity by a pulse the area of which (pulse height times pulse duration) is equal to the retinal difference. This view is called a retinotopic organization because calculations are presumed to be made only in a retinal coordinate system.

The latter view is shown in Figure 4.3. Based on the coordinates of the eye position at the beginning of a saccade and the coordinate of eye position that is desired, the pulse generator (a negative feedback system) drives the eye with a high velocity until it reaches its goal. This is called a spatially organized system because the main signals are specified in a head-coordinate reference frame. The former hypothesis superficially appears to be simplest but only because it glosses over many of the details. It is inherent so far in most control systems models of saccadic eye movements (Young and Stark, 1963; Robinson, 1973).

However, we know that the brain makes saccades when there is no retinal error. For example, we make saccades in the dark to tactile and auditory stimuli without any retinal error. As another example, if a point source of

Figure 4.2

This figure shows the outline of the control scheme for retinotopic organization, in which the saccadic commands (neural pulses) are coded in distance (the difference between two points on the retina) by which the eye must be moved.

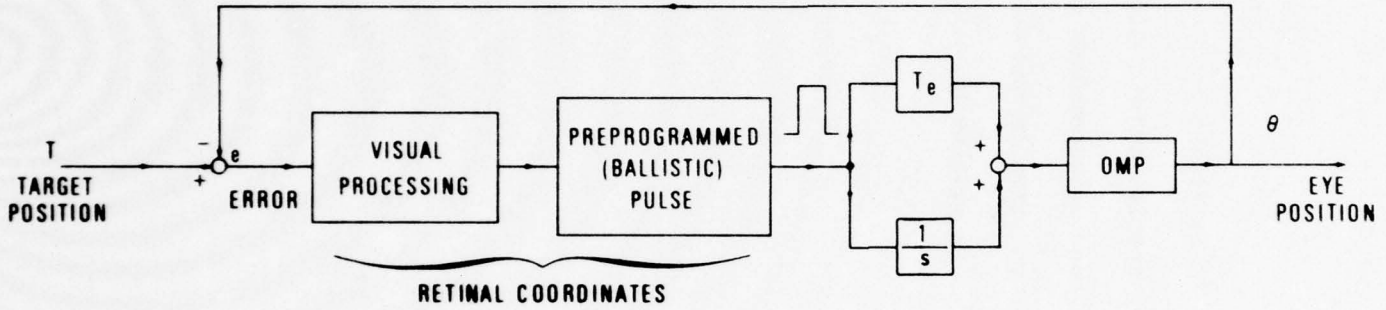

Figure 4.2 The Outline of the Control Scheme for Retinotopic Organization

Figure 4.3

This figure outlines the scheme for spatial organization, in which the saccadic commands are coded in the position in the orbit to which the eye must be brought.

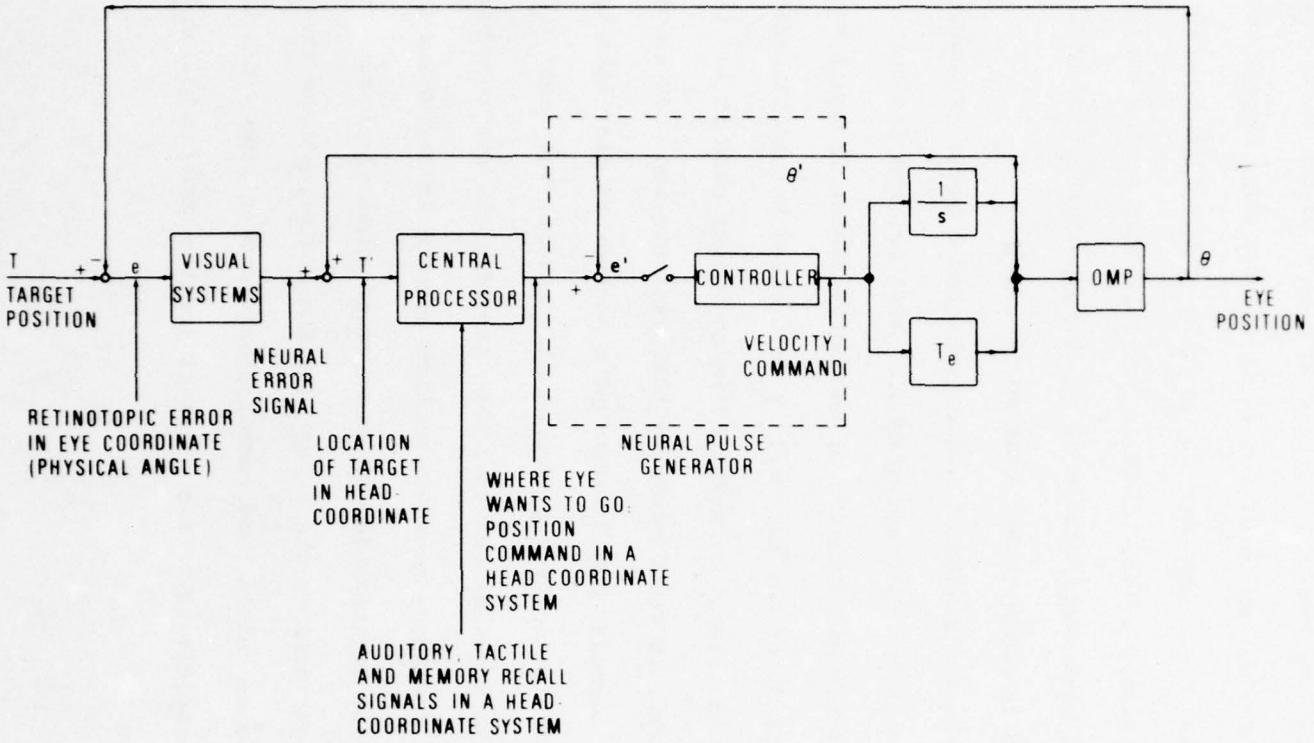

Figure 4.3 The Outline of the Control Scheme for Spatial Organization

light is briefly flashed on the fovea of an eye moving during a saccade, the subject, who has been told to track the target, makes another saccade back to the light source from the end point of the first saccade even though the retinal error was zero at the time of the flash (Hallet and Lightstone, 1976). This is possible only if the subject could know the position of the target at the time of the flash in space rather than on the retina.

In retinotopic organization, the saccade is assumed to be ballistic or preprogrammed. That is, the product of the amplitude and duration of the pulse (which is equal to the magnitude of the saccade) is determined before it begins and thus cannot be modified in midflight once it has started. However, it was discovered that patients who made abnormally slow saccades could interrupt a saccade in midflight to acquire a new target (Zee et al., 1976). This cast considerable doubt on the idea that saccades are preprogrammed.

For these reasons, we have adopted in our model the spatial organization of saccades in which the brain computes the position of the target (or the position where the eye wants to go) in head coordinates and then simply drives the eye rapidly towards the target (or its goal) until it gets there.

The brain could monitor the eye position in the head either by using an "efference copy" of the eye position derived from internally monitored commands to the OMN or by using direct afferent information from extraocular muscle spindles and other sensory receptors. Most studies (e.g., Skavenski et al., 1972) suggest efference copy is used to compute the location of seen objects in head coordinates. Thus, in our model, the eye position in head coordinates is obtained from the efference copy (θ' in Figure 4.1) for the purpose of saccadic pulse generation.

4.3 Control scheme for the pulse generator

We want a mode of control which drives the eye as rapidly as possible to the point where it wants to go from the point where it is now based on the knowledge of the coordinates of both points in the head-coordinate frame.

A classic mode of a control system which performs this kind of function is the bang-bang control system. We use a modified version of it to match the behavior of our cat as shown in Figure 4.4. It consists of a simple negative feedback system designed to drive error signal to a null. Its forward path contains a high-gain saturating amplifier. The reference input C(t) to the system is the target position or the point in space where the eye wants to go. The output of the amplifier is integrated by the NI whose output

Figure 4.4

This is a bang-bang control system with high-gain amplifier modified for our purpose from the standard form. The reference input C(t) is the target position. The control system drives the efference copy $\theta'(t)$ of the eye position to the target position C(t) by means of feedback control.

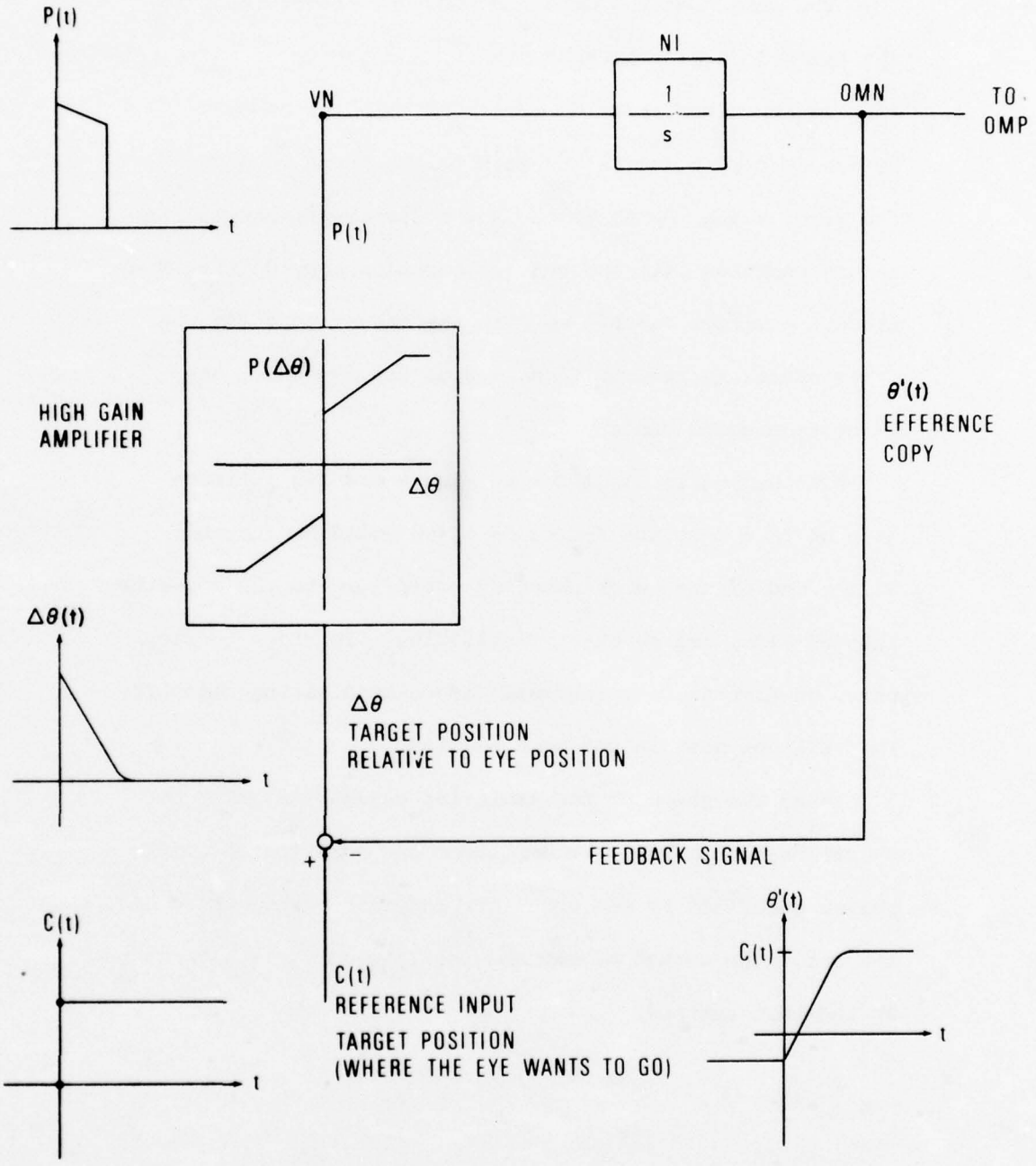

Figure 4.4 Modified Bang-Bang Control System

becomes the efference copy of the eye position. It follows that the output of the amplifier must be proportional to the eye velocity. For this reason, the output of the amplifier is sometimes referred to as the velocity command. The efference copy $\theta'(t)$ is fed back to the input to produce the error signal $\Delta\theta(t)$ which is the difference between the target position $C(t)$ and the eye position copy $\theta'(t)$. When the eye position catches up with the target position, the error signal is reduced to zero and, consequently, the velocity command vanishes.

The high-gain amplifier in Figure 4.4 has infinite gain at $\Delta\theta = 0$ so the system as shown would be unstable. At the end of one quick-phase it could jump to the opposite limb of $P(\Delta\theta)$ and so start oscillating. In order to stop this, we have to construct some associated gating circuitry. This will be done in the next section.

Also the shape of the amplifier curve $P(\Delta\theta)$ must be chosen in such a way that amplitude and duration of quick-phases generated by the model are compatible with those of the cat. The method of determining this curve is also given in the next section.

4.4 The description of the quick-phase generation mechanism

The proposed mechanism of quick-phase generation is shown in more detail in Figure 4.5. The trigger signal which initiates a quick-phase is called the "WHEN signal." The trigger signal is assumed to be discrete. The continuous signal which represents the target position C(t) where the eye should be driven is called the "WHERE signal."

Referring to Figure 4.5, a discrete WHEN signal actuates the OR-gate, thus closing the switch s_2 which starts the quick-phase. Once a quick-phase is initiated, a branch of the output P(t) of the amplifier is channeled back to the OR-gate so that, even after the WHEN signal (being a discrete trigger signal by assumption) disappears, the OR-gate is kept activated as long as the output of the amplifier persists at non-zero values. If, during a quick-phase, the efference copy $\theta'(t)$ matches the WHERE signal C(t), thus making $\Delta\theta = 0$, the output of the amplifier first becomes zero which in turn opens the switch s_2 by deactivating the OR-gate. This makes the QP timing autonomous. Once started, it runs its course to completion, independent of the WHEN signal.

The expanded view of the modified version of the high-gain amplifier as used in Figure 4.5 is shown in Figure 4.6. It has a built-in arrangement to prevent the oscillation which would otherwise be induced because in digital simulation the last increment of input reaching the origin from

Figure 4.5

This figure shows the outline of the quick-phase generation mechanism. A discrete WHEN signal closes the switch s_2 through the OR-gate. Once s_2 is closed, it remains closed by the output P(t) of the amplifier through the OR-gate until the efference copy $\theta'(t)$ of the eye position matches the WHERE signal C(t) which is the target position.

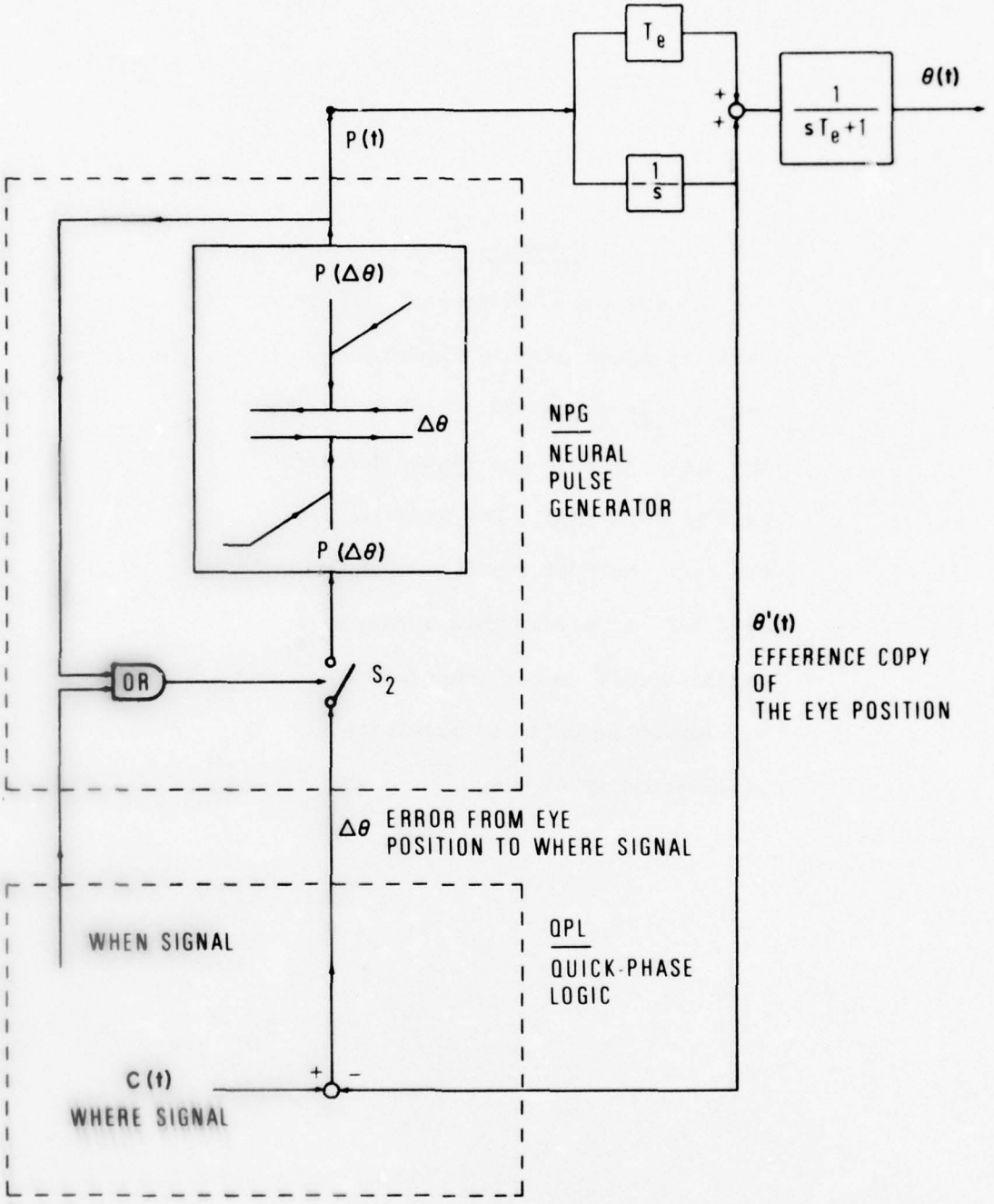

Figure 4.5 Outline of the Quick-Phase Generation Mechanism

Figure 4.6

This is the expanded view of the high-gain amplifier used in Figure 4.5. For positive $\Delta\theta$ [where $\Delta\theta = C(t) - \theta'(t)$], the upper half of the figure denoted by $P^+(\Delta\theta)$ is used. For negative $\Delta\theta$, the lower half of the figure denoted by $P^-(\Delta\theta)$ is used. This arrangement pertains only to our computer simulation in order to eliminate the oscillation at $\Delta\theta = 0$.

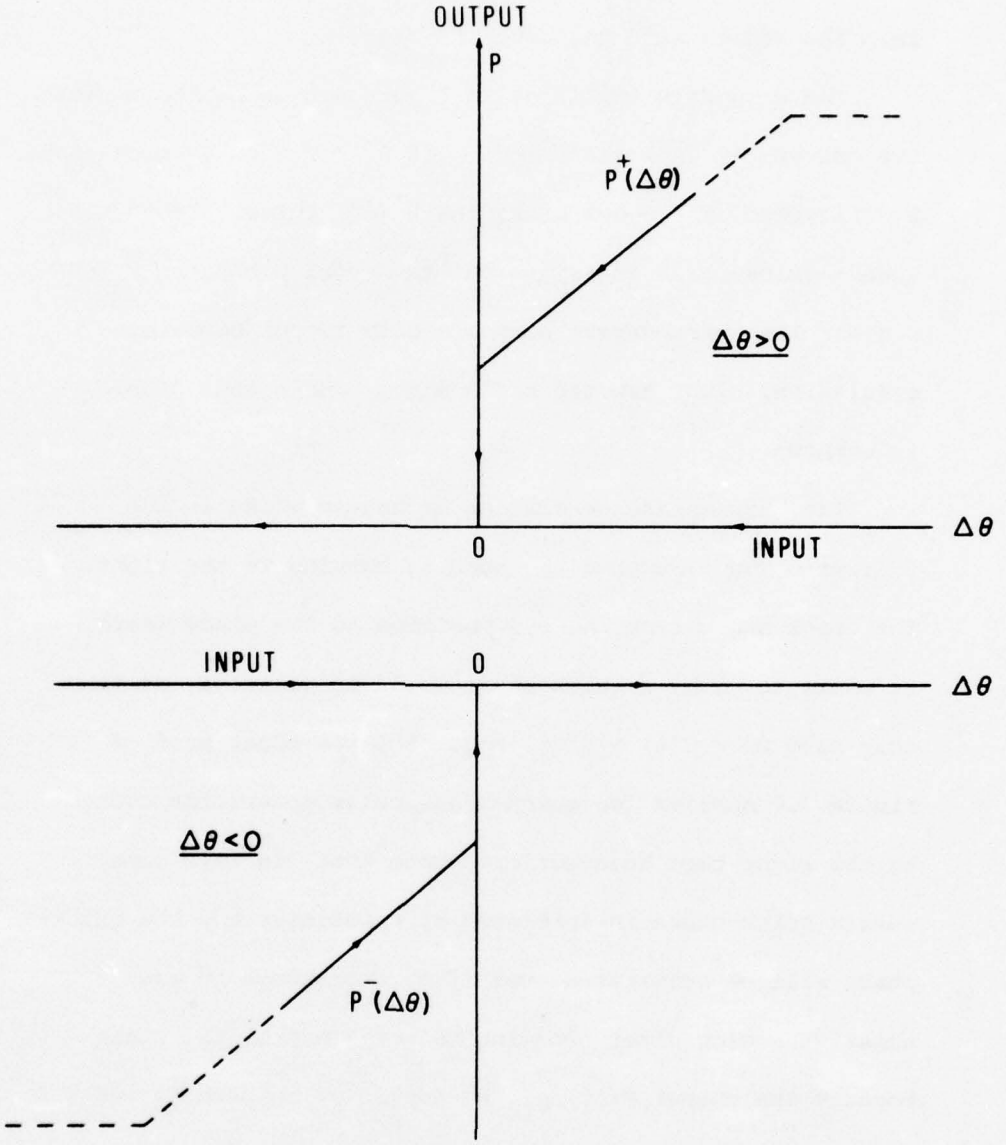

$\Delta\theta = C(t) - \theta'(t)$
THE ERROR ANGLE FROM THE EYE POSITION
TO THE WHERE CURVE

Figure 4.6 The High Gain Amplifier (used in Figure 4.5)

one side of the input axis generally overshoots slightly into the region with the opposite sign.

The high-gain amplifier in Figure 4.6 is broken up into two curves: $P^{+}(\Delta\theta)$ and $P^{-}(\Delta\theta)$. If $\Delta\theta > 0$ when a quick-phase is triggered, the model picks the $P^{+}(\Delta\theta)$ curve. If $\Delta\theta < 0$ when a quick-phase is triggered, the model picks the $P^{-}(\Delta\theta)$ curve. This arrangement pertains only to our computer simulation. Just how the brain might handle this problem is unknown.

The quick-phase generation mechanism works in the following way. Suppose the head is turning to the right. The error angle from the eye position to the place where it wants to go by a quick-phase would be positive, or in this case $\Delta\theta = C(t) - \theta'(t) > 0$. So, the upper half of Figure 4.6 applies for quick-phase pulse generation caused by the right turn head motion. Note that, in this case, once a quick-phase is initiated by a positive $\Delta\theta$, the quick-phase will be terminated even if $\Delta\theta$ overshoots to the negative region after crossing the origin from the right because the output $P(\Delta\theta)$ of the amplifier is zero for $\Delta\theta < 0$ in the upper half of Figure 4.6, thus preventing the oscillations. For the left turn head motion, the error angle is negative or $\Delta\theta < 0$. So, for the quick-phase pulse generation, the lower left half of Figure 4.6 is used in an

exactly opposite way from the case for that caused by the right turn head motion. The upper and lower halves correspond to two unidirectional pulse generators in each half of the pons.

The logic which determines the WHEN signals and the WHERE signals, that is, the timings and the amplitudes of quick-phase, is the central problem of this thesis and will be discussed in detail in the next chapter.

The next step is to determine the input-output relationship $P(\Delta\theta)$ of the amplifier in order to generate saccades with appropriate velocities for the cat. In general, $P(\Delta\theta)$ increases with $\Delta\theta$ to reflect the physiological observation that large saccades have a higher velocity than small saccades. Let the input to the amplifier be denoted by $\Delta\theta(t)$. Note that

$$\Delta\theta(t) = C(t) - \theta'(t) \qquad (4.4.1)$$

For the steady state response of the step input head velocity, $C(t)$ changes only slowly compared to the rapidity of quick-phases. Therefore, it follows that

$$\Delta\dot{\theta}(t) \simeq -\dot{\theta}'(t) \qquad (4.4.2)$$

Since $\dot{\theta}'(t)$ is the approximate input to the neural integrator, it must be approximately equal to the output $P(t)$ of the amplifier because during the quick-phase the only input to the neural integrator is the output from the amplifier. It follows that

$$P(\Delta\theta(t)) \simeq \dot{\theta}'(t) \simeq -\Delta\dot{\theta}(t) \qquad (4.4.3)$$

The actual curve $P(\Delta\theta)$ is smooth; that is, it has a continuous derivative (see Zee et al., 1976: Keller, 1974) but a straight line segment approximation is adequate. In fact, because this model is only concerned with QP's as events and is not concerned with great accuracy concerning intra-saccadic dynamics, we shall assume a simple linear relationship between the input and the output of the amplifier (shown in Figure 4.7 for $\Delta\theta > 0$) in the form of

$$P^{+}(\Delta\theta) = a\Delta\theta + b \text{ for } \Delta\theta > 0 \qquad (4.4.4)$$

and

$$P^{-}(\Delta\theta) = a\Delta\theta - b \text{ for } \Delta\theta < 0 \qquad (4.4.5)$$

Equation (4.4.4), using (4.4.3), may be expressed as

$$\Delta\dot{\theta}(t) = -a\Delta\theta(t) - b \qquad (4.4.6)$$

The solution of (4.4.6) is

$$\Delta\theta(t) = e^{-at}\Delta\theta(0) + \int_0^t e^{-a(t-\tau)}(-b)d\tau \qquad (4.4.7)$$

or

$$\Delta\theta(t) = e^{-at}\Delta\theta(0) - \frac{b}{a}(1 - e^{-at}) = e^{-at}\left(\Delta\theta(0) + \frac{b}{a}\right) - \frac{b}{a} \qquad (4.4.8)$$

We want to determine the value of a knowing $\Delta\theta(0)$ at the beginning $t = 0$ of the quick-phase, $\Delta\theta(t_Q)$ at the end $t = t_Q$ of the quick-phase and the intercept point b of $P^{+}(\Delta\theta)$ with the output axis in Figure 4.7. The lowest quick-phase

Figure 4.7

This is the model used to determine the equation for the bang-bang amplifier (for $\Delta\theta > 0$). The figure describes the case for right turn head motion in which $\Delta\theta > 0$. The problem is to determine the slope, a, and the intercept point b for the equation $P^{+}(\Delta\theta) = a\Delta\theta + b$ which describes the input-output relationship of the bang-bang amplifier.

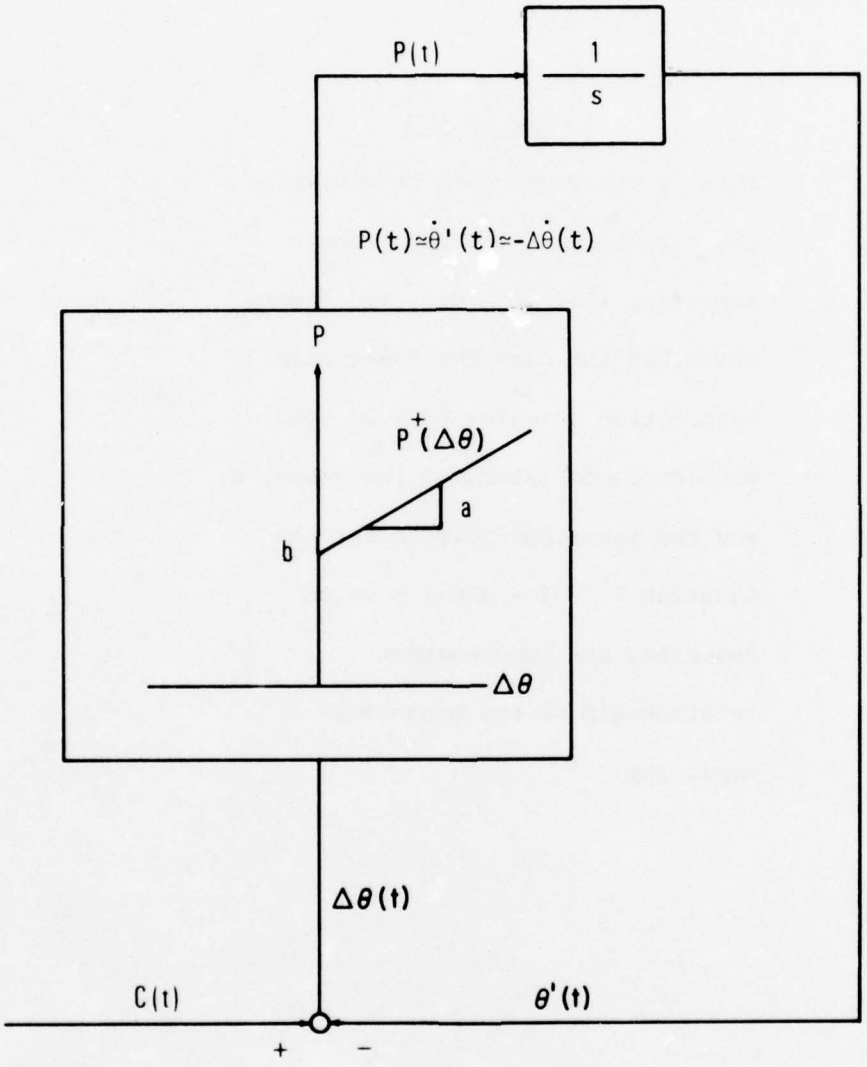

Figure 4.7 Model Used to Determine the Equation for the Bang-Bang Amplifier (for $\Delta\theta > 0$)

velocity $\dot{\theta}_Q$ from our cat is 40.5 deg/sec corresponding to the slow-phase velocity of 3.6 deg/sec. Thus, we chose the value of 40 for b. The largest mean quick-phase amplitude in this study (for the highest mean input head velocity of 60.6 deg/sec) is 13.5 deg with the mean quick-phase duration of 0.115 sec. The quick-phase duration of 0.115 sec for a 13.5 deg rapid eye movement also coincides with the results obtained on the cat's saccadic amplitude - duration relationship (an unpublished observation by D. A. Robinson).

Substituting $\Delta\theta(0) = 13.5$, $\Delta\theta(t) = \Delta\theta(t_Q) \simeq 0$, $t = t_Q = 0.115$ and $b = 40$ in (4.4.8), we have

$$0 = e^{-a(0.115)}(13.5 + \frac{40}{a}) - \frac{40}{a} \qquad (4.4.9)$$

Solving (4.4.10) for a (by trial and error) we obtain $a \simeq 16.2$. It follows from (4.4.4) and (4.4.5) that

$$P^+(\Delta\theta) = 16.2\ \Delta\theta + 40 \qquad (4.4.10)$$

and similarly for $P^-(\Delta\theta)$.

This model will now automatically generate cat saccades which have roughly the correct amplitude - duration and amplitude - velocity relationship for saccades of all sizes.

CHAPTER V

THE INTEGRATED MODEL OF THE SLOW-PHASE AND THE QUICK-PHASE

5.1 The outline of the integrated model

The first attempt to integrate the slow-phase and the quick-phase models is made simply by summing the output $\phi(t)$ of the SCC and the output $P(t)$ of the NPG as shown conceptually in Figure 5.1. This idea conforms with the observed modulation of saccade velocity during head movement in a study of monkey head-eye coordination (Morasso, et al., 1973). However, in those studies it is the case that for monkey $P(t) >> \phi(t)$.

But cat behaves differently. For our cat, which was typical, the quick-phase or saccade eye velocity for amplitudes of 13 deg is about 120 deg/sec compared with about 850 deg/sec for monkey (Fuchs and Luschei, 1970). The arrangement of Figure 5.1 would work so long as $P(t)$ is always much greater than $\phi(t)$. However, if $P(t)$ is near or less than $\phi(t)$ there is trouble. Suppose, for instance, $P(t) = 60$ deg/sec and $\phi(t) = 80$ deg/sec. The arrangement would not function properly because the eye would still be moving in the direction of the slow-phase instead of the quick-phase while the neural pulse was being generated by the NPG for a quick-phase. Thus, a proper quick-phase could not occur, contrary to fact. This raises a question as to

Figure 5.1

This figure depicts the hypothesis that SP and QP commands linearly summate. This hypothesis is rejected because it contradicts existing evidence and leads to contradictions when the output of the neural pulse generator is near or less than the output of the SCC.

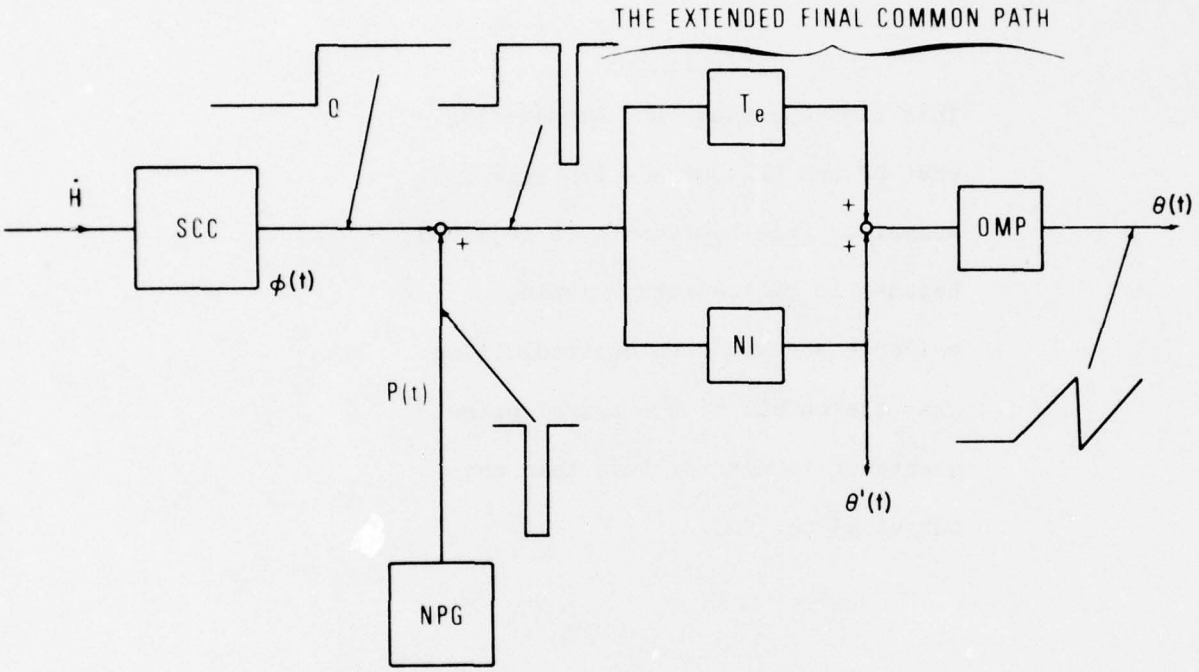

Figure 5.1 The Hypothesis that Integration of SP and QP Commands Linearly Summate. (To be rejected)

whether the output from the SCC should be suppressed from entering the extended final common path (Figure 5.1) during quick-phases.

For example as supporting evidence, many cells in the vestibular nucleus which fire with a rate proportional to head velocity (the $\phi(t)$ signal) pause during all quick-phases (Fuchs and Kimm, 1975). This is neural evidence that the vestibular signal is suppressed during quick-phases. Furthermore, a recent study (Jürgens and Becker 1975) indicates that the hypothesis of a linear addition of saccades and pursuit eye movements does not work. That is, the smooth pursuit signal did not appear to continue during a saccade and therefore, did not appear to be simply added or subtracted from the saccadic signal. Using these findings as supporting evidence for suppressing the slow-phase signal during quick-phases, our model implements this by introducing a switch s_1 at the output of the SCC as shown in Figure 5.2. s_1 is closed during slow-phases and open during quick-phases. With this arrangement the input to the extended final common path is the signal from the SCC only during slow-phases and the signal from the NPG only during quick-phases.

Incorporating Figure 5.2 with Figure 4.5, we obtain Figure 5.3 which represents the outline of the integrated model. The role of the AND-gate is to assure a reaction

Figure 5.2

This figure depicts the hypothesis that the canal signal is suppressed by quick-phases. The switch s_1 is closed for slow-phases and open for quick-phases thus making the output from the neural pulse generator the only input to the extended final common path during quick-phases. This arrangement is adopted in this study.

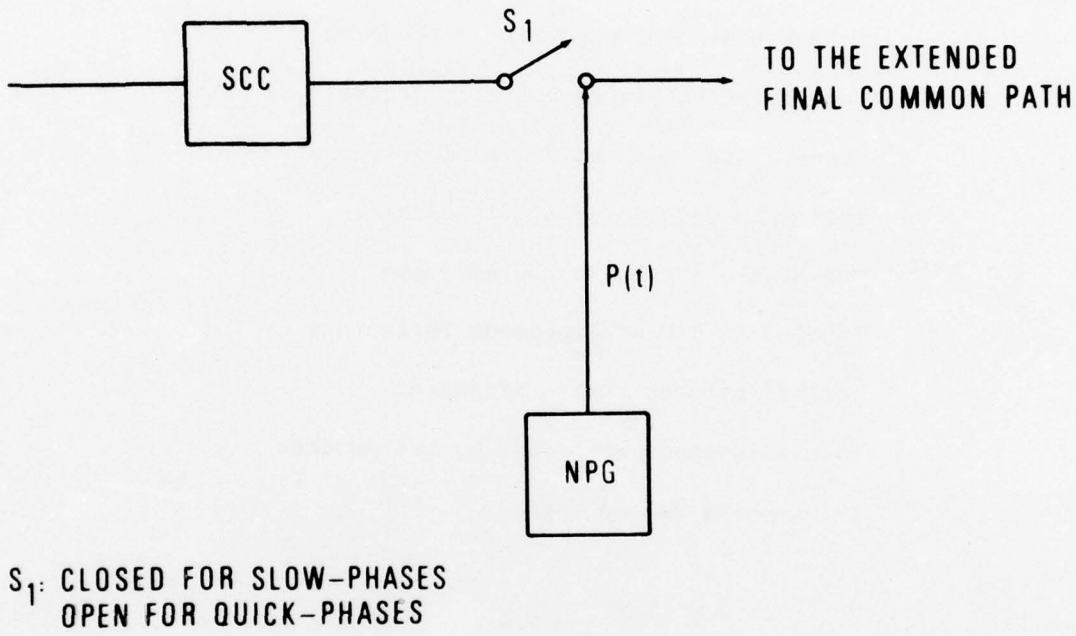

Figure 5.2 The Hypothesis that the Canal Signal is Suppressed by Quick-Phases. (This scheme is used in this study)

Figure 5.3

This figure shows the outline of the integrated model which is achieved by incorporating Figure 5.2 with Figure 4.5. Since s_1 is open and s_2 is closed, the system is undergoing a quick-phase. One of the inputs to the AND-gate labeled as "50 milliseconds refractory period" assures that a period of 50 milliseconds must pass before another quick-phase can be made.

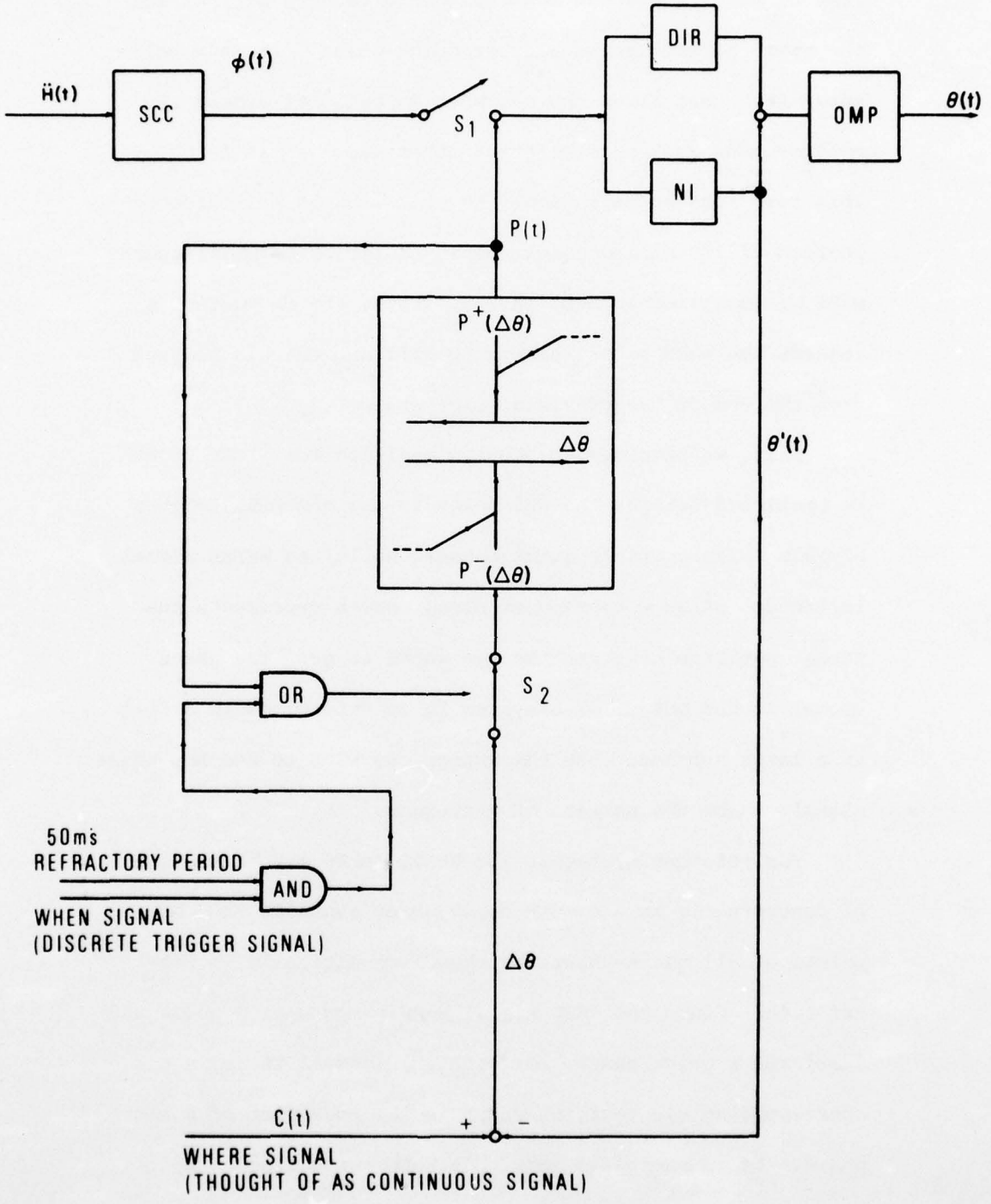

Figure 5.3 Outline of the Integrated Model (s_1 and s_2 in QP Mode)

time of 50 milliseconds (called the refractory period) for the brain before making another quick-phase. It is a well-known fact that after one saccade, a period of around 200 milliseconds must pass before another saccade can be made. This rule also seems to apply to QP's with 50 milliseconds instead of 200 milliseconds. This choice of 50 milliseconds will be justified in Section 7.4. Thus, the AND-gate disregards the WHEN signal unless 50 milliseconds has elapsed from the end of the previous quick-phase.

Next, we consider the WHEN signal and the WHERE signal. As mentioned before, the WHEN signals are discrete trigger signals which initiate quick-phases, while the WHERE signal is thought of as a continuous signal which represents the target position of where the eye wants to go. The WHERE signal is the output of a system to be determined in detail in a later section. For the moment, we want to see how these signals shape the pattern of nystagmus.

For rotatory nystagmus the WHERE curve may be thought of conceptually as a smooth curve which contains the end-points of all quick-phases as shown schematically in Figure 5.4A. Since the WHEN signal terminates a slow-phase and initiates a quick-phase, for each WHEN signal there is a corresponding eye position which is the end-point of a slow-phase. It is useful to imagine a WHEN curve also as a

Figure 5.4A

This figure shows a typical VOR response from our cat for step head input velocity of about 60 deg/sec. The WHEN signals and the WHERE signals are thought of as continuous curves that are sampled by the occurrence of a QP. The WHERE curve C(t) is divided into two parts: the deterministic part $\bar{C}(t)$, equal to the mean value of C(t), and noisy part n(t) with zero mean. Similar considerations apply for the WHEN curve.

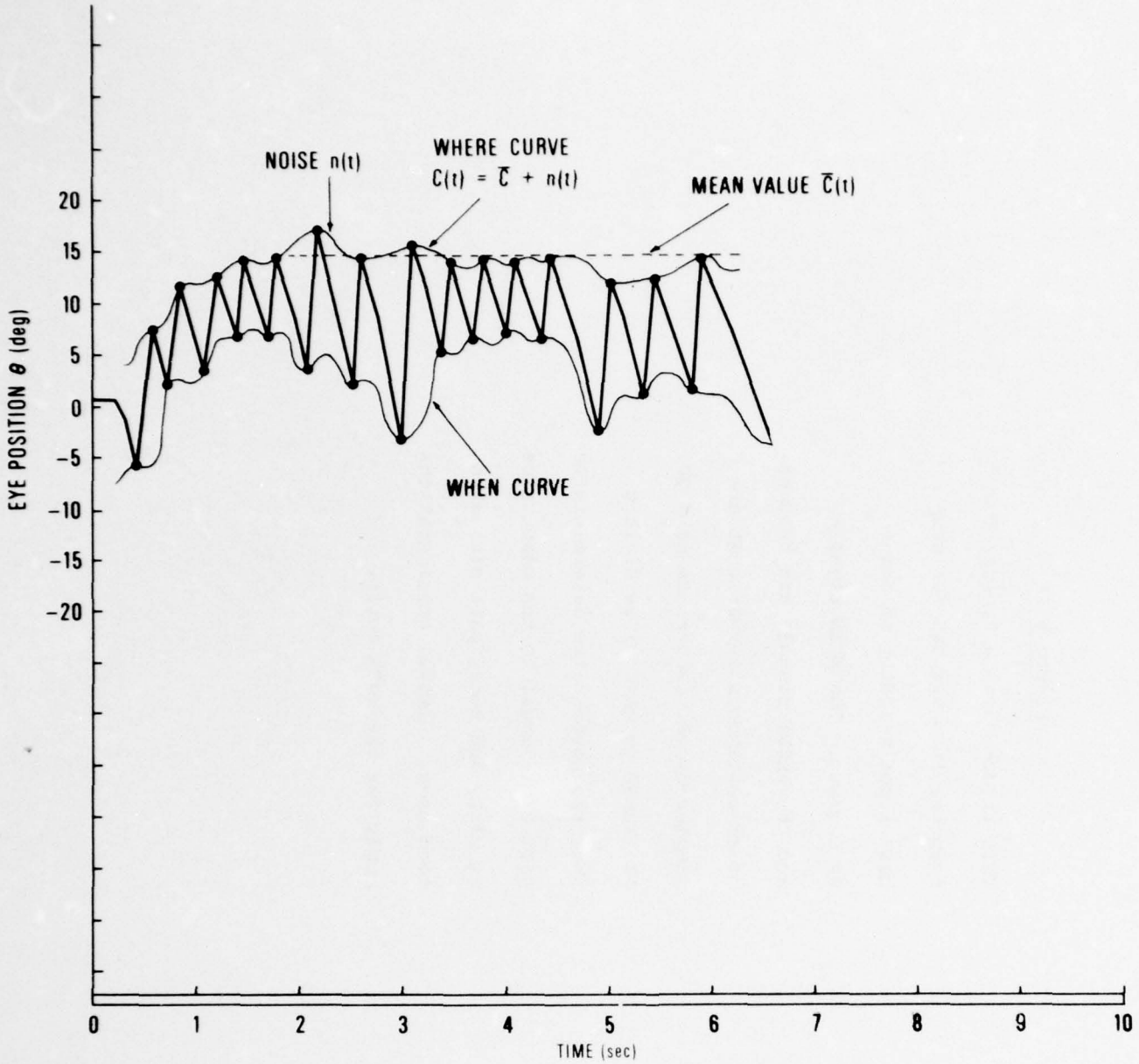

Figure 5.4A A Typical VOR Response from our Cat for $\dot{H} \simeq 60$ deg/sec

continuous signal. Whenever the eye reaches it, a quick-phase is triggered. Consequently, it contains the end-points of all the slow-phases as shown in Figure 5.4A. The WHEN signal is the output of another system to be determined in a later section. The typical appearances of the WHERE curve and the WHEN curve are similar to those shown in Figure 5.4A, which is a typical VOR response from our cat for the step head input velocity of about 60 deg/sec, the highest value we have used. Actual responses from our cat for this input velocity are shown in Figures 5.4B, 5.4C, 5.4D, 5.4E, and 5.4F.

The WHERE and WHEN curves are internal signals which cannot be observed as continuous signals. However, each time a quick-phase occurs, these signals are made explicit. Thus, experimentally we observe them as sampled signals indicated by the dots in Figure 5.4A.

These signals are obviously noisy. When head velocity is constant, however, nystagmus is more or less in a steady state. In this situation we can divide these signals into their mean value (deterministic part) and a noisy part which has zero mean value. Thus, the curve C(t) can be divided into

$$C(t) = \bar{C}(t) + n(t) \qquad (5.1.1)$$

where $\bar{C}(t)$ is the deterministic WHERE curve and n(t) is the noise, (Figure 5.4A). Similar considerations apply for the WHEN curve.

Figures: 5.4B, 5.4C, 5.4D, 5.4E and 5.4F

These figures show more VOR responses from our cat for step head input velocity of about 60 deg/sec. Figures 5.4B and 5.4E show the responses from left turn head motion, while Figures 5.4C, 5.4D, and 5.4F show the responses from right turn head motion. Note that variations in the QP end-points (WHERE the eye is going) are considerably less than the variations in the SP end-points (WHEN the QP is initiated).

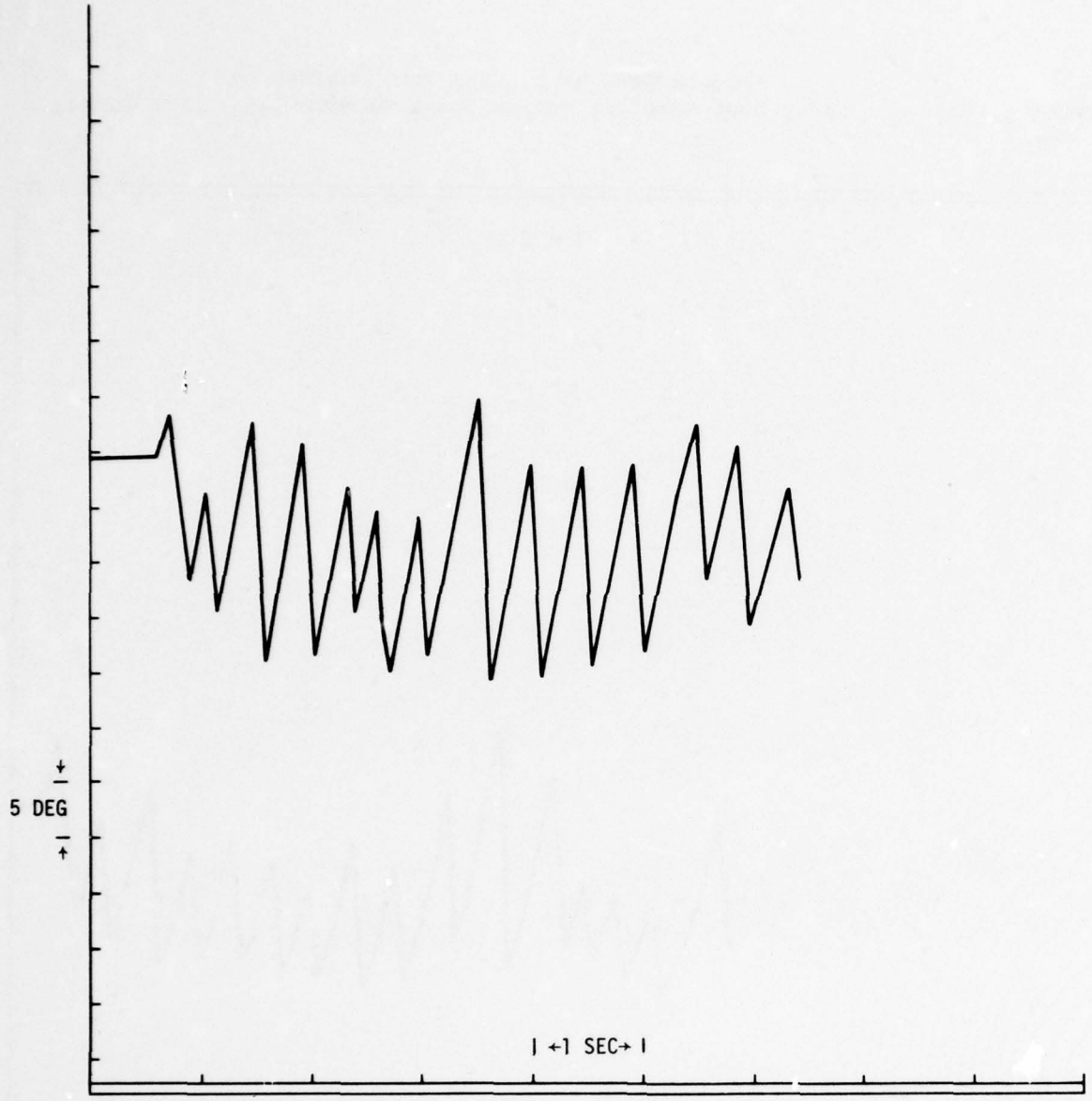

Figure 5.4B VOR Response from Our Cat for Step Head Input Velocity of About 60 deg/sec (for Left Turn Head Motion)

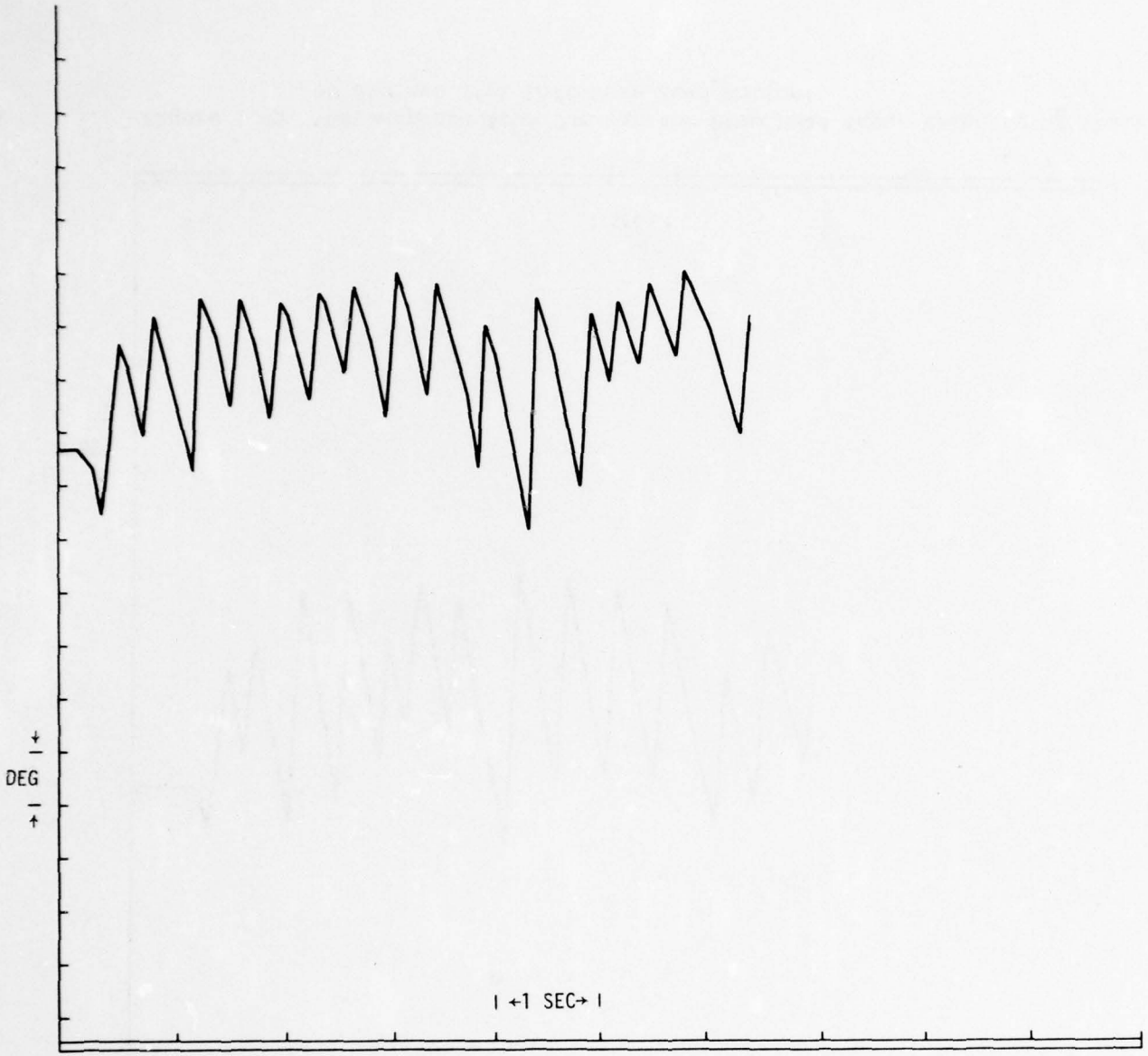

Figure 5.4C VOR Response from Our Cat for Step Head Input Velocity of About 60 deg/sec (for Right Turn Head Motion)

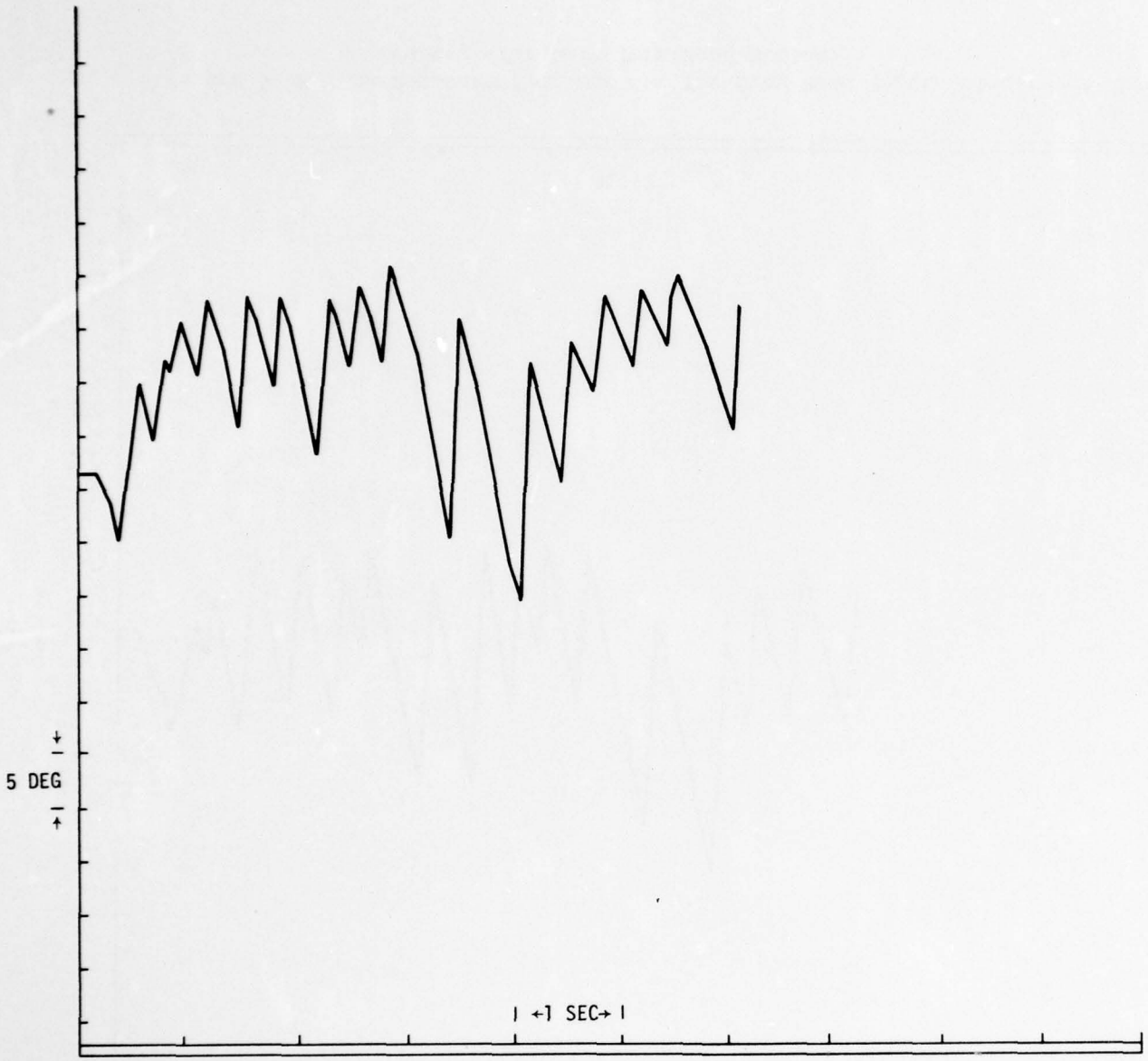

Figure 5.4D VOR Response from Our Cat for Step Head Input Velocity of About 60 deg/sec (for Right Turn Head Motion)

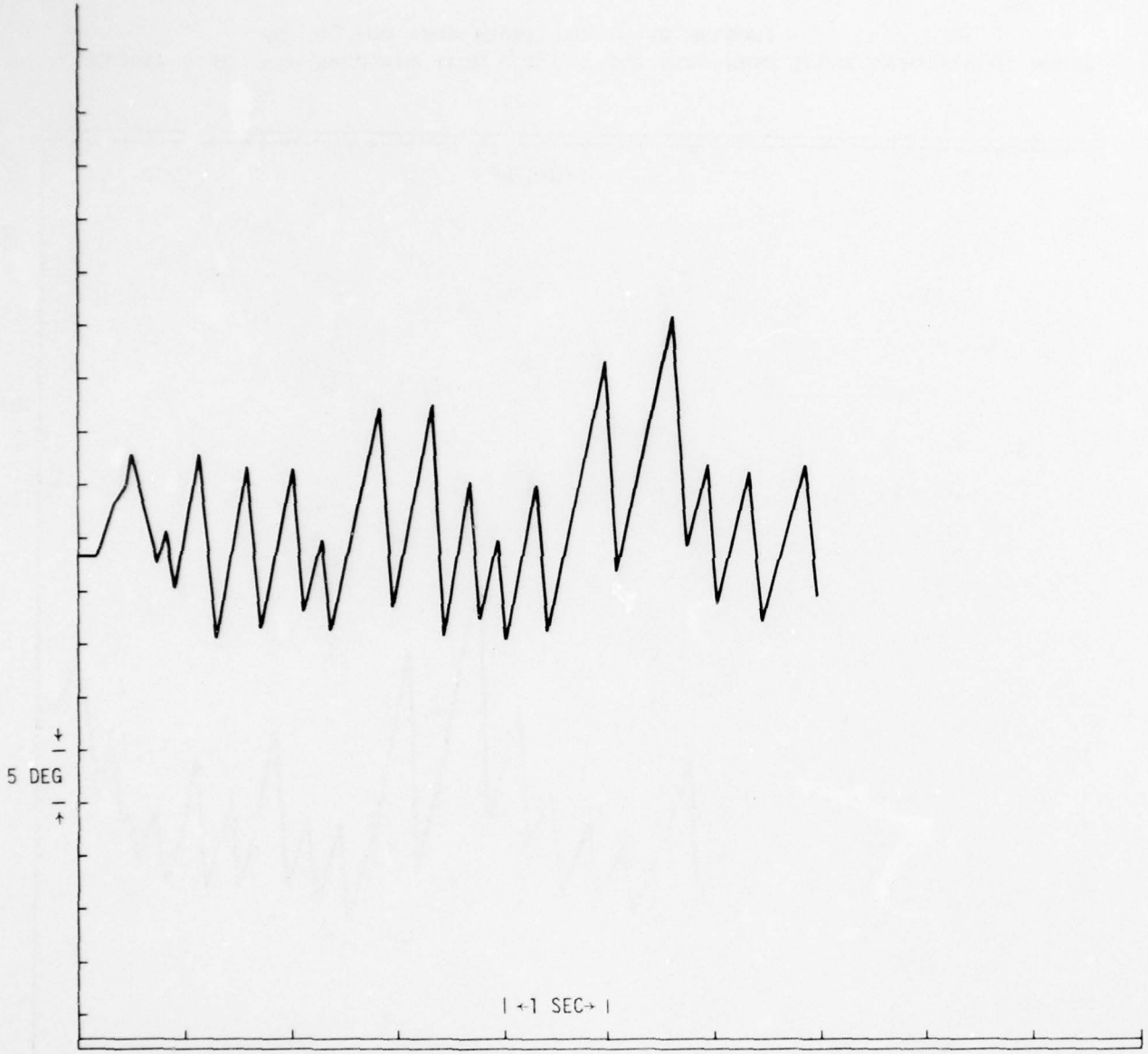

Figure 5.4E VOR Response from Our Cat for Step Head Input Velocity of About 60 deg/sec (for Left Turn Head Motion)

AD-A042 342 NAVAL SURFACE WEAPONS CENTER DAHLGREN LAB VA F/G 6/4
MATHEMATICAL MODEL OF THE VESTIBULOOCULAR REFLEX.(U)
JUN 77 K S CHUN
UNCLASSIFIED NSWC/DL-TR-3669 NL

2 OF 3
AD A042342

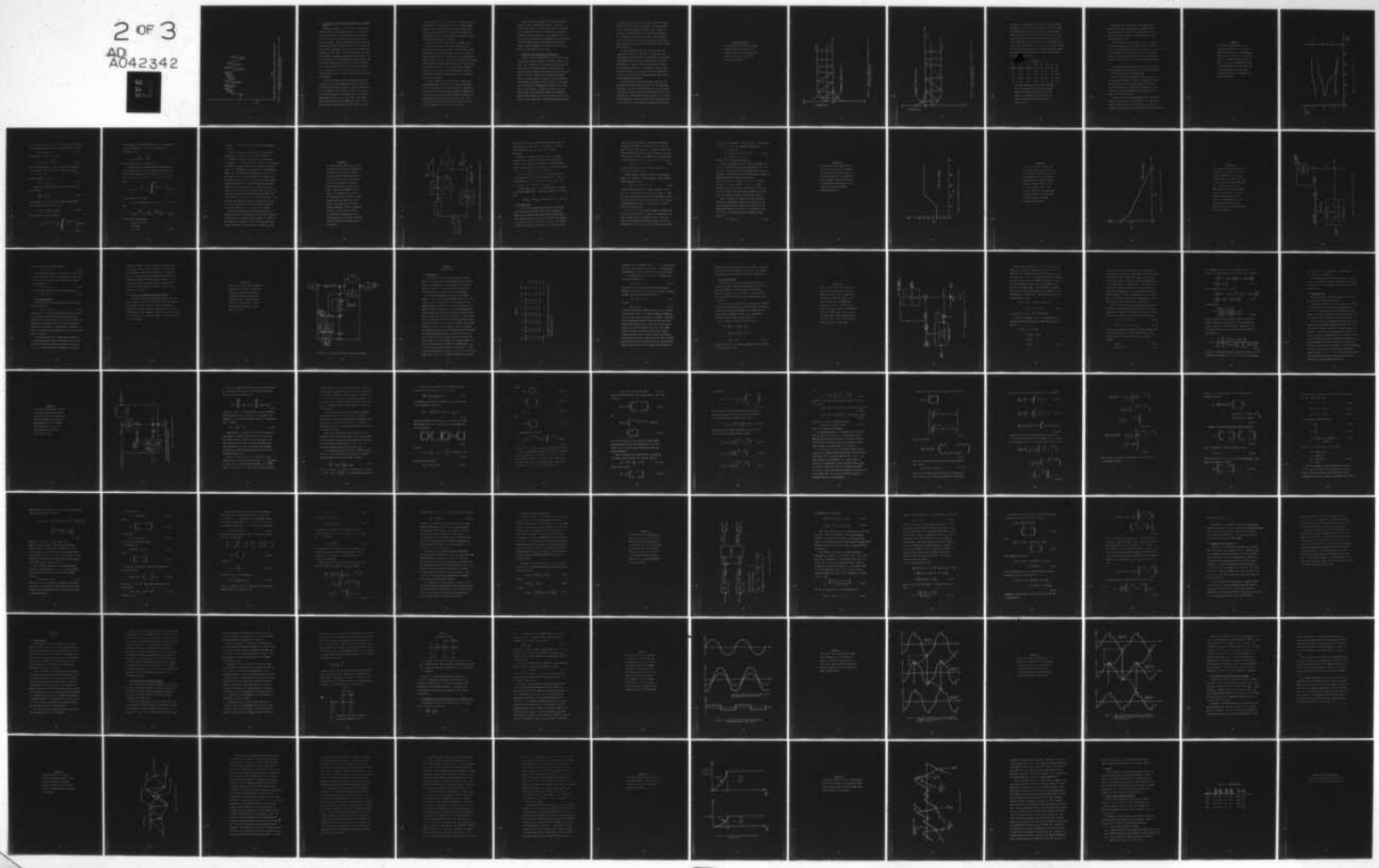

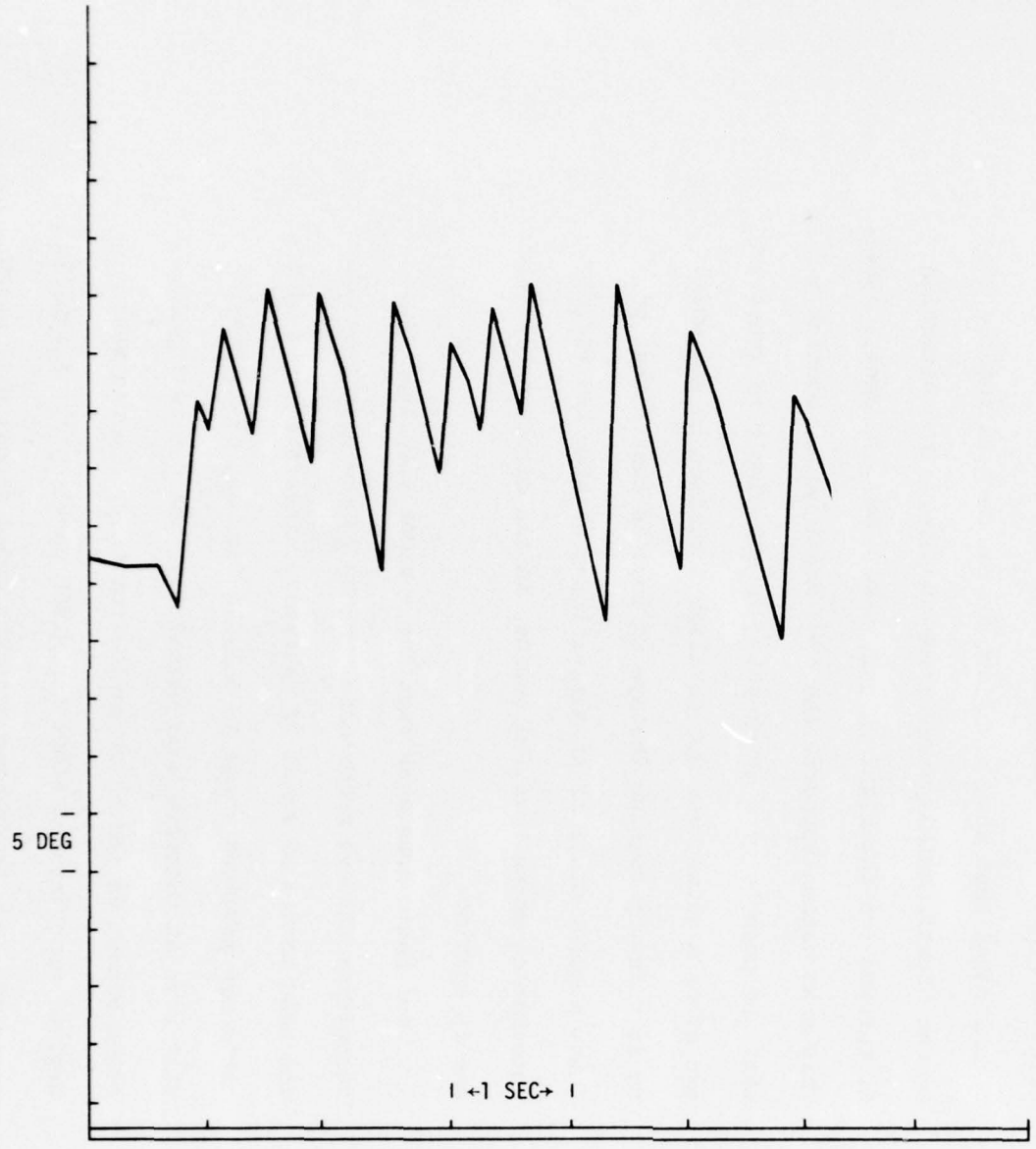

Figure 5.4F VOR Response from Our Cat for Step Head Input Velocity of About 60 deg/sec (for Right Turn Head Motion)

5.2 The contours of the deterministic WHEN curve and WHERE curve

Referring to Figure 5.4 in the last section, the most striking aspect of the nystagmus pattern is that the mean eye position of our cat at the conclusion of quick-phases in the steady state is shifted well into the direction of the head rotation. Earlier experiments with human subjects demonstrated that when a subject in the dark is rotated (say to the right), quick-phases drive the eye in the direction of turning (to the right in this case) (Melvill Jones, 1964). This observation supports the idea mentioned in section 4.1 that the purpose of a quick-phase is not simply to reset the eye after a slow-phase but to allow a subject to see where he is going by turning the eye to look in that direction. Thus, a quick-phase is an active thing seeking new visual information which lies, of course, in the direction in which one is turning.

Our cat's data show that for various step input head velocities the eye makes quick-phases in the direction of the head motion by about 12 degrees. Since the limit of the cat's eye movement range is only 20 degrees, it is clear that even at moderate head velocities, the cat is looking ahead almost as far as it can. From this, one can make several observations about the WHERE curve C(t). First, it obviously must be derived from the canal signal $\phi(t)$ since

in the dark that is the only signal which informs the brain that rotation is taking place. Second, it should promptly call for an eye position in the direction of turning and, finally, since the range of eye position is limited, one might expect an early saturation effect by which $\bar{C}(t)$ stops increasing as $\dot{H}$ continues to increase.

Thus, during each nystagmus beat, the WHERE curve is the "center of interest" or the place where the eye is purposefully driven by quick-phases. Once there, the slow-phase maintains the visual axis at that point in space in search of new information. This requires a certain minimum amount of time for visual processing (at least 50 milliseconds) but beyond that the gap between the position of the eye and the "center of interest" $C(t)$ is widening and eventually, probably by some sort of threshold phenomenon, the eye is released and is then quickly returned to $C(t)$ in search of new visual information.

As we can observe in Figure 5.4A, the steady state deterministic WHEN curve from our cat seems to be shifted by a constant amount Q in the direction of the slow-phase eye motion from the steady state deterministic WHERE curve in such a way that the deterministic WHEN curve appears to approximately coincide with the zero degree line. This suggests that the difference between $\theta(t)$ and $C(t)$ is the critical parameter which triggers a quick-phase.

Another observation supports the idea that the quick-phase is an active goal-seeking process. Even casual inspection of Figure 5.4 shows that the noise on the WHERE curve is about half of that on the WHEN curve (analysis of the data is given in Chapter 6). This suggests from the systems control viewpoint that the WHERE curve is considered to be more important than the WHEN curve and the system might be organized purposely to effect more control (less noise) over the former than the latter.

5.3 The model of the deterministic WHERE curve

A set of the VOR responses from our cat for step input head velocity of about 60 deg/sec is shown in Figures 5.4B, 5.4C, 5.4D, 5.4E and 5.4F. The head velocity of 60 deg/sec is selected for the model because the higher the input velocity the more frequent and uniformly spaced are the quick-phases. The step responses of the deterministic WHERE curves are drawn for best fits based on visual inspection. Unfortunately, the sampling rate is still not very high and one has difficulty in determining any details in the shape of any early transients. However, by running each test several times one can observe ensembles of responses and make a better estimate, but still the fitting process is all based on visual inspection. Idealized deterministic curves

are shown in Figure 5.5 for a right turn head motion and in Figure 5.6 for a left turn head motion. The step response of the deterministic WHERE curve $\bar{C}(t)$ seems to consist of two parts. The first part is the portion which appears to be a response of a first-order lag system (time constant, T_L) to a step input with steady state response magnitude f_0. The second part is the portion represented by a step function with magnitude g_0.

As already mentioned, we must use $\phi(t)$ as the input signal from which $C(t)$ is generated. In fact, since the compensatory slow-phase model is a second order linear system, the velocity signal and the position signal are the state variables of the system. We have already used the latter in the bang-bang controller. Consequently, the use of $\phi(t)$, the velocity signal, as the other input to the mechanism of the neural pulse generation seems appropriate simply from a system engineering viewpoint.

For each nominal intended head input velocity $\dot{H}_0$, the mean values of actual input head velocity $\dot{H}$, the slow-phase eye velocity $\dot{\theta}_s$, and the time constant T_L of the first-order lag system as well as f_0 and g_0 are determined from our cat's analogue data. The results are shown in Table 5.1. $\dot{H}$ is the actual head input velocity recorded in the VOR analogue data. $\dot{H}$ is not identical to $\dot{H}_0$ because the apparatus used for our

Figures 5.5 and 5.6

These figures show deterministic WHERE and WHEN curves for step input head velocity for the right turn head motion (Figure 5.5) and for the left turn head motion (Figure 5.6).

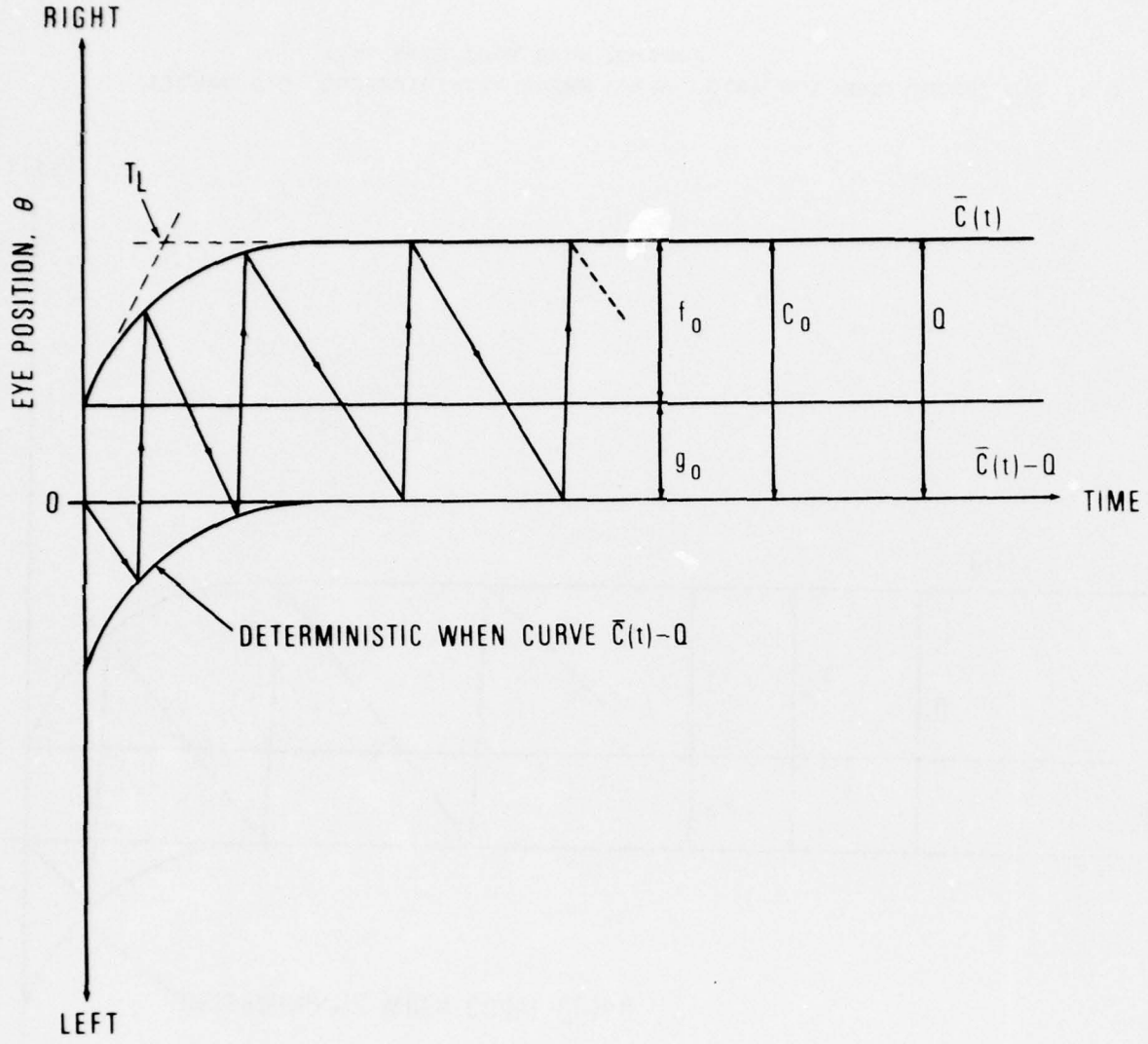

Figure 5.5 Deterministic WHERE Curve, $\bar{C}(t)$ and WHEN Curve, $\bar{C}(t) - Q$ (For Right Turn Head Motion)

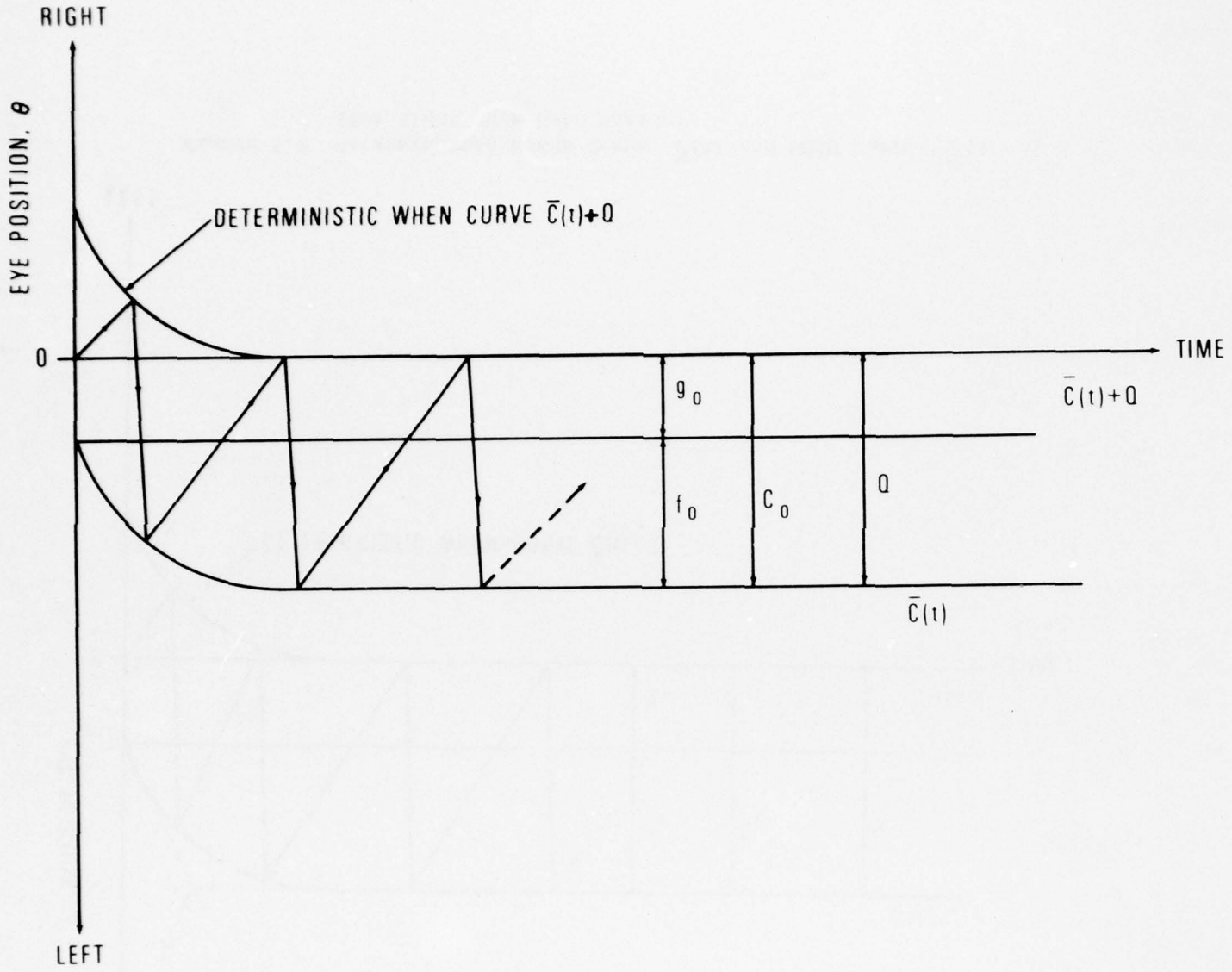

Figure 5.6 Deterministic WHERE Curve, $\bar{C}(t)$ and WHEN Curve, $\bar{C}(t) + Q$
(For Left Turn Head Motion)

experiment is a hand-operated instrument without a feedback arrangement. $\dot{\theta}_s$ is the mean slow-phase eye velocity in deg/sec obtained by dividing the mean of all slow-phase magnitudes of several runs for a given $\dot{H}$ by the mean of all slow-phase durations of the same several runs for the same $\dot{H}$. T_L is the time constant of the first-order system determined by visual inspection based on the fact that, in the step response of the first-order lag system, the initial slope line crosses the steady state response position one time constant later (as shown in Figure 5.5).

Table 5.1

$\dot{H}_0$	$\dot{H}$	$\dot{\theta}_s$	gain	g_0	f_0	C_0	T_L
deg/sec	deg/sec	deg/sec	($\dot{\theta}_s/\dot{H}$)	deg	deg	deg	sec
10	10.0	8.9	0.890	4.2	9.5	13.7	0.9
20	23.4	21.0	0.897	4.2	10.3	14.5	0.8
40	42.0	30.8	0.733	3.6	11.9	15.5	0.4
60	60.6	46.5	0.767	2.3	13.0	15.3	0.3

All values are mean values of about seven runs for each nominal head velocity with standard deviations ranging from 30% to 50% of their values. The symbols used in this table are defined and explained elsewhere in this section (5.3).

There were about seven runs for each nominal head velocity, with each run lasting about 6 seconds, which is about one half of the effective time constant T_c' for cat. The values listed in Table 5.1 have standard deviations ranging from 30% to 50%.

The values from our cat of f_0, g_0, $C_0 = f_0 + g_0$ and T_L are plotted in Figure 5.7 as a function of $\dot{\theta}_s$. Apparently, f_0 and g_0 reach constant saturation values above $\dot{\theta}_s \simeq 9$ deg/sec. The mean value of the gain $\dot{\theta}_s/\dot{H}$ is 0.82. This is somewhat smaller than the VOR reflex gain of 0.9 which is adopted in our model (see section 3.5) but is within the normal range for cat.

The values used in the model for f_0 and g_0 are picked in consideration of responses with step and sinusoidal inputs in both deterministic and stochastic modes.

Table 5.1 gives no information in the range of eye velocity below 8.9 deg/sec. Details in this range are left to a consideration of sinusoidal responses which contain such low velocities. To implement the decrease of T_L as $\dot{\theta}_s$ increases, we have incorporated a special scheme in our model to be discussed shortly.

Next, we derive the equation by which $\bar{C}(t)$ may be generated from $\phi(t)$ (which is proportional to $\dot{\theta}_s$). The deterministic WHERE curve $\bar{C}(t)$ may be viewed as the sum of two functions, one denoted by $f(t)$ which appears to be the response

Figure 5.7

This figure shows the plot of f_0, g_0, C_0, and T_L as functions of the slow-phase eye velocity $\dot{\theta}_s$. For the meanings of f_0, g_0, C_0, and T_L refer to Figures 5.5 and 5.6. Our model assumes that f_0, g_0, and $C_0 = f_0 + g_0$ are constants, while T_L, the time constant of the first-order lag system, decreases as the input head velocity and, hence, the slow-phase eye velocity increases.

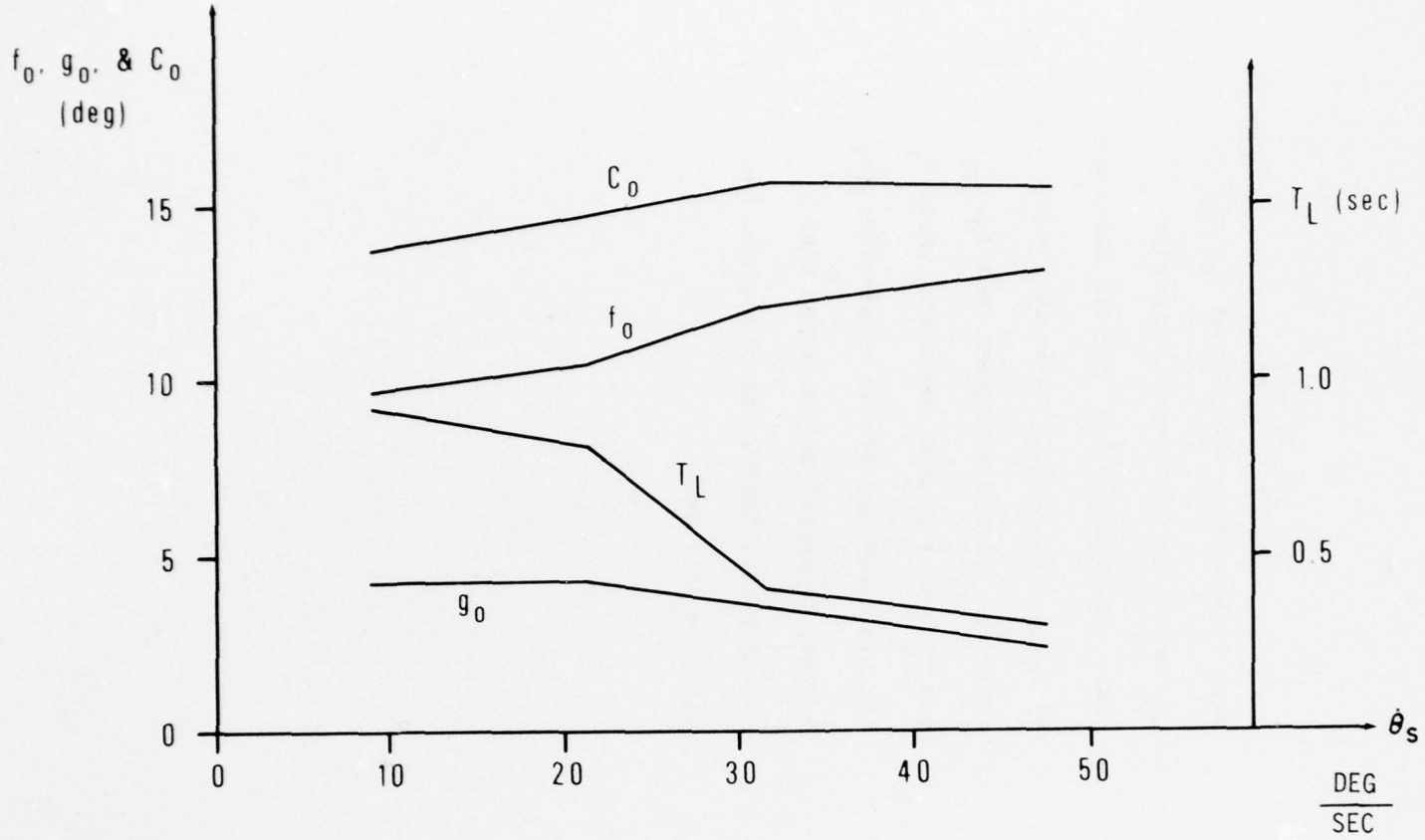

Figure 5.7 Plot of f_0, g_0, C_0, and T_L vs $\dot{\theta}_s$

of a first-order system to a step input, and the other denoted by g(t) which may be considered as a step function. That is,

$$\bar{C}(t) = f(t) + g(t) \tag{5.3.1}$$

From Figure 5.5, f(t) is in the form

$$f(t) = f_0\left(1 - e^{-\frac{t}{T_L}}\right) \tag{5.3.2}$$

with the time constant T_L (which we assume to be constant for the moment). Then, g(t) has a constant value g_0 or

$$g(t) = g_0 \tag{5.3.3}$$

We note that for $t >> T_L$

$$\bar{C}(t) \simeq f_0 + g_0 = C_0 \tag{5.3.4}$$

Thus, the transfer function between f(t) and $\phi(t)$ is in the form of

$$\frac{f(s)}{\phi(s)} = \frac{G}{sT_L + 1} \tag{5.3.5}$$

with the gain G. The differential equation corresponding to 5.3.5 with zero initial condition is

$$\dot{f}(t) = -\frac{1}{T_L} f(t) + \frac{G}{T_L} \phi(t) \tag{5.3.6}$$

The solution of (5.3.6) is given by

$$f(t) = e^{-\frac{1}{T_L}(t - t_0)} f(t_0) + \int_{t_0}^{t} e^{-\frac{1}{T_L}(t - \tau)} \frac{G}{T_L} \phi(\tau) d\tau \tag{5.3.7}$$

If we assume for a step response that $\phi(\tau)$ is approximately a constant denoted by ϕ, then (5.3.7) reduces, with $t_0 = 0$ and $f(t_0) = 0$, to

$$f(t) = G\phi\left(1 - e^{-\frac{t}{T_L}}\right) \tag{5.3.8}$$

which is the same as (5.3.2) with $G\phi = f_0$.

For the purpose of further analysis and computer simulation we want to put this into a time discrete form. Consider periodic sampling every T seconds or at $t = kT$ for $k = 0, 1, 2, \ldots,$. In (5.3.7), let $t = (k+1)T$ and $t_0 = kT$ Then,

$$f[(k+1)T] = e^{-\frac{1}{T_L}T} f(kT) + \int_{kT}^{(k+1)T} e^{-\frac{1}{T_L}[(k+1)T-\tau]} \frac{G}{T_L}\phi(\tau)d\tau \tag{5.3.9}$$

If we assume in (5.3.9) that

$$\phi(\tau) \simeq \phi(kT) \text{ for } kT \leq \tau < (k+1)\tau \tag{5.3.10}$$

Then

$$f_{k+1} = e^{-\frac{1}{T_L}T} f_k + G\left(1 - e^{-\frac{1}{T_L}T}\right)\phi_k \tag{5.3.11}$$

in which, for simplification

$$\begin{aligned} f_{k+1} &= f[(k+1)T] \\ f_k &= f(kT) \\ \phi_k &= \phi(kT) \end{aligned} \tag{5.3.12}$$

are used. (5.3.11) is the discrete equation corresponding to (5.3.7).

Now it is necessary to deal with this system's non-linearities. First, f_0 reaches a saturation value at $\phi \simeq 9$ deg/sec. Second, T_L decreases as ϕ increases from 0.9 seconds at $\phi \simeq 9$ deg/sec to 0.3 seconds at $\phi \simeq 46.5$ deg/sec. To model these characteristics, the arrangement as shown in Figure 5.8 is adopted for the generation of the deterministic WHERE curve. The upper channel corresponds to 5.3.11 if the non-linear limiter is short-circuited. The limiter clips the output f_{k+1} at $\pm f'(f' > 0)$ if the input to the limiter exceeds the bounds $\pm f'$. A possible danger with the type of system in which a first-order lag is simply followed by a limiter is that some internal variable such as f_k in (5.3.11) should not be allowed to become large compared with f' for then, when input ϕ and, hence, $G\phi$ suddenly drops back to zero, the system will momentarily hang-up in saturation until f_k has time to drop below f' due to the effect corresponding to the first term of (5.3.7), unless properly handled.

Thus, system dynamics must be removed when it is in saturation and this is guaranteed by the location of the non-linearity within the feedback loop in Figure 5.8. Thus, if the system is in saturation (for $\phi > 0$) but $G\phi_k$ falls back within the bounds $\pm f'$ of the limiter, the output f_{k+1} also

Figure 5.8

This figure shows a mathematical scheme to generate the deterministic WHERE curve. The upper branch creates the portion of the deterministic WHERE curve which is the output of the first-order system to a step head velocity. The lower branch creates the step portion of the curve. With this arrangement, if the output is in saturation ($\pm f'$), and if the input falls in such a way as to make $G\phi_k$ fall within the bounds $\pm f'$ of the limiter, the output f_{k+1} also starts falling immediately. This is illustrated at point a. Also with this scheme, the effective time constant T_L of the system decreases as the input ϕ increases, due to the increasing clipping action of the limiter.

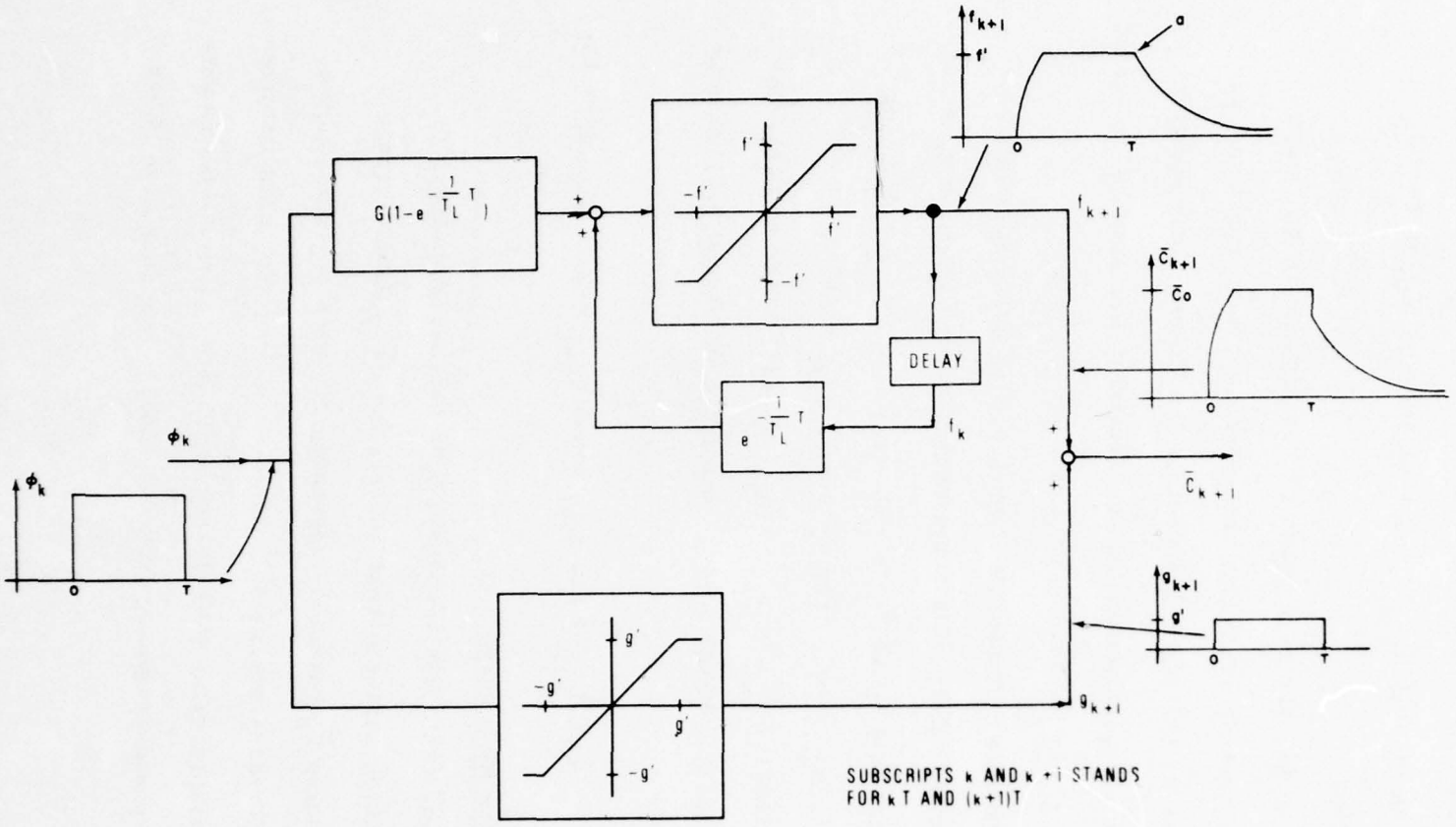

Figure 5.8 The Model for Generation of the Deterministic WHERE Curve

starts to fall at once. This follows from the fact that, if one assumes in (5.3.11) that $f_k = f'$ and $G\phi_k < f'$, then it can be shown that $f_{k+1} < f'$, that is, the output is decreasing.

However, the main point of the limiter in the upper channel is that it causes the effective "time constant" to decrease as the input ϕ increases due to the increasingly earlier clipping action of the limiter. For reasons discussed later, $f' = f_0 = 11$ deg is chosen tentatively.

The lower channel of Figure 5.8 is self-explanatory, consisting solely of a non-linear limiter with $g' = g_0 = 1.0$ corresponding to (5.3.3). For $|\phi_k| < g'$, $g_{k+1} = \phi_k$. For $\phi_k \geq g'$, $g_{k+1} = g'$. For $\phi_k \leq -g'$, $g_{k+1} = -g'$.

Finally, $\bar{C}_{k+1} = f_{k+1} + g_{k+1}$ is equivalent to $\bar{C}(t)$, the deterministic WHERE curve. Referring to Figure 5.8, we note that

$$\max \bar{C}_{k+1} = \max f_{k+1} + \max g_{k+1} = f' + g' \qquad (5.3.13)$$

5.4 The WHEN curve

Our cat's VOR responses from various step input head velocities indicate that the steady state deterministic WHEN curve $\bar{D}_0$ coincides approximately with the zero degree line (Primary position). For $\dot{\theta}_s > 30$ deg/sec, this requires a threshold value Q of 12 deg which also gives an acceptable quick-phase frequency from the model. Our data also shows

that at $\dot{\theta}_s \simeq 10$ we need $Q \simeq 6$ to match the quick-phase frequency of our model with that of our cat. Since we want $\bar{D}_0$ for the step input of $\phi \simeq 10$ (with ϕ being the SCC output signal) to coincide with the zero degree line, the magnitude of the steady state WHERE curve $\bar{C}_0$ must be equal to six, that is $|\bar{C}_0| = Q = 6$. Since $\bar{C}_0 = G\phi + g$, we set

$$G|\phi| + 1 = 10G + 1 = 6 \qquad (5.4.1)$$

in which G is the gain of the transfer function 5.3.5. From 5.4.1, we obtain G = 0.5.

Next, we want to find $|\phi|$ at which the deterministic WHERE curve saturates. For this purpose, since ϕ would be greater than one, we set

$$G|\phi| + 1 = 0.5|\phi| + 1 = 12 \qquad (5.4.2)$$

from which we obtain $|\phi| = 22$. Thus, we make $Q = 12$ for $|\phi| \geq 22$. For $10 < |\phi| \leq 22$, we set $Q = 0.5|\phi| + 1$. This will make the line $\bar{D}_0$ coincide with the zero degree line for any step input head velocity which results in $|\phi| \geq 10$ with the understanding that $|\phi| \simeq |\dot{\theta}_s|$ because $\dot{\theta}_s = 0.9\phi$ as a result of the reflex gain.

For $0 < |\phi| < 10$, we do not have data to determine the value of Q for this region. However, the simulation of our model indicates that a constant value of $Q = 6$ for this region yields acceptable sinusoidal response for the test frequencies of 0.05, 0.25, and 1.2 Hz, with peak velocities

of 10, 20, and 30 deg/sec. For this reason, we have adopted $Q = 6$ for $0 < \phi < 10$. The summary is given below:

$$Q = 12 \text{ for } |\phi| > 22$$

$$Q = 0.5|\phi| + 1 \text{ for } 22 \geq |\phi| > 10 \qquad (5.4.3)$$

$$Q = 6 \text{ for } 10 \geq |\phi| > 0$$

Equation 5.4.3 is plotted in Figure 5.9.

If Q given by Equation 5.4.3 is used in the model, $\bar{D}_0$ for $|\phi| > 10$ would coincide with the zero degree line. For $10 \geq |\phi| > 0$, $\bar{D}_0$ would shift in the compensatory direction (opposite to the direction of the head motion) by the amounts explained below (for left turn head motion).

For $1 \geq |\phi| > 0$, $\bar{D}_0 = -(0.5|\phi| + |\phi|) + 6 = 6 - 1.5|\phi|$.

For $10 \geq \phi > 1$, $\bar{D}_0 = -(0.5|\phi| + 1) + 6 = 5 - 0.5|\phi|$.

The plot of $\bar{D}_0$ vs $|\phi|$ is given in Figure 5.10. Note that $\bar{D}_0$ is the "steady state" deterministic WHEN curve for step input head velocity, which is a constant for given $|\phi|$.

Next, we consider the condition for the quick-phase initiation. Referring to Figure 5.6 (in section 5.3) for left turn step input head velocity, the equation for the deterministic WHEN curve is $\bar{C}(t) + Q$. The efference copy $\theta'(t)$ of the eye position during the slow-phase always satisfies

$$\theta'(t) < \bar{C}(t) + Q \qquad (5.4.4)$$

Figure 5.9

This plot shows the threshold value Q in degrees as a function of the magnitude $|\phi|$ of the SCC output signal. ϕ has units of deg/sec. The dependence of Q on stimulus intensity yields not only acceptable QP frequencies in step responses, but also reasonable sinusoidal responses.

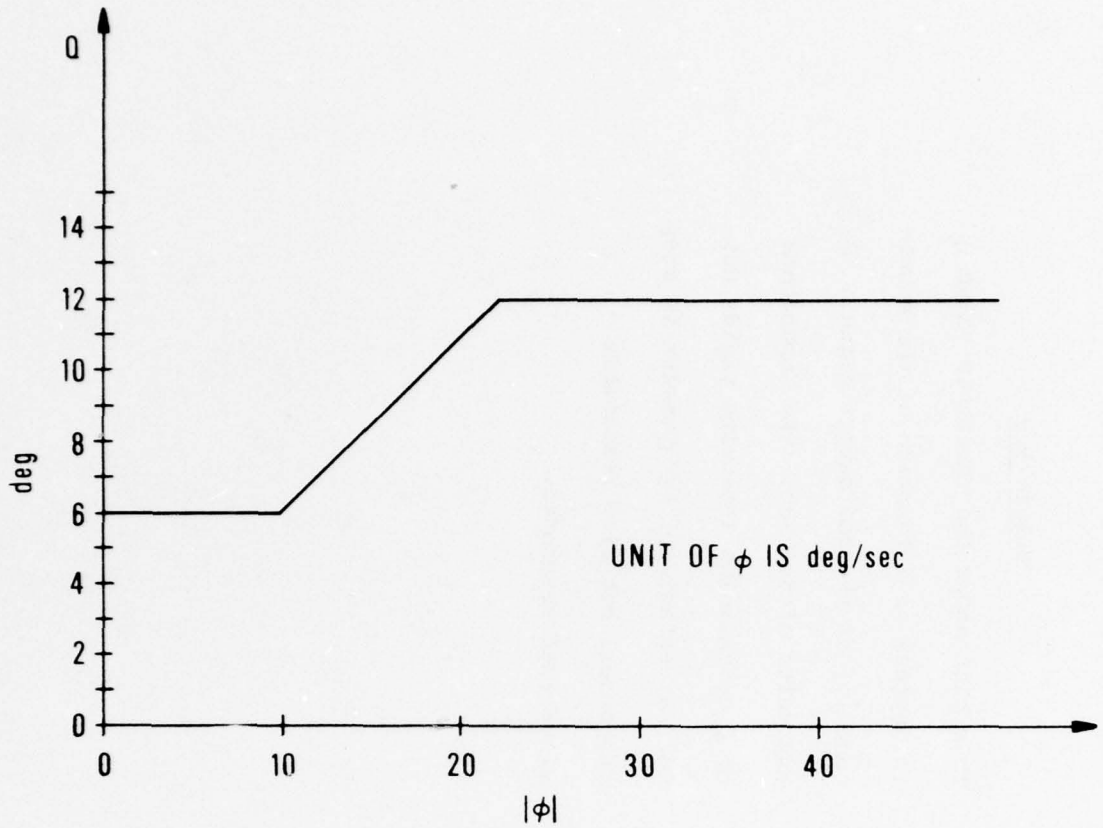

Figure 5.9 The Threshold Vaue Q vs the SCC Signal ϕ

Figure 5.10

This plot shows (for left turn head motion) the steady state value $\bar{D}_0$ of the deterministic WHEN curve (for step input head velocity) as a function of the magnitude $|\phi|$ of the SCC output signal. It shows that $\bar{D}_0 = 0$ for $|\phi| > 10$. However, for $0 < |\phi| < 10$, $\bar{D}_0$ is shifted to the compensatory direction (opposite to the direction of head motion) by the amount indicated in the figure.

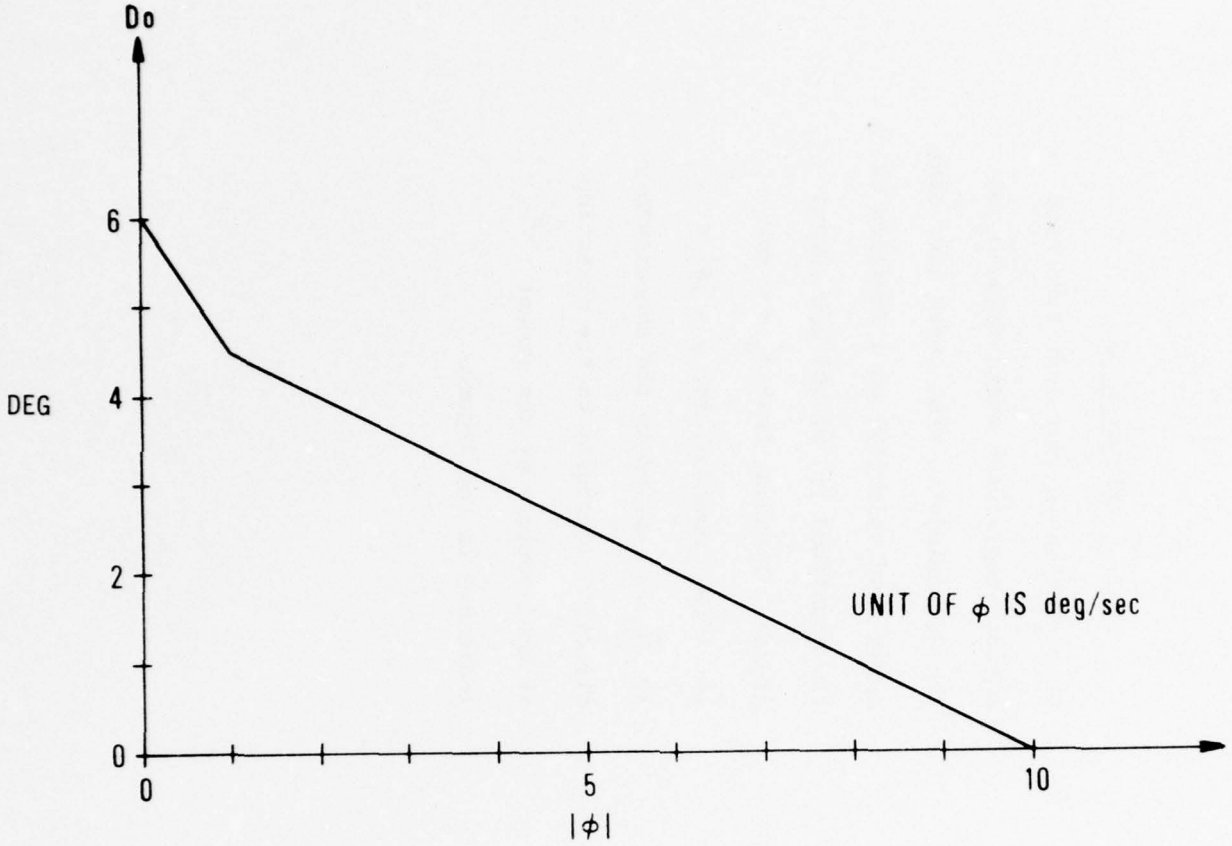

Figure 5.10 $\bar{D}_0$ vs $|\phi|$ for Step Input Head Velocity

Figure 5.11

This figure shows the threshold device as used for the generation of quick-phases. Whenever $\Delta\theta$, which is the distance from the efference copy $\theta'(t)$ of the eye position to the WHERE curve $C(t)$, exceeds the thresholds $\pm Q$, a WHEN signal is generated and intiates a process (if it meets the 50 milli-seconds refractroy period) which results in a generation of a quick-phase as explained in the text. The value of Q is determined according to 5.4.3 and Figure 5.9.

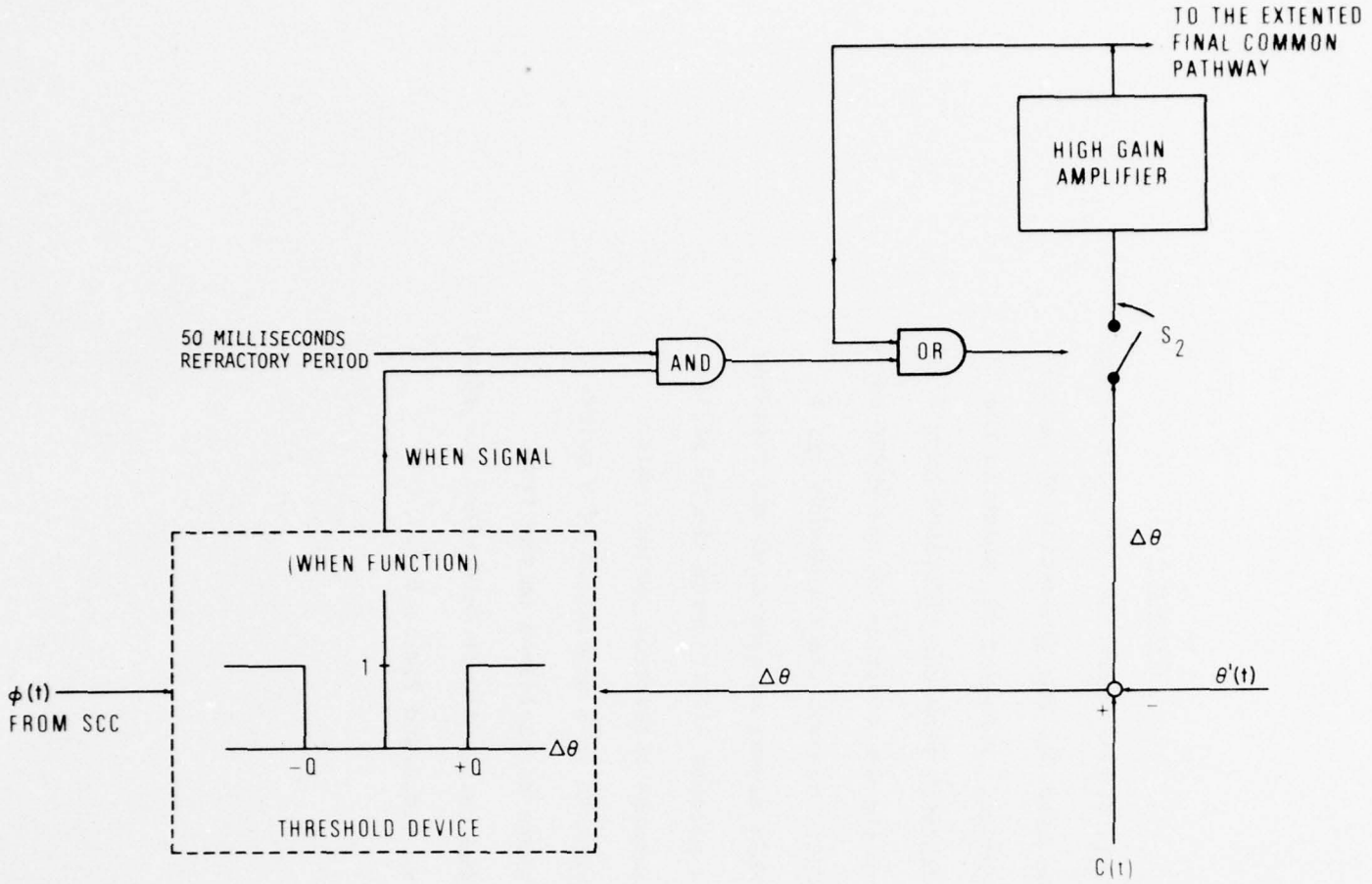

Figure 5.11 The Threshold Device for Quick-Phases

Thus a quick-phase is initiated whenever

$$\theta'(t) \geq \bar{C}(t) + Q \tag{5.4.5}$$

Now, referring to Figure 5.5 (in section 5.3) for right turn step head input velocity, the deterministic WHEN curve is $\bar{C}(t) - Q$. For this case, $\theta'(t)$ during the slow-phase always satisfies

$$\theta'(t) > C(t) - Q \tag{5.4.6}$$

It follows that the quick-phase is initiated whenever

$$\theta'(t) \leq \bar{C}(t) - Q \tag{5.4.7}$$

5.5 The threshold device

The condition for the quick-phase initiation is from (5.4.5) and (5.4.7).

$$|C(t) - \theta'(t)| \geq Q \tag{5.5.1}$$

Equation (5.5.1) is the unified condition for QP initiation for both left and right turn head motion which sets the threshold for the quick-phase at $\pm Q$ as shown in Figure 5.11. Whenever the error angle $\Delta\theta$ from $\theta'(t)$ to $\bar{C}(t)$ matches or exceeds the thresholds $\pm Q$, a quick-phase is initiated. As long as $\Delta\theta$ stays within the boundaries + Q and - Q, no quick-phase is initiated.

Referring to Figure 5.11, a WHEN signal generated by the threshold device actuates the AND-gate if it also meets the 50 milliseconds refractory period condition (see section 7.4). Once the AND-gate is actuated, s_2 is closed

through the OR-gate. Once s_2 is closed, it remains closed as long as the output from the amplifier persists because of the feedback signal from the amplifier. The threshold device is also referred to as the WHEN function because it generates the WHEN signal from the error signal. It is to be noted that once the threshold value is exceeded (from either direction for whatever reasons), the eye is always driven to C(t) by a QP.

5.6 The total integrated deterministic VOR model

The total integrated deterministic (without noise) VOR model is shown in Figure 5.12 with each block being explained in previous sections. The final values of parameters of each block in the model will be determined after the overall considerations of the responses to step and sinusoidal inputs and the behavior of the stochastic model. These are discussed in a later chapter.

Figure 5.12

This figure shows the total integrated deterministic VOR model, in which the mechanism of quick-phase generation is integrated with the compensatory slow-phase model. During the slow-phase, s_1 is closed and s_2 is open. During the quick-phase, s_1 is open and s_2 is closed.

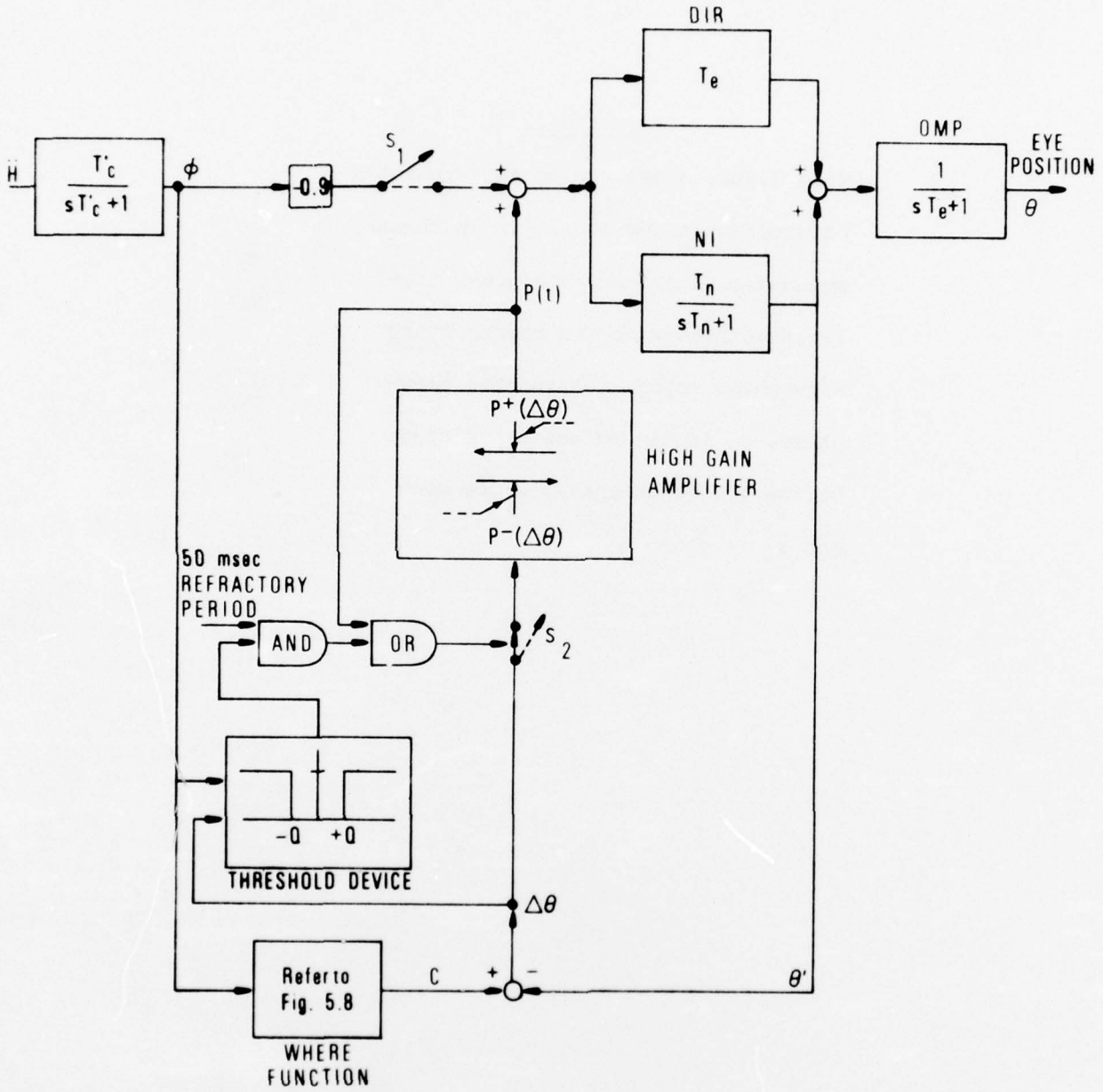

Figure 5.12 The Total Integrated Deterministic VOR Model

CHAPTER VI

STOCHASTIC MODEL

6.1 Introduction

The stochastic model is necessitated by the random behavior of the nystagmus (more specifically by the fluctuations of the WHEN curves and the WHERE curves) as illustrated in Figure 5.4. We have observed that as the eye velocity increases, fluctuations are more pronounced.

We view the quick-phase end-points as the sampled sequence, $C^*(t)$, of the continuous WHERE curve, $C(t)$. Similarly, we view the quick-phase initiation points as the sampled sequence, $D^*(t)$, of the continuous WHEN curve, $D(t)$. Based on several VOR responses of our cat corresponding to various nominal step input head velocities, relevant measurements are made and statistics are computed. The mean values of various relevant quantities for each nominal head velocity are shown in Table 6.1, in which $\dot{H}_0$, $\dot{H}$, and $\dot{\theta}_s$ have the same meaning as in Table 5.1 in section 5.3 and $\dot{\theta}_Q$ is the mean quick-phase velocity in *deg/sec* obtained by dividing the mean of all quick-phase magnitudes of several runs for a given $\dot{H}$ by the mean of all quick-phase durations of several runs for the same $\dot{H}$. Q is the separation in degrees between the steady state deterministic WHEN curve and WHERE curve. f_Q is the mean quick-phase frequency in beats per sec. $\sigma(D^*)$ is the standard deviation of the sampled sequence $D^*(t)$ of the WHEN curve. $\sigma(C^*)$ is the standard deviation of the sampled

Table 6.1

$\dot{H}_0$	$\dot{H}$	$\dot{\theta}_s$	$\dot{\theta}_Q$	Q	f_Q	$\sigma(D^*)$	$\sigma(C^*)$	R_{12}
deg/sec	deg/sec	deg/sec	deg/sec	deg	per/sec	deg	deg	
10	10.0	8.9	43.0	7.2	1.18	3.9	2.5	0.46
20	23.4	21.0	63.5	9.2	1.70	5.0	2.7	0.34
40	42.0	30.8	93.0	11.6	2.15	4.7	2.1	0.30
60	60.6	46.5	118.0	13.5	2.49	4.9	2.8	0.27
mean						4.6	2.5	0.34

The meanings of the symbols used in this table are explained elsewhere in section 6.1.

sequence $C^*(t)$ of the WHERE curve. R_{12} is the linear correlation coefficient between $D^*(t)$ and $C^*(t)$. The mathematical approximations for these quantities are derived as follows.

As we have discussed in section 5.1, the WHERE curve, $C(t)$, may be thought of as

$$C(t) = \bar{C}(t) + r_2(t) \tag{6.1.1}$$

in which $\bar{C}(t)$ is the mean location of the deterministic WHERE curve and $r_2(t)$ is its noise with zero mean. Similarly the WHEN curve, $D(t)$, may be thought of as

$$D(t) = \bar{D}(t) + r_1(t) \tag{6.1.2}$$

in which

$$\bar{D} = \bar{C}(t) \pm Q \tag{6.1.3}$$

is the mean deterministic WHEN curve and $r_1(t)$ is its noise with zero mean. This line of thought suggests introducing noise sources at certain locations in the model. The noises thus introduced are generated through filters from purely random (white) Gaussian noise sources and located in such places as to create noisy WHEN curves and a noisy WHERE curve with certain statistical characteristics such as standard deviations and a linear correlation coefficient, and with certain spectral compositions which would reasonably match those of our cat's VOR step responses. We have chosen Gaussian inputs to the filters because that distribution is

mathematically tractable and the noise histograms constructed from the limited data available from our cat's step responses seem sufficiently bell-shaped to permit this approximation.

6.2 The stochastic model

Let $x_2(t)$ and $z_2(t)$ be two independent Gaussian noise signals both with zero means and with desired variances and spectral components. How these noises are generated is discussed in section 6.3. $x_2(t)$ and $z_2(t)$ are introduced into the VOR model at points p_1 and p_2 respectively, as shown in Figure 6.1.

The point p_2 is selected for $z_2(t)$ because noise injected at this point would simulate the resultant effect of combining all the noise sources from anywhere in the WHERE function and the neural integrator circuits. It is reasonable to assume that these circuits are not noise free.

Now, referring to Figure 6.1, we note that

$$\Delta\theta = \left[\bar{C}(t) - \theta'(t)\right] + z_2(t)$$

$$= \left[\bar{C}(t) + z_2(t)\right] - \theta'(t)$$

$$= C(t) - \theta'(t) \qquad (6.2.1)$$

According to (6.2.1), $z_2(t)$ may be treated as noise on either $\bar{C}(t)$ or on $[\bar{C}(t) - \theta'(t)]$.

Figure 6.1

Noises are introduced into the model to create a noisy WHERE curve and a noisy WHEN curve. Noise $z_2(t)$ is added to the deterministic WHERE curve $\bar{C}(t)$ at p_2 to create the noise on the WHERE curve. Another noise, $x_2(t)$, is added at p_1 so that the resultant noise on the threshold, thus on the WHEN curve, is $x_2(t) + z_2(t)$. This would cause correlation between the noises on the two curves because $z_2(t)$ is common in noises of both curves.

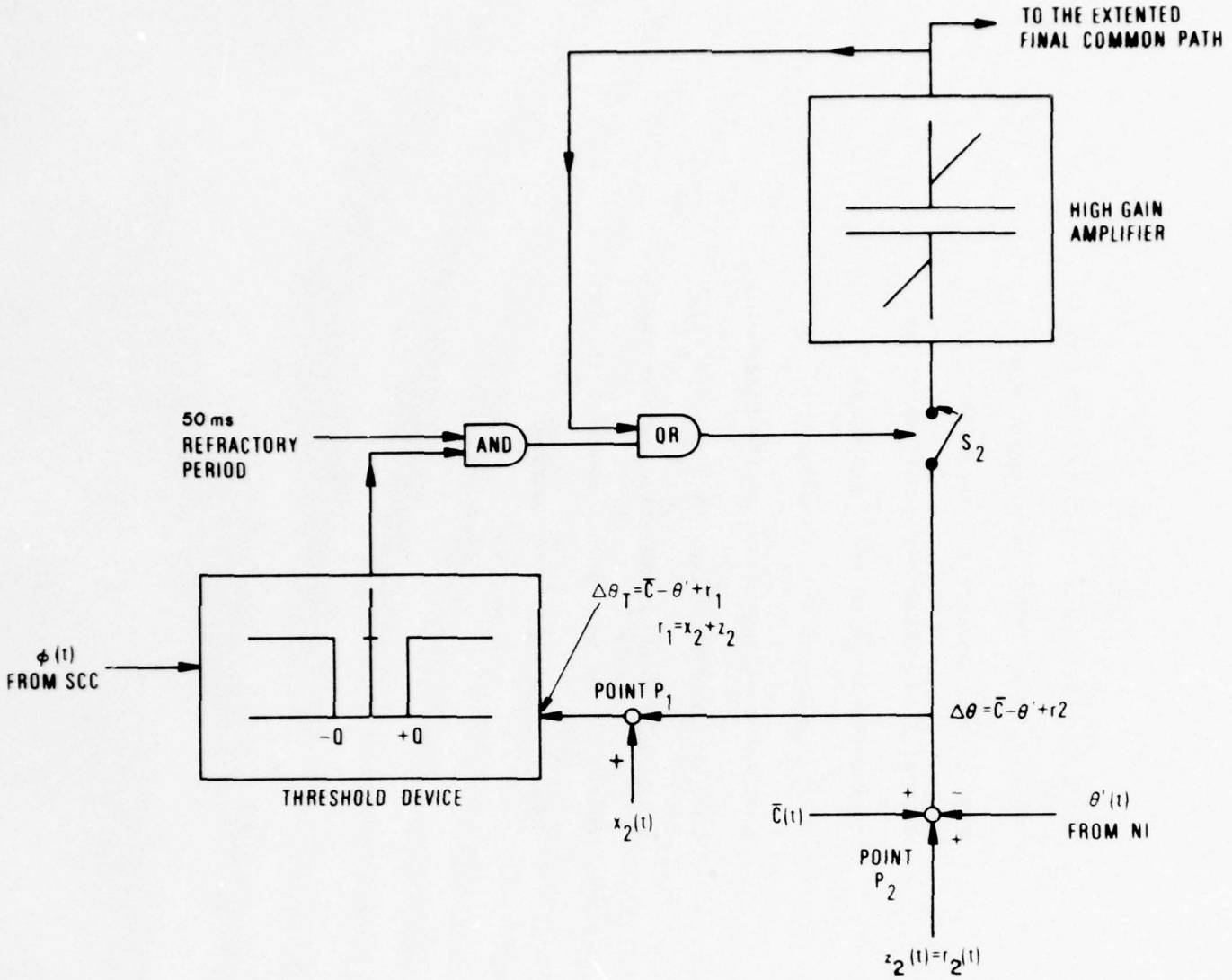

Figure 6.1 Introduction of Noises on the Deterministic WHEN and WHERE Curves

Next we consider the noise $r_1(t)$ on the deterministic WHEN curve. One way to interpret the fluctuations of the WHEN curve is to attribute them to the fluctuations of the threshold value of Q. It is neurophysiologically reasonable to assume that the decision process in the brain is so complex and unpredictable that it can be represented by the addition of a random signal. For this noise, a separate noise source $x_2(t)$ is introduced at p_1 in addition to $z_2(t)$ introduced at p_2 (Figure 6.1). The input signal $\Delta\theta_T$ to the threshold device is now

$$\Delta\theta_T(t) = \bar{C}(t) - \theta'(t) + x_2(t) + z_2(t)$$

$$= \bar{C}(t) - \theta'(t) + r_1(t) \qquad (6.2.2)$$

so that $x_2(t) + z_2(t) = r_1(t)$ by definition.

With this arrangement, $r_1(t)$ is correlated with $r_2(t)$ because the expected value of $r_1 r_2$ expressed by $E(r_1 r_2)$ is given by

$$E(r_1 r_2) = E\,(x_2 + z_2)z_2$$

$$= E(x_2 z_2) + E(z_2^2)$$

$$= E(z_2^2)$$

$$= E(r_2^2) \qquad (6.2.3)$$

since x_2 and z_2, both with zero means, are uncorrelated. In the model, the noise $z_2(t)$ would cause correlation between the WHEN curve and the WHERE curve because $z_2(t)$ affects each of them through the high-gain amplifier (WHERE curve) and the threshold device (WHEN curve). This correlation was first noted by casual inspection of the raw data and then confirmed by measurement. It is intellectually satisfying that this model is not only compatible with such a correlation, but it would be difficult and unrealistic to introduce noise in such a way that there was no correlation.

Next, we want to derive the expression for the linear correlation coefficient R_{12} between the eye position at the beginning (t_1) and the eye position at the end (t_2) of each quick-phase. From (6.1.1), (6.1.2), and (6.1.3) we have

$$C^*(t_2) = \bar{C}(t_2) + r_2^*(t_2) \tag{6.2.4}$$

$$D^*(t_1) = \bar{C}(t_1) \pm Q + r_1^*(t_1) \tag{6.2.5}$$

in which the superscript * denotes the sampled values either at the beginnings or at the ends of quick-phases. From (6.2.4) and (6.2.5), noting that $E(r_1^*) = 0$ and $E(r_2^*) = 0$, we obtain

$$E(C^*) = \bar{C} \tag{6.2.6}$$

$$E(D^*) = \bar{C} \pm Q \tag{6.2.7}$$

Thus, remembering that t_1 is at the beginning and t_2 is at the end of each quick-phase, the numerator of R_{12} is given by

$$E\left\{\left[D^*(t_1) - E\left(D^*(t_1)\right)\right]\left[C^*(t_2) - E\left(C^*(t_2)\right)\right]\right\}$$

$$= E\left[r_1^*(t_1) r_2^*(t_2)\right] \qquad (6.2.8)$$

and the denominator of R_{12} is given by

$$\left\{E\left[D^*(t_1) - E\left(D^*(t_1)\right)\right]^2 E\left[C^*(t_2) - E\left(C^*(t_2)\right)\right]^2\right\}^{\frac{1}{2}}$$

$$= \left\{E\left[\left(r_1^*(t_1)\right)^2\right] \quad E\left[\left(r_2^*(t_2)\right)^2\right]\right\}^{\frac{1}{2}} \qquad (6.2.9)$$

It follows that

$$R_{12} = \frac{\left[E\left(r_1^*(t_1)\ r_2^*(t_2)\right)\right]}{\sqrt{E\left[\left(r_1^*(t_1)\right)^2\right] E\left[\left(r_2^*(t_2)\right)^2\right]}} \qquad (6.2.10)$$

which is identical with the definition for the linear correlation coefficient between r_1^* at t_1 (the beginning) and r_2^* at t_2 (the end) of each quick-phase. Equation (6.2.10) is utilized in section 6.4. Note that (6.2.10) may also be approximated by

$$\hat{R}_{12} = \frac{\frac{1}{n} \sum_{k',k''=1}^{n} \left\{\left[r_1^*(k'T)\right] \left[r_2^*(k''T)\right]\right\}}{\sqrt{\left\{\frac{1}{n} \sum_{k'=1}^{n} \left[r_1^*(k'T)\right]^2\right\}\left\{\frac{1}{n} \sum_{k''=1}^{n} \left[r_2^*(k''T)\right]^2\right\}}} \qquad (6.2.11)$$

in which T is a periodic sampling interval (see section 6.3) and in which $k'T$ corresponds to t_1 in (6.2.10) and $k''T$ corresponds

to t_2 in (6.2.10). $\hat{R}_{12}$ approaches R_{12} asymptotically, (if it is ergodic) as n increases.

The resulting stochastic VOR model, which is shown in Figure 6.2, is acheived by simply incorporating the scheme of Figure 6.1 into the deterministic VOR model as presented in Figure 5.12.

6.3 Noise generation

We want the output from our stochastic model to match the random behavioral data from our cat.

Knowing the variance of the noise signals is not enough. It is important to know the spectral composition of the noise. It is likely that the actual neural noise is band-limited, and computer simulations in which very high or very low frequencies were allowed gave unrealistic behavior.

For this reason, we attempted to determine the spectral composition of the WHERE and WHEN curves of our cat's VOR responses by frequency analysis of the sampled curves C*(t) and D*(t). Since the inter-saccadic interval which corresponds to the inter-sampling period is not uniform, we could not use the discrete Fourier transform which assumes a uniform inter-sampling period. We overcame this difficulty by using a trigonometric interpolation. In this interpolation, a finite Fourier series is forced to pass through data values x_n (with n = 1, 2, - - -, N) of N data points, which may not be equally spaced, by proper choices of the coefficients of the truncated Fourier series.

Figure 6.2

The stochastic VOR model is achieved by simply incorporating the scheme of Figure 6.1 into the deterministic model as presented in Figure 5.12. This model will create the WHERE curve with noise $r_2(t) = z_2(t)$ and the WHEN curve with noise $r_1(t) = x_2(t) + z_2(t)$.

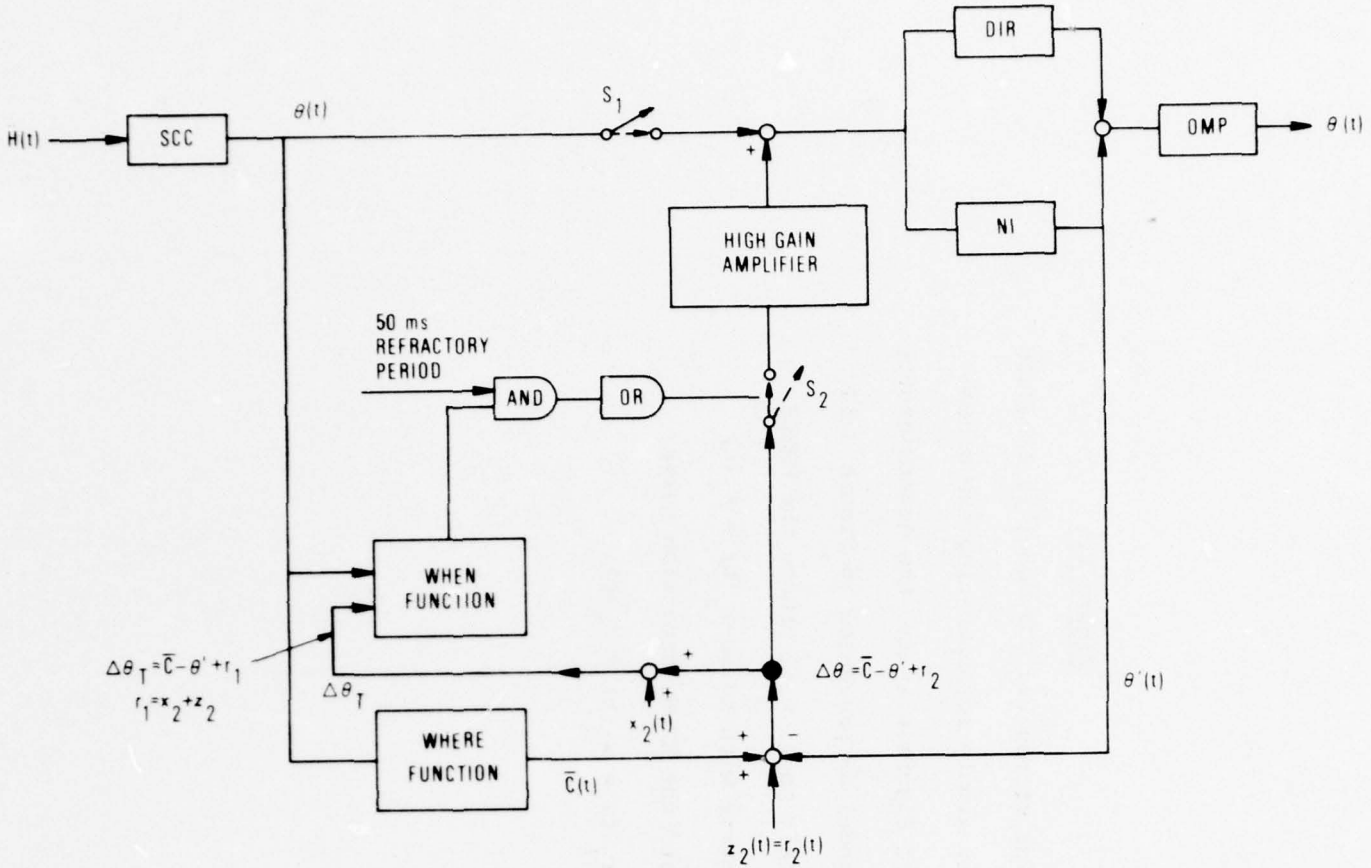

Figure 6.2 The Stochastic VOR Model

For an even number of data points N with the data length T_L', the value of x(t) which is the deviation from the mean, for $0 \leq t \leq T_L'$, may be expressed as

$$x(t) = \sum_{q=1}^{\left(\frac{N}{2}\right)} A_q\left(\cos qw_o t\right) + \sum_{q=1}^{\left(\frac{N}{2}\right)} B_q\left(\sin qw_o t\right) \tag{6.3.1}$$

in which $w_o = 2\pi/T_L'$. For N data points, we have N equations with N unknowns, N/2 A_q's and N/2 B_q's, to be solved. The magnitude F_q at a particular angular frequency (in radians/sec) of $qw_o = 2\pi q/T_L'$ is

$$F_q = \sqrt{A_q^2 + B_q^2} \tag{6.3.2}$$

Unfortunately, the length of the records from our cat's step response is typically only about 5 to 6 sec long with each record consisting of about a dozen data points. The short duration of the record is inherently imposed by the leaky integration of the SCC, which causes the slow-phase eye velocity to gradually decrease with an effective time-constant of about 12 sec.

For $T_L' \simeq 5$ and $N \simeq 12$ in (6.3.1), the lowest angular frequency (in the available frequency range) is $w_1 = \frac{2\pi}{5}$ rad/sec (0.2 Hz) for q = 1 and the highest frequency is $w_2 = \left(\frac{2\pi}{5}\right)6$ rad/sec (1.2 Hz) for q = 6. The result of spectral analysis

by this method for these data was very erratic. However, the results showed no consistent trend in the power spectrum over this bandwidth, suggesting that in the range of roughly 0.2 to 1.2 Hz, there is no reason to assume the spectrum to be other than flat. The Fourier analysis described above would give no information about frequency components outside this frequency range.

It turns out that the plot of the computer-simulated noise with components of w greater than w_2 fluctuates so rapidly that it presents an unphysiological appearance, while the plot of the noise with components of w less than w_1 is undesirable because it has long periods in which QP's are all too short or too long.

Under these circumstances and constraints, we have designed a filter which would produce, from a purely random Gaussian sequence, another Gaussian sequence with flat band-pass characteristics (with gain of 1) for $w_1 < w < w_2$ and rejects frequencies above or below this range.

The transfer function of the filter between the output noise y(t) and the input noise u(t), which is the purely random Gaussian noise with zero mean, is given by

$$\frac{y(s)}{u(s)} = \frac{s\tau_1}{(s\tau_1 + 1)(s\tau_2 + 1)} \qquad (6.3.3)$$

with $\tau_1 = 1$ from $w_1\tau_1 = 1$ and $\tau_2 = 1/8$ from $w_2\tau_2 = 1$ using $w_1 = \frac{2\pi}{5} \simeq 1$ and $w_2 = \left(\frac{2\pi}{5}\right)6 \simeq 8$ for computational simplicity.

As the first step to obtain the time-discrete equation, we define $x(s)$ such that $y(s) = \tau_1 s x(s)$ so that

$$\frac{x(s)}{u(s)} = \frac{1}{(s\tau_1 + 1)(s\tau_2 + 1)} \tag{6.3.4}$$

The differential equation corresponding to (6.3.4) with zero initial conditions is given by

$$\ddot{x}(t) = -\frac{\tau_1 + \tau_2}{\tau_1 \tau_2}\dot{x}(t) - \frac{1}{\tau_1 \tau_2}x(t) + \frac{1}{\tau_1 \tau_2}u(t) \tag{6.3.5}$$

With state variable notation of $x_1(t) = x(t)$ and $x_2(t) = \dot{x}(t)$, which implies that $y(t) = \tau_1 x_2(t)$, (6.3.5) may be expressed in a matrix form as

$$\begin{pmatrix} \dot{x}_1(t) \\ \dot{x}_2(t) \end{pmatrix} = \begin{pmatrix} 0 & 1 \\ a_{21} & a_{22} \end{pmatrix} \begin{pmatrix} x_1(t) \\ x_2(t) \end{pmatrix} + \begin{pmatrix} -a_{21} \end{pmatrix} \begin{pmatrix} 0 \\ u_2(t) \end{pmatrix} \tag{6.3.6}$$

in which

$$a_{21} = -\frac{1}{\tau_1 \tau_2}, \quad a_{22} = -\frac{\tau_1 + \tau_2}{\tau_1 \tau_2}, \text{ and } u_2(t) = u(t). \tag{6.3.7}$$

(6.3.6) is in the form of

$$\dot{X}(t) = AX(t) + BU(t) \tag{6.3.8}$$

in which

$$X(t) = \begin{pmatrix} x_1(t) \\ x_2(t) \end{pmatrix} \tag{6.3.9}$$

$$A = \begin{pmatrix} 0 & 1 \\ a_{21} & a_{22} \end{pmatrix} \tag{6.3.10}$$

$$B = -a_{21} \tag{6.3.11}$$

and

$$U(t) = \begin{pmatrix} 0 \\ u_2(t) \end{pmatrix} \tag{6.3.12}$$

The solution of (6.3.8) is

$$X(t) = e^{A(t - t_0)} X(t_0) + \int_{t_0}^{t} e^{A(t - \tau)} BU(\tau) d\tau \tag{6.3.13}$$

in which $e^{A(t-t_0)}$ is the transition matrix from $X(t_0)$ to $X(t)$.

Now, consider periodic sampling at every T sec (computation interval) or at $t = kT$ for $k = 0, 1, 2, - - -$. We seek to find the output of the filter, $y[(k + 1)T]$, given the input $U(kT)$ and the filter properties A. Substituting $t_0 = kT$ and $t = (k + 1)T$ in (6.3.13), we obtain

$$X\left[(k+1)T\right] = \Phi(T)X(kT) + W_x(kT) \qquad (6.3.14)$$

where the transition matrix $\Phi(T)$ (because $\Phi[k+1)T - kT] = \Phi(T)$) is given by

$$\Phi(T) = e^{AT} \triangleq \begin{pmatrix} \phi_{11}(T) & \phi_{12}(T) \\ \phi_{21}(T) & \phi_{22}(T) \end{pmatrix} \qquad (6.3.15)$$

and

$$W_x(kT) = \int_{kT}^{(k+1)T} e^{A[(k+1)T - \tau]} BU(\tau)\, d\tau$$

$$\triangleq \begin{pmatrix} w_{x_1}(kT) \\ w_{x_2}(kT) \end{pmatrix} \qquad (6.3.16)$$

In (6.3.16), both $w_{x_1}(kT)$ and $w_{x_2}(kT)$ are purely random Gaussian sequences with zero mean because of (6.3.12) in which $u_2(t)$ is a purely random Gaussian noise with zero mean by assumption.

Next, we determine the elements of $\Phi(T) = \exp(AT)$ by the inverse Laplace transform (L^{-1}) method. That is,

$$\Phi(T) = e^{AT} = L^{-1}\left[(sI - A)^{-1}\right] \qquad (6.3.17)$$

From (6.3.10), we get

$$(sI - A) = \begin{pmatrix} s & -1 \\ -a_{21} & s-a_{22} \end{pmatrix} \qquad (6.3.18)$$

It follows that

$$(sI - A)^{-1} = \frac{1}{s^2 - a_{22}s - a_{21}} \begin{pmatrix} s-a_{22} & 1 \\ a_{21} & s \end{pmatrix} \tag{6.3.19}$$

The fact that (6.3.19) is the correct expression may be confirmed by multiplying it by (6.3.18), which results in the identity matrix as it should. Using (6.3.7),

$$s^2 - a_{22}s - a_{21} = \left(s + \frac{1}{\tau_1}\right)\left(s + \frac{1}{\tau_2}\right) \tag{6.3.20}$$

Finding the inverse Laplace transforms of (6.3.19) with (6.3.20) using the standard table, we obtain

$$\phi_{11}(T) = \frac{1}{\tau_1 - \tau_2}\left(\tau_1 e^{-\frac{T}{\tau_1}} - \tau_2 e^{-\frac{T}{\tau_2}}\right) \tag{6.3.21}$$

$$\phi_{12}(T) = \frac{\tau_1\tau_2}{\tau_1 - \tau_2}\left(e^{-\frac{T}{\tau_1}} - e^{-\frac{T}{\tau_2}}\right) \tag{6.3.22}$$

$$\phi_{21}(T) = \frac{1}{\tau_1 - \tau_2}\left(e^{-\frac{T}{\tau_2}} - e^{-\frac{T}{\tau_1}}\right) \tag{6.3.23}$$

and

$$\phi_{22}(T) = \frac{1}{\tau_1 - \tau_2}\left(\tau_1 e^{-\frac{T}{\tau_2}} - \tau_2 e^{-\frac{T}{\tau_1}}\right) \qquad (6.3.24)$$

Equation (6.3.14) may now be expressed in terms of (6.3.21) to (6.3.24) as

$$x_1[(k+1)T] = \phi_{11}(T)x_1(kT) + \phi_{12}(T)x_2(kT) + w_{x_1}(kT) \qquad (6.3.25)$$

$$x_2[(k+1)T] = \phi_{21}(T)x_1(kT) + \phi_{22}(T)x_2(kT) + w_{x_2}(kT) \qquad (6.3.26)$$

Because $y(t) = \tau_1 x_2(t)$ as mentioned before,

$$y[(k+1)T] = \tau_1 x_2[(k+1)T] \qquad (6.3.27)$$

which is the output we are seeking.

The remaining problem is to determine $w_{x_2}(kT)$ such that $E(y^2) = E(x_2^2) \triangleq \sigma^2(x_2)$, for $\tau_1 = 1$, matches the variance obtained from our cat's VOR responses. E denotes the operation of taking the expected value of its argument (which is equal to taking its time-average if it is ergodic).

In (6.3.14), $X[(k+1)T]$ is a Gaussian random sequence if $W_x(kT)$ is a Gaussian purely random sequence and the initial state vector $X(0)$ is Gaussian (Bryson and Ho, 1975). In our case, $E[W_x(kT)] = 0$ and $E[X(kT)] = 0$. Next, we want to generate a two-dimensional, jointly Gaussian sequence $W_x'(kT)$ by a digital computer such that it is equivalent to $W_x(kT)$ of (6.3.16), to the extent that the statistical characteristics of the output $X[(k+1)T]$ of (6.3.14) forced by $W_x'(kT)$ is identical with those forced by $W_x(kT)$.

From (6.3.16) using (6.3.15) we obtain (denoting B by b)

$$W_x(kT) = \begin{pmatrix} w_{x_1}(kT) \\ \\ w_{x_2}(kT) \end{pmatrix}$$

$$= \begin{Bmatrix} b \int_{KT}^{(k+1)T} \phi_{12}[(k+1)T - \tau]\, u_2(\tau)\, d\tau \\ \\ b \int_{KT}^{(k+1)T} \phi_{22}[(k+1)T - \tau]\, u_2(\tau)\, d\tau \end{Bmatrix} \tag{6.3.28}$$

We want to determine

$$E\left[W_x(kT)W_x^T(kT)\right] = E\begin{pmatrix} w_{x_1}^2(kT) & w_{x_1}(kT)w_{x_2}(kT) \\ \\ w_{x_1}(kT)w_{x_2}(kT) & w_{x_2}^2(kT) \end{pmatrix} \tag{6.3.29}$$

with $u_2(t)$ representing a continuous white (purely random) noise, that is

$$E[u_2(t)u_2(\tau)] = \psi\delta(t-\tau) \tag{6.3.30}$$

in which ψ is the power spectral density of the white noise $u_2(t)$, and $\delta(t-\tau)$ is the Dirac delta function. Substituting

from (6.3.28) into (6.3.29) and using (6.3.30), we obtain

$$E\left[w_{x_1}^2(kT)\right] = \psi b^2 \int_0^T \phi_{12}^2(T-\tau)d\tau \qquad (6.3.31)$$

$$E\left[w_{x_2}^2(kT)\right] = \psi b^2 \int_0^T \phi_{22}^2(T-\tau)\,d\tau \qquad (6.3.32)$$

$$E\left[w_{x_1}(kT)w_{x_2}(kT)\right] = \psi b^2 \int_0^T \phi_{12}(T-\tau)\phi_{22}(T-\tau)d\tau \qquad (6.3.33)$$

in which $\phi_{12}(T-\tau)$ and $\phi_{22}(T-\tau)$ are given by (6.3.22) and (6.3.24) with T replaced by the new argument $(T-\tau)$. Carrying out integrations in (6.3,31), (6.3.32), and (6.3.33), we have

$$E\left[w_{x_1}^2(kT)\right] = \frac{\psi}{(\tau_1-\tau_2)^2}\left[\frac{\tau_1}{2}\left(1-e^{-\frac{2}{\tau_1}T}\right)\right.$$

$$-\frac{2}{\left(\frac{1}{\tau_1}+\frac{1}{\tau_2}\right)}\left(1-e^{-\left(\frac{1}{\tau_1}+\frac{1}{\tau_2}\right)T}\right)$$

$$\left.+\frac{\tau_2}{2}\left(1-e^{-\frac{2}{\tau_2}T}\right)\right] \qquad (6.3.34)$$

$$E\left[w_{x_2}^2(kT)\right] = \frac{\psi}{\left(\tau_1 - \tau_2\right)^2}\left[\frac{1}{2\tau_2}\left(1 - e^{-\frac{2}{\tau_2}T}\right)\right.$$

$$- \frac{2}{\left(\tau_1 + \tau_2\right)}\left(1 - e^{-\left(\frac{1}{\tau_1} + \frac{1}{\tau_2}\right)T}\right)$$

$$\left. + \frac{1}{2\tau_1}\left(1 - e^{-\frac{2}{\tau_1}T}\right)\right] \qquad (6.3.35)$$

$$E\left[w_{x_1}(kT)w_{x_2}(kT)\right] = \frac{\psi}{\left(\tau_1 - \tau_2\right)^2}\left[\frac{1}{2}\left(e^{-\frac{2}{\tau_1}T} + e^{-\frac{2}{\tau_2}T}\right)\right.$$

$$\left. - e^{-\left(\frac{1}{\tau_1} + \frac{1}{\tau_2}\right)T}\right] \qquad (6.3.36)$$

where τ_1 and τ_2 are originally introduced in (6.3.3), and T is the computation interval.

With $\tau_1 = 1$, $\tau_2 = 0.125$, and $T = 0.01$ in the above three equations, we obtain

$$Q_x = E\left[W_x(kT)W_x^T(kT)\right] \triangleq \begin{pmatrix} w_{11} & w_{12} \\ w_{12} & w_{22} \end{pmatrix} \psi$$

$$= \begin{pmatrix} 1.9918 \times 10^{-5} & 2.9258 \times 10^{-3} \\ 2.9258 \times 10^{-3} & 0.58556 \end{pmatrix} \psi \qquad (6.3.37)$$

Suppose we have another covariance matrix Q_x' given by

$$Q_x' \triangleq \begin{pmatrix} q'_{x_{11}} & q'_{x_{12}} \\ q'_{x_{12}} & q'_{x_{22}} \end{pmatrix} \triangleq \begin{pmatrix} \sigma_1^2 & \rho\sigma_1\sigma_2 \\ \rho\sigma_1\sigma_2 & \sigma_2^2 \end{pmatrix} \qquad (6.3.38)$$

If σ_2^2 is specified, σ_1^2 may be related to σ_2^2 by

$$\sigma_1^2 = C^2\sigma_2^2 \qquad (6.3.39)$$

in which the value of C^2 is to be determined subsequently. This allows us to express (6.3.38) by

$$Q_x' = \begin{pmatrix} C^2\sigma_2^2 & \rho C\sigma_2^2 \\ \rho C\sigma_2^2 & \sigma_2^2 \end{pmatrix} \qquad (6.3.40)$$

We want to make (6.3.40) equal to (6.3.37), that is, we want $Q_x = Q_x'$. This requires that

$$w_{22}\psi = \sigma_2^2 \tag{6.3.41}$$

$$w_{11}\psi = C^2\sigma_2^2 = C^2 w_{22}\psi \tag{6.3.42}$$

$$w_{12}\psi = \rho C\sigma_2^2 = \rho C w_{22}\psi \tag{6.3.43}$$

It follows that, cancelling ψ's out,

$$C^2 = \frac{w_{11}}{w_{22}} \tag{6.3.44}$$

$$\rho C = \frac{w_{12}}{w_{22}} \tag{6.3.45}$$

$$\rho = \frac{1}{C}\,\frac{w_{12}}{w_{22}} = \frac{w_{12}}{\sqrt{w_{11}w_{22}}} \tag{6.3.46}$$

For $\tau_1 = 1$, $\tau_2 = 0.125$, and $T = 0.01$, we get

$$\begin{aligned} C^2 &= 3.4016 \times 10^{-5} \\ C &= 5.8323 \times 10^{-3} \\ \rho C &= 4.9966 \times 10^{-3} \\ \rho &= 0.8567 \end{aligned} \tag{6.3.47}$$

With the knowledge of the covariance matrix given by (6.3.40), $w_{x_1}(kT)$ and $w_{x_2}(kT)$ are generated by a computer routine (Scheuer and Stoller, 1962) such that the joint probability density of w_{x_1} and w_{x_2} corresponds to the jointly

Gaussian density function $f\left(w_{x_1}, w_{x_2}\right)$ (Papoulis, 1965) given by (since w_{x_1} and w_{x_2} have zero mean)

$$f\left(w_{x_1}, w_{x_2}\right) = \frac{1}{2\pi\sigma_1\sigma_2(1-\rho^2)^{\frac{1}{2}}} \exp\left(-\frac{1}{2(1-\rho^2)}\right)$$

$$\left[\frac{w_{x_1}^2}{\sigma_1^2} - \frac{2\rho w_{x_1} w_{x_2}}{\sigma_1\sigma_2} + \frac{w_{x_2}^2}{\sigma_2^2}\right] \tag{6.3.48}$$

in which $\sigma_1 = \sigma(w_{x_1})$, $\sigma_2 = \sigma(w_{x_2})$, and $\sigma_1 = C\sigma_2$. $W_x(kT) = \left[w_{x_1}(kT) \quad w_{x_2}(kT)\right]^T$ thus generated becomes the input of (6.3.14). Since $W_x(kT)$ is related to $u_2(\tau)$ by (6.3.28) and $u_2(\tau)$ is assumed to be a purely random (white) Gaussian noise, $y[(k+1)T] = \tau_1 x_2[(k+1)T]$ given by (6.3.27) would have the same band-pass characteristics as the output of the filter equation given by (6.3.3).

Next, we want to determine the relationship between $E[x_2^2(kT)] = \sigma_{x_2}^2$ and $E[W_{x_2}^2(kT)] = \sigma_{wx_2}^2$. To do this (Bryson and Ho, 1975), we start with (6.3.8) which is repeated below as

$$\dot{X}(t) = AX(t) + BU(t) \tag{6.3.49}$$

Since $u_2(t)$ of $U(t)$ is a Gaussian random process with zero mean, $X(t)$ is also a Gaussian random process with zero mean because linear transformations of a Gaussian vector preserve its Gaussian character.

We define $P(t)$ by

$$P(t) = E[X(t)X^T(t)] \tag{6.3.50}$$

in which

$$P(t) = \begin{pmatrix} P_{11}(t) & P_{12}(t) \\ P_{12}(t) & P_{22}(t) \end{pmatrix} \tag{6.3.51}$$

We assume that

$$P(0) = E[X(0)X^T(0)] \tag{6.3.52}$$

is a purely Gaussian random variable.

We define Ψ by

$$E[U(t)U^T(\tau)] = \Psi\delta(t-\tau) \tag{6.3.53}$$

in which

$$\Psi = \begin{pmatrix} \psi_{11} & \psi_{12} \\ \psi_{12} & \psi_{22} \end{pmatrix} \tag{6.3.54}$$

Because of (6.3.12) and (6.3.30), we have from the above two equations,

$$E[U(t)U^T(\tau)] = \begin{pmatrix} 0 & 0 \\ 0 & \psi \end{pmatrix} \delta(t-\tau) \tag{6.3.55}$$

in which $\psi_{22} = \psi$ is used. Under these conditions, it can be shown that

$$\dot{P}(t) = AP(t) + P(t)A^T + B\Psi B^T \tag{6.3.56}$$

with $P(t_0)$ given.

Since the characteristic matrix A has two eigenvalues both of which are real and negative being $-\frac{1}{\tau_1}$ and $-\frac{1}{\tau_2}$ ($\tau_1 > 0$ and $\tau_2 > 0$), asymptotically as t approaches infinity, P(t) in (6.3.56) approaches a statistically stationary value of constant P making $\dot{P}(t) = 0$. In this case, 6.3.56 becomes

$$AP + PA^T + B\Psi B^T = 0 \tag{6.3.57}$$

Substituting from (6.3.10), (6.3.51), (6.3.11), and (6.3.55) into (6.3.57), we obtain

$$\begin{pmatrix} 0 & 1 \\ a_{21} & a_{22} \end{pmatrix} \begin{pmatrix} p_{11} & p_{12} \\ p_{12} & p_{22} \end{pmatrix} + \begin{pmatrix} p_{11} & p_{12} \\ p_{12} & p_{22} \end{pmatrix} \begin{pmatrix} 0 & a_{21} \\ 1 & a_{22} \end{pmatrix}$$

$$= a_{21}^2 \begin{pmatrix} 0 & 0 \\ 0 & \psi \end{pmatrix} \tag{6.3.58}$$

which gives

$$p_{22} = -\frac{a_{21}^2}{2a_{22}} \psi \tag{6.3.59}$$

In view of (6.3.7), (6.3.59) becomes

$$P_{22} = \frac{1}{2\tau_1 \tau_2 (\tau_1 + \tau_2)} \psi \tag{6.3.60}$$

Since $P_{22} = E[X_2^2(t)]$ for large t and $y(t) = \tau_1 x_2(t)$, we have, denoting $E[y^2(t)]$ for large t by σ_y^2,

$$\sigma_y^2 = \tau_1^2 P_{22} \tag{6.3.61}$$

It follows from (6.3.60) that

$$\sigma_y^2 = \frac{\tau_1}{2\tau_2(\tau_1 + \tau_2)} \psi \tag{6.3.62}$$

As a check, by rewriting (6.3.62), since τ_1 and τ_2 are related to the break-frequencies w_1 and w_2 by $w_1\tau_1 = 1$ and $w_2\tau_2 = 1$ by (6.3.3),

$$\sigma_y^2 = \frac{1}{2} \frac{w_2^2}{w_1 + w_2} \psi \tag{6.3.63}$$

We can clearly see that σ_y^2 increases as w_2 increases, as it should, because this increases the band-width, while σ_y^2 decreases as w_1 increases, as it should, because this decreases the band-width.

Now dividing (6.3.35) by (6.3.62) on both sides, and denoting $E[W_{x_2}^2(kT)]$ for large kT by $\sigma_{wx_2}^2$, we obtain

$$\frac{\sigma_{wx_2}^2}{\sigma_y^2} = \frac{2\tau_2(\tau_1 + \tau_2)}{\tau_1(\tau_1 - \tau_2)^2}\left[\frac{1}{2\tau_2}\left(1 - e^{-\frac{2}{\tau_2}T}\right) - \frac{2}{(\tau_1 + \tau_2)}\left(1 - e^{-\left(\frac{1}{\tau_1} + \frac{1}{\tau_2}\right)T}\right) + \frac{1}{2\tau_1}\left(1 - e^{-\frac{2}{\tau_1}T}\right)\right] = F(\tau_1, \tau_2, T) \tag{6.3.64}$$

From (6.3.64) with $\tau_1 = 1$, $\tau_2 = 0.125$ and $T = 0.01$, we obtain

$$\sigma_{wx_2} = 0.4058\ \sigma_y \tag{6.3.65}$$

in which σ_y is related to the standard deviation of experimentally obtained data. If (6.3.14) is driven by $W_x(kT)$ generated by (6.3.48) using $\sigma_2 = \sigma_{wx_2}$ above, $\sigma_1 = C\sigma_2$ and the values of ρ and C as given by (6.3.47) for $\tau_1 = 1$, $\tau_2 = 0.125$ and $T = 0.01$, then the output $y[(k+1)T]$ as given by (6.3.27) would have the same band-pass characteristics as the output $y(t)$ from (6.3.3). Note that since $\tau_1 = 1$, $y[(k+1)T] = X_2[(k+1)T]$ in (6.3.27).

The validity of the computer routine of generating $w_{x_1}(kT)$ and $w_{x_2}(kT)$ according to $f(w_{x_1}, w_{x_2})$ given by (6.3.48) was confirmed by recomputing the values of C and ρ from the computer-generated $w_{x_1}(kT)$ and $w_{x_2}(kT)$. The validity of (6.3.64) was confirmed by recomputing the value of $\sigma_y = \tau_1 \sigma_{x_2}$ based on $x_2[(k+1)T]$ obtained by simulating (6.3.25) and (6.3.26), which are driven by $w_{x_1}(kt)$ and $w_{x_2}(kT)$. The σ_y in (6.3.65) is related to the experimental data obtained from our cat (see the following section).

As a check for (6.3.62), we made $\tau_1 = 2$ and $\tau_2 = 1/16$, thus increasing the band-width of the filter given by (6.3.3). σ_y^2 obtained from the simulation of (6.3.25), (6.3.26), and (6.3.27) gave a good match with the value predicted by (6.3.62), which shows the soundness of (6.3.62).

6.4 Statistical analysis in the model

Referring to Figure 6.3, $r_1(kT)$ and $r_2(kT)$ are discrete noise signals coming out every computation interval of T seconds. However, $r_1^*(k'T)$ is the sampled noise on the WHEN curve at k'T when a QP is triggered and $r_2^*[(k' + L)T]$ is the sampled noise on the WHERE curve at $(k' + L)T$ where LT is equal to the QP duration. L is an appropriate integer. For example, L = 11 for a QP duration of 0.11 sec because T = 0.01 sec. k' is the value of k when each QP is triggered. Working backwards from the outputs r_1^* and r_2^* to the inputs $w_{x_2}(kT)$ and $w_{z_2}(kT)$ in Figure 6.3, we want to determine the standard deviations $\sigma\left(w_{x_2}\right)$ and $\sigma\left(w_{z_2}\right)$ in terms of experimentally obtained standard deviations corresponding to $\sigma\left(r_1^*\right)$ and $\sigma\left(r_2^*\right)$.

Referring to Figure 6.3, since $r_1 = \tau_1 x_2 + \tau_1 z_2$ and since x_2 and z_2 are uncorrelated with each other, both with zero means, we have

$$\sigma_1^2\left(r_1\right) = \tau_1^2\sigma^2\left(x_2\right) + \tau_1^2\sigma^2\left(z_2\right) \tag{6.4.1}$$

Because

$$\tau_1^2\sigma^2\left(z_2\right) = \sigma^2\left(r_2\right) \tag{6.4.2}$$

we have

$$\sigma^2\left(x_2\right) = \frac{1}{\tau_1^2}\left[\sigma^2\left(r_1\right) - \sigma^2\left(r_2\right)\right] \tag{6.4.3}$$

Figure 6.3

This figure shows an arrangement by which the sampled noise r_1^* on the WHEN curve and the sampled noise r_2^* on the WHERE curve are created through the VOR model such that respective variance of r_1^* and r_2^* as well as the correlation between r_1^* and r_2^* would match the corresponding values from our cat's data.

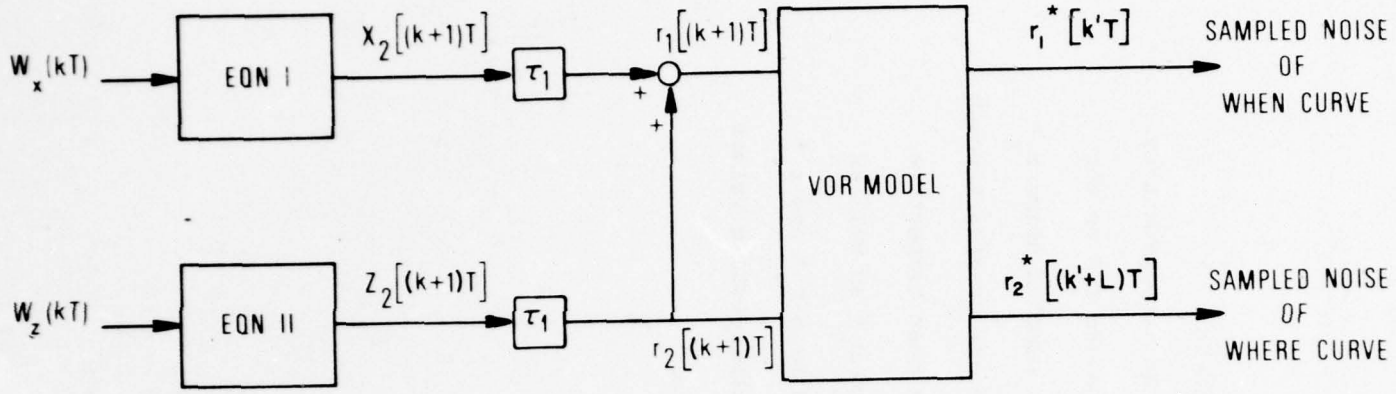

$$X[(k+1)T] = \Phi(T)X(kT) + W_x(kT) \qquad (I)$$

$$Z[(k+1)T] = \Phi(T)Z(kT) + W_z(kT) \qquad (II)$$

$$X = \begin{pmatrix} x_1 \\ x_2 \end{pmatrix} ; \quad Z = \begin{pmatrix} z_1 \\ z_2 \end{pmatrix} ; \quad W_x = \begin{pmatrix} w_{x1} \\ w_{x2} \end{pmatrix} ; \quad W_z = \begin{pmatrix} w_{z1} \\ w_{z2} \end{pmatrix}$$

THE ELEMENTS OF $\Phi(T)$ ARE GIVEN IN 6.3.21 ~ 6.3.24

Figure 6.3 Noise Generation

It follows from (6.3.64) that

$$\sigma^2\left(w_{x_2}\right) = \tau_1^2 F\left(\tau_1, \tau_2, T\right) \sigma^2\left(x_2\right) \tag{6.4.4}$$

$$\sigma^2\left(w_{z_2}\right) = \tau_1^2 F\left(\tau_1, \tau_2, T\right) \sigma^2\left(z_2\right) \tag{6.4.5}$$

Once $\sigma^2\left(w_{x_2}\right)$ and $\sigma^2\left(w_{z_2}\right)$ are thus determined, $x_2[(k+1)T]$ and $z_2[(k+1)T]$ are generated by filters represented by equation I and equation II in Figure 6.3 from $w_{x_2}(kT)$ and $w_{z_2}(kT)$, both of which are purely random Gaussian sequences with zero means but with different variances of $\sigma^2\left(w_{x_2}\right)$ and $\sigma^2\left(w_{z_2}\right)$ respectively.

Next, we want to determine the linear correlation coefficient R_{12} between $r_1^*(k'T)$ and $r_2^*[(k'+L)T]$. $k'T$ is the time at the beginning of a quick-phase, while $(k'+L)T$ is the time at the end of the same quick-phase. Thus, LT is equal to the quick-phase duration. R_{12} is obtained from (6.2.10) by replacing t_1 by $k'T$ and t_2 by $(k'+L)T$ and designating $E\left[\left(r_1^*(t_1)\right)^2\right]$ by $\sigma^2(r_1^*)$ and $E\left[\left(r_2^*(t_2)\right)^2\right]$ by $\sigma^2(r_2^*)$. Thus,

$$R_{12} = \frac{E\left[r_1^*(k'T)\ r_2^*\ (k'+L)T\right]}{\sigma(r_1^*)\ \sigma(r_2^*)} \tag{6.4.6}$$

Now, for the sampled noise r_2^* of the WHERE curve

$$\sigma(r_2^*) \simeq \sigma(r_2) = \tau_1 \sigma\ (z_2) \tag{6.4.7}$$

However, for the sampled noise r_1^* of the WHEN curve we can say

$$\sigma(r_1^*) \simeq \sigma(r_1) \tag{6.4.8}$$

only for a relatively high slow-phase eye velocity. As the eye velocity becomes slower, the eye position tends to touch only the nearest part of the noisy WHEN curve because of its smaller slope. (This is illustrated in Figure 7.6.) This would make $\sigma(r_1^*)$ smaller than $\sigma(r_1)$ as the eye velocity becomes slower. This effect, which we might call "shading," is not too significant although noticeable in our model output at the lowest available step input head velocity of about 10 deg/sec compared with the highest input head velocity of about 60 deg/sec for our cat. This point is further discussed in Chapter 7.

With this understanding, we have

$$\begin{aligned} E\left[r_1^*(k'T)r_2^*\left((k'+L)T\right)\right] &\simeq E\left[r_1(kT)r_2\left((k+L)T\right)\right] \\ &= \tau_1^2 E\left[\left(x_2(kT)+z_2(kT)\right)\ z_2\left((k+L)T\right)\right] \\ &= \tau_1^2 E\left[z_2(kT)z_2\left((k+L)T\right)\right] \end{aligned} \tag{6.4.9}$$

because x and z are uncorrelated. It follows from (6.4.6) that

$$R_{12} \simeq \frac{\tau_1^2 E\left[z_2(kT)z_2\ (k+L)T\right]}{\sigma(r_1)\ \sigma(r_2)} \tag{6.4.10}$$

To express (6.4.10) in terms of known quantities, first we define $P_z(kT)$ and $C(kT, (k + L)T)$ such that

$$P_z(kT) = E\left[Z(kT)Z^T(kT)\right] = \begin{pmatrix} p_{z_{11}} & p_{z_{12}} \\ p_{z_{12}} & p_{z_{22}} \end{pmatrix} \tag{6.4.11}$$

and

$$C\left(kT, (k + L)T\right) = E\left[Z(kT)Z^T((k + L)T)\right] = \begin{pmatrix} c_{11} & c_{12} \\ c_{21} & c_{22} \end{pmatrix} \tag{6.4.12}$$

Now, (Bryson and Ho, 1975),

$$C\left(kT, (k + L)T\right) = P_z(kT)\Phi^T\left((k + L)T, kT\right) = P_z(kT)\Phi^T(LT) \tag{6.4.13}$$

We are interested in the c_{22} element of (6.4.12) which is, using (6.4.11), (6.4.12), and (6.4.13),

$$c_{22}[kT, (k + L)T] = E\left[Z_2(kT)Z_2(k + L)T\right] = \phi_{21}(LT)p_{z_{12}} + \phi_{22}(LT)p_{z_{22}} \tag{6.4.14}$$

Equation (6.4.14) becomes, using (6 3.23) and (6.3.24) with T replaced by LT,

$$c_{22}[kT,\ (k+L)T] = \frac{1}{\tau_1 - \tau_2}\left[\begin{pmatrix} -\frac{LT}{\tau_2} & -\frac{LT}{\tau_1} \\ e & -e \end{pmatrix} p_{z_{12}} + \begin{pmatrix} -\frac{LT}{\tau_2} & -\frac{LT}{\tau_1} \\ \tau_1 e & -\tau_2 e \end{pmatrix} p_{z_{22}}\right] \tag{6.4.15}$$

For L = 0, (6.4.15) reduces to $p_{z_{22}}$, as it should, because $c_{22}(kT, kT) = E\left[z_2(kT)\ z_2(kT)\right] = P_{z_{22}}$. For a typical quick-phase duration of 0.05 sec to 0.2 sec, L is 5 ~ 20 with T = 0.01 sec. For these values of L with $\tau_1 = 1$ and $\tau_2 = 1/8$, the first term inside the square bracket of the right hand side of (6.4.15) is negligible compared with the second term because it turns out that $|p_{z_{12}}| << |p_{z_{22}}|$ for T = 0.01. Thus,

$$c_{22}[kT,\ (k+L)T] \simeq \frac{1}{\tau_1 - \tau_2}\begin{pmatrix} -\frac{LT}{\tau_2} & -\frac{LT}{\tau_1} \\ \tau_1 e & -\tau_2 e \end{pmatrix} p_{z_{22}} \tag{6.4.16}$$

It follows from (6.4.10) with (6.4.14) and (6.4.16) that

$$R_{12} \simeq \frac{\sigma(r_2)}{\sigma(r_1)}\begin{pmatrix} -\frac{LT}{\tau_2} & -\frac{LT}{\tau_1} \\ \tau_1 e & -\tau_2 e \end{pmatrix} \frac{1}{\tau_1 - \tau_2} \tag{6.4.17}$$

because $p_{z_2 2} = \frac{1}{\tau_1^2}\sigma^2(r_2)$.

Equation (6.4.17) allows us to take the physiologically measured variables $\sigma(r_1)$, $\sigma(r_2)$ and LT and the estimated frequency limits of the noise, $\frac{1}{\tau_1}$ and $\frac{1}{\tau_2}$, and allows us to predict the correlation coefficient R_{12}. The success of this prediction is discussed in the next chapter.

6.5 Summary (Refer to Figure 6.3)

The noise on the WHEN curve corresponds to r_1^* and the noise on the WHERE curve corresponds to r_2^*. From our cat's step responses, we determine variances $\sigma^2(r_1^*)$ and $\sigma^2(r_2^*)$ as well as the linear correlation coefficients R_{12} between the eye position at the beginning and that at the end of each quick-phase. From the experimentally determined values of $\sigma^2(r_1^*)$ and $\sigma^2(r_2^*)$, we estimate $\sigma^2(r_1)$ and $\sigma^2(r_2)$ by (6.4.8) and (6.4.7). Next, we determine $\sigma^2(z_2)$ and $\sigma^2(x_2)$ by (6.4.2) and (6.4.1). After that, we determine $\sigma^2(w_{x_2})$ and $\sigma^2(w_{z_2})$ by (6.4.4) and (6.4.5).

$w_{x_1}(kT)$ and $w_{x_2}(kT)$ are generated by a computer routine in such a way as to meet the probability density function $f(w_{x_1}, w_{x_2})$ given by (6.3.48). $w_{z_1}(kT)$ and $w_{z_2}(kT)$ are generated in a similar way according to $f(w_{x_1}, w_{x_2})$ in (6.3.48) with w_{x_1} and w_{x_2} replaced by w_{z_1} and w_{z_2} and with the

understanding that $\sigma_1 = \sigma(w_{z1})$ and $\sigma_2(w_{z2})$. For given $\sigma(r_1^*)$ and $\sigma(r_2^*)$ corresponding to experimentally obtained standard deviations, the computer program takes care of the rest of the procedure which yields $W_x(kT)$ and $W_z(kT)$.

Referring to Figure 6.3, $x_2[(k + 1)T]$ and $z_2[(k + 1)T]$ are generated respectively through equations (I) and (II) from $W_x(kT)$ and $W_z(kT)$. x_2 and z_2 have the same frequency band-pass characteristics as the filter equation (6.3.4). $\sigma(r_1^*)$ and $\sigma(r_2^*)$ as well as R_{12} (see section 6.2) computed from our VOR model would be compared with those obtained from our cat's data. R_{12} may be estimated by (6.4.17), in which LT may be interpreted as the mean quick-phase duration. In the computer program, R_{12} is determined by (6.4.6) using running averages. The R_{12} from the VOR model has shown a reasonable match with our cat's data.

CHAPTER VII

RESULTS

7.1 General approach

The parameters of the model developed thus far are adjusted so that the output of the model obtained by simulation would approximately match the responses from our cat. This is done in two stages. Initially, the parameters are adjusted for the deterministic model without noise inputs. After this, the parameters of the noise inputs for the stochastic model are adjusted to meet the statistical characteristics from our cat's data.

First, the quick-phase frequency f_Q from the deterministic model for various step input head velocities is made to match approximately with the mean f_Q of our cat's VOR responses by adjusting the threshold value Q. Next, the deterministic model thus obtained is further modified to obtain reasonable sinusoidal responses by slightly readjusting Q and adjusting the time constant T_L of the lag network in the WHERE function, so that the shapes of deterministic sinusoidal responses at test frequencies of 1.2, 0.25, and 0.05 Hz are reasonably comparable with typical sinusoidal responses from our cat at these frequencies.

The final results and comparison with our cat's data are shown towards the end of this chapter.

Many of the system's parameters are fixed by physiological measurements and are not adjustable. Thus, we note in Figure 3.1 that $T_c' = 12$ sec, $T_N = 25$ sec, $T_e = 0.15$ sec fall into this category. In the high-gain amplifier of the neural pulse generator, the slope $a = 16.2$ and the intercept point $b = 40$ (both in Figure 4.7) are also based on neurophysiological observations as explained previously and, in any event, would not influence the main nystagmus pattern. This leaves the threshold value Q (Figure 5.11), and G and T_L (Figure 5.8) for making relatively small amounts of adjustments. However, G is constrained by (5.4.1) to the value of 0.5. Thus we are left with only Q and T_L as available for minor adjustments. Adjustment of these two parameters is discussed in the following two sections.

7.2 The adjustment of the threshold value Q

The initial estimate of the threshold value Q is adjusted so that the quick-phase frequency (in beats per sec) f_Q for the model step response and the quick-phase frequency per cycle f_Q' for the model sinusoidal response would match reasonably those from our cat.

After some trials and errors, we have obtained the final profile of Q as a function of the SCC output signal ϕ greater than 10 deg/sec as shown in Figure 5.9 and explained in section 5.4. For $0 < |\phi| < 10$, although we do not have data

from step responses to determine the value of Q for this region, we found a constant value of Q = 6 yields acceptable sinusoidal responses as explained in section 5.4.

According to Table 5.1 in Chapter 5, the mean value C_0 of the steady state deterministic WHERE curve is about 15 deg. Yet, in our model we saturated the deterministic WHERE curve at 12 deg for a canal signal greater than 22 deg/sec. This modification is concerned with the location of the WHEN curve which is $C_0 \pm Q$.

Although for the step inputs the deterministic WHEN curve appears to be shifted about a few degrees beyond 0 deg (e.g., 3 deg) in the direction of head motion, for the sinusoidal responses at 0.05 Hz with input peak head velocity of about 30 deg/sec the mean initiation point of quick-phases appears to be on the 0 degree line. Because of the large amount of uncertainty in the determination of C_0 and the location of the WHEN curve for step inputs and sine waves, and also because of the uncertainty in the determination of the 0 degree line and the smallness of the discrepancy, we arbitrarily chose C_0 as 12 deg.

The comparison of f_Q (for step input) and f_Q' (for sinusoidal input) from the model and from our cat is shown in Table 7.1 and 7.2, respectively. The results from the model are obtained with the parameter values as specified

in section 7.1 and with the noises (as described in section 7.4) added. Since the cat's data is noisy, the noises must be added to the model for consistent comparison on the same basis. In Table 7.1 the fact that f_Q matches fairly well between the cat and the model output indicates that our original estimation of the threshold value Q is approximately correct. This is because f_Q is approximately inversely proportional to Q at a constant slow-phase velocity since

$$f_Q = \frac{1}{\frac{Q}{V_Q} + \frac{Q}{V_s}} \simeq \frac{V_s}{Q} \qquad (7.2.1)$$

in which V_Q and V_s are respectively QP and SP mean velocity, and in which $|V_Q| >> |V_s|$. Equation 7.2.1 shows that f_Q is proportional to slow-phase eye velocity. Because of (7.2.1) we note that f_Q, for velocity steps, is not a very demanding criteria. All one needs to do is to get Q correct.

Table 7.1

Step Responses

	Cat	Model
$\dot{\theta}_s$	f_Q	f_Q
deg/sec	sec^{-1}	sec^{-1}
8.9	1.2	1.3
21.0	1.7	1.8
30.8	2.2	2.6
46.5	2.5	2.9

$\dot{\theta}_s$ slow-phase eye velocity in deg/sec

f_Q quick-phase frequency per sec

Table 7.2

Sinusoidal Response

		Cat	Model
f	$\dot{H}_M$	f'_Q	f'_Q
Hz	deg/sec	cycle^{-1}	cycle^{-1}
1.2	30	1.1	2.0
0.25	30	6.6	7.9
0.05	30	23.0	24.0

f frequency of the input sinusoidal head velocity in Hz

$\dot{H}_M$ amplitude of the input sinusoidal head velocity in deg/sec

f'_Q quick-phase frequency (in beats) per cycle of the input frequency

In Table 7.2, f'_Q also matches fairly well except at $f = 1.2$ Hz. Although the model makes a quick-phase at each half-cycle without fail at $f = 1.2$ Hz, the cat makes on the average only one quick-phase each cycle. The reason that might account for this will be discussed in a later section on hysteresis.

7.3 The adjustment of the time constant T_L in the WHERE function

The transfer function of the lagged portion of the WHERE function is given by (5.3.5) as

$$\frac{f(s)}{\phi(s)} = \frac{G}{sT_L + 1} \qquad (7.3.1)$$

For G = 0.5 and T_L near 0.6 as a rough estimate, the break-frequency of (7.3.1) is about 0.27 Hz. Thus, for an input frequency of f =1.2 Hz, (7.3.1) reduces to

$$\frac{f(s)}{\phi(s)} = \frac{G}{T_L} \frac{1}{s} \qquad (7.3.2)$$

which acts as a pure integrator. For this reason, at f = 1.2 Hz the phase shift is close to 90 degrees and its change due to variation of T_L is small compared with the amplitude change due to the same cause.

Figure 7.1 describes how the component of the deterministic WHERE curve $\bar{C}(t)$ is shaped for an input $\phi(t)$ given by

$$\phi(t) = A \sin 2\pi ft \qquad (7.3.3)$$

with f = 1.2. In Figure 7.1, g(t) is the step portion of $\bar{C}(t)$ as described in the lower portion of Figure 5.8 with $g' = 1$. Thus, $\bar{C}(t) = f(t) + g(t)$.

In Figure 7.2, the interaction of the eye position with $\bar{C}(t)$ and the deterministic WHEN curve $\bar{D}(t)$ is shown [it is drawn parallel to $\bar{C}(t)$ for simplicity although in the model it is not quite (see section 5.4)]. As T_L is increased, the quick-phase end-points q_1, q_2, and q_3 would move closer to the line $\bar{C}(t) = 0$, and the slow-phase end-points S_1, S_2, and S_3 would move further away from it. If we denote by $|\theta_s|_M$ the maximum magnitude of the slow-phase eye position change in the transition region (Figure 7.2), this would make $|\theta_s|_M$ bigger, thus altering the shape of the VOR response. Figure 7.3 shows the effect of increasing the value of T_L by a factor of about two.

Figure 7.1

This figure describes a sinusoidal SCC signal $\phi(t)$ around 1.2 Hz, and the components $f(t)$ and $g(t)$ of the corresponding deterministic WHERE curve which is generated by $\phi(t)$. Two curves are shown for $f(t)$. The dashed curve shows what happens if T_L is doubled. At this frequency the amplitude of $f(t)$ is so small, even for A equal to 30 deg/sec, that it does not reach the clipping level.

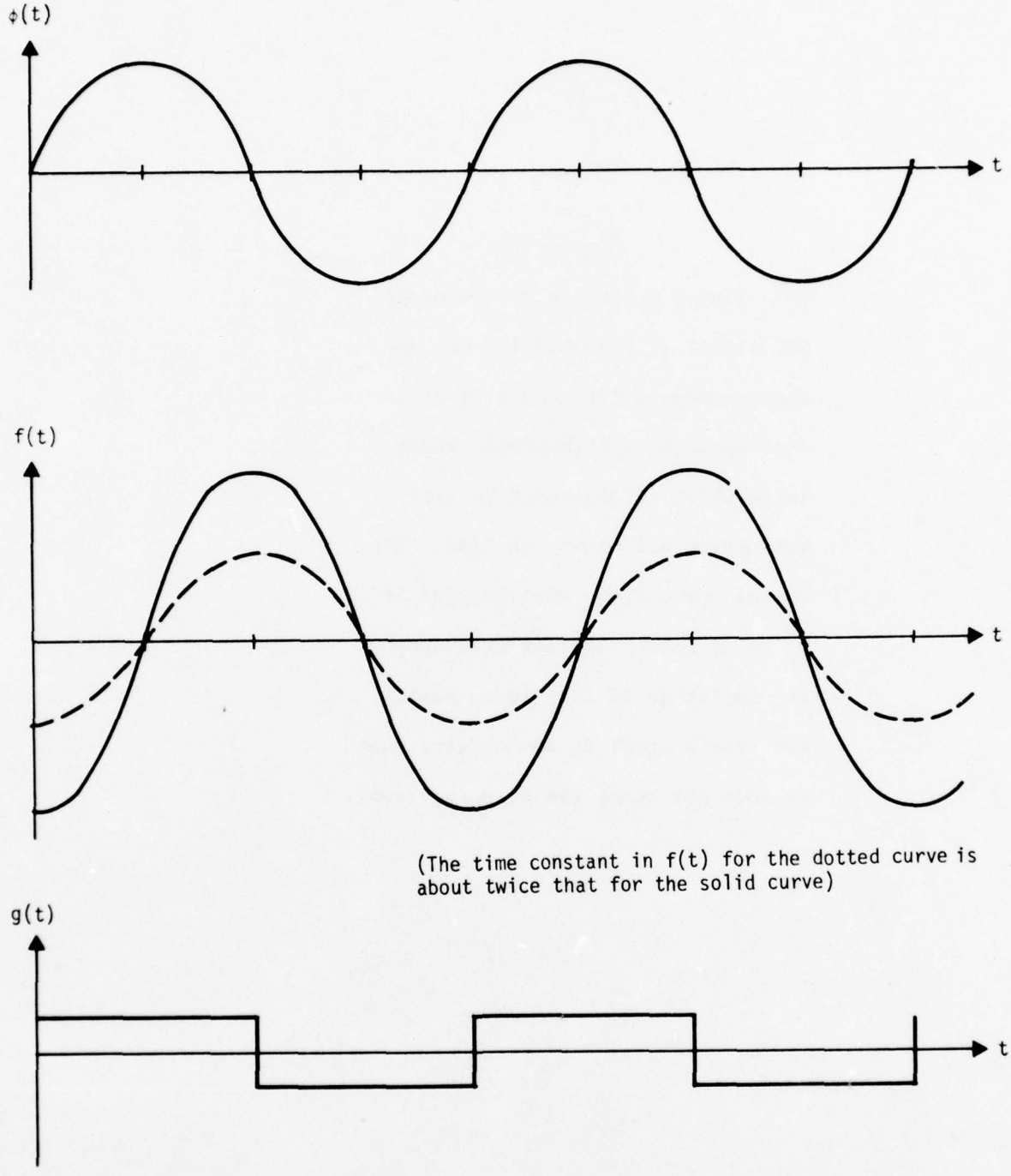

Figure 7.1 The Components of the Deterministic WHERE Curve for Sinusoidal Input (1.2 Hz).

Figure 7.2

This figure shows the deterministic WHERE curve and WHEN curves corresponding to Figure 7.1 (with f(t) represented by the solid line), and also shows the interaction between eye position and the deterministic WHERE and WHEN curves.

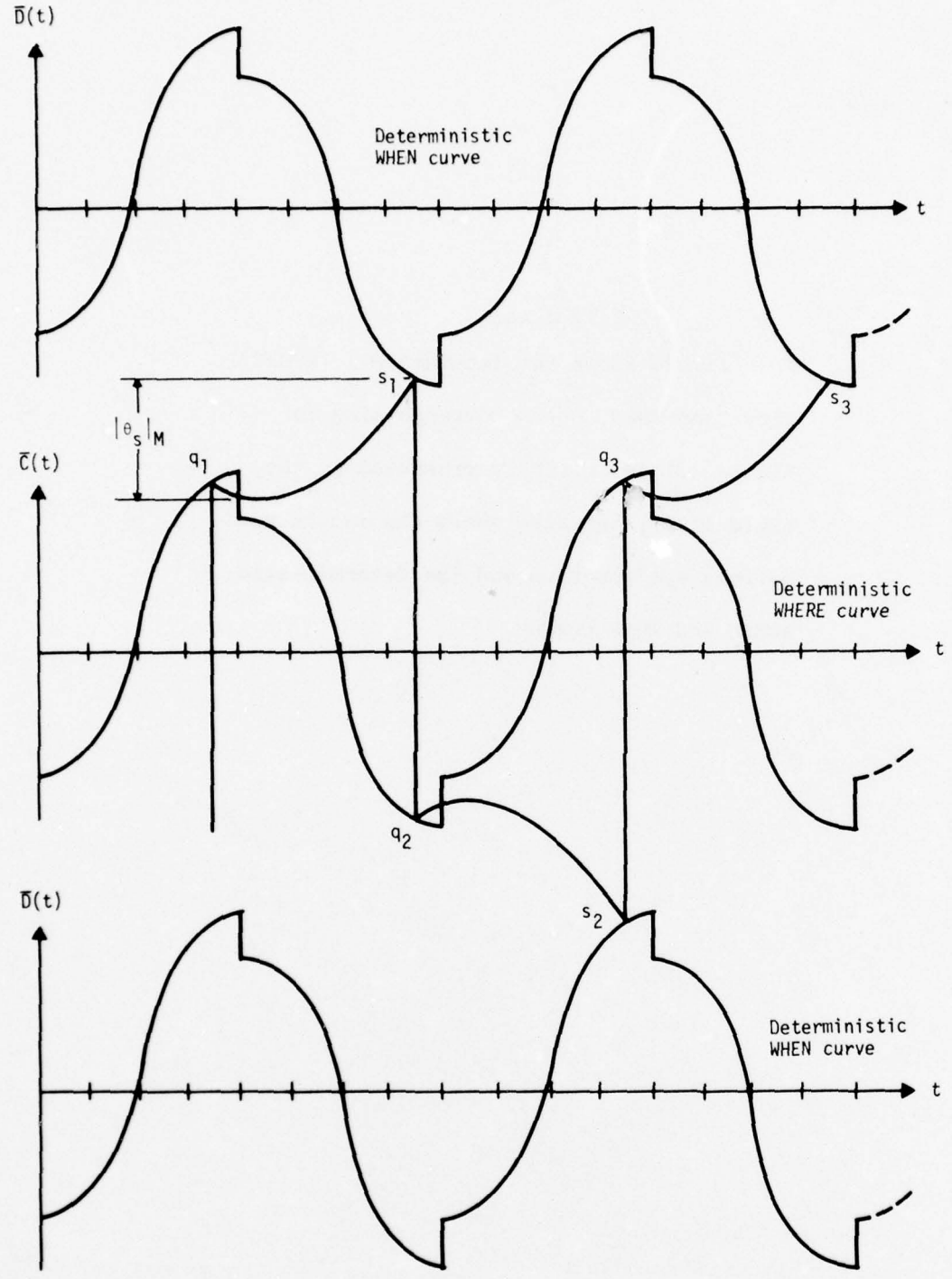

Figure 7.2 Interaction Between Eye Position and WHERE and and WHEN Curves (corresponds to the solid curve of f(t) in Figure 7.1)

Figure 7.3

This figure shows the deterministic WHERE curve and WHEN curves corresponding to Figure 7.1 (with f(t) represented by the dotted line), and also shows the interaction between eye position and the deterministic WHERE and WHEN curves.

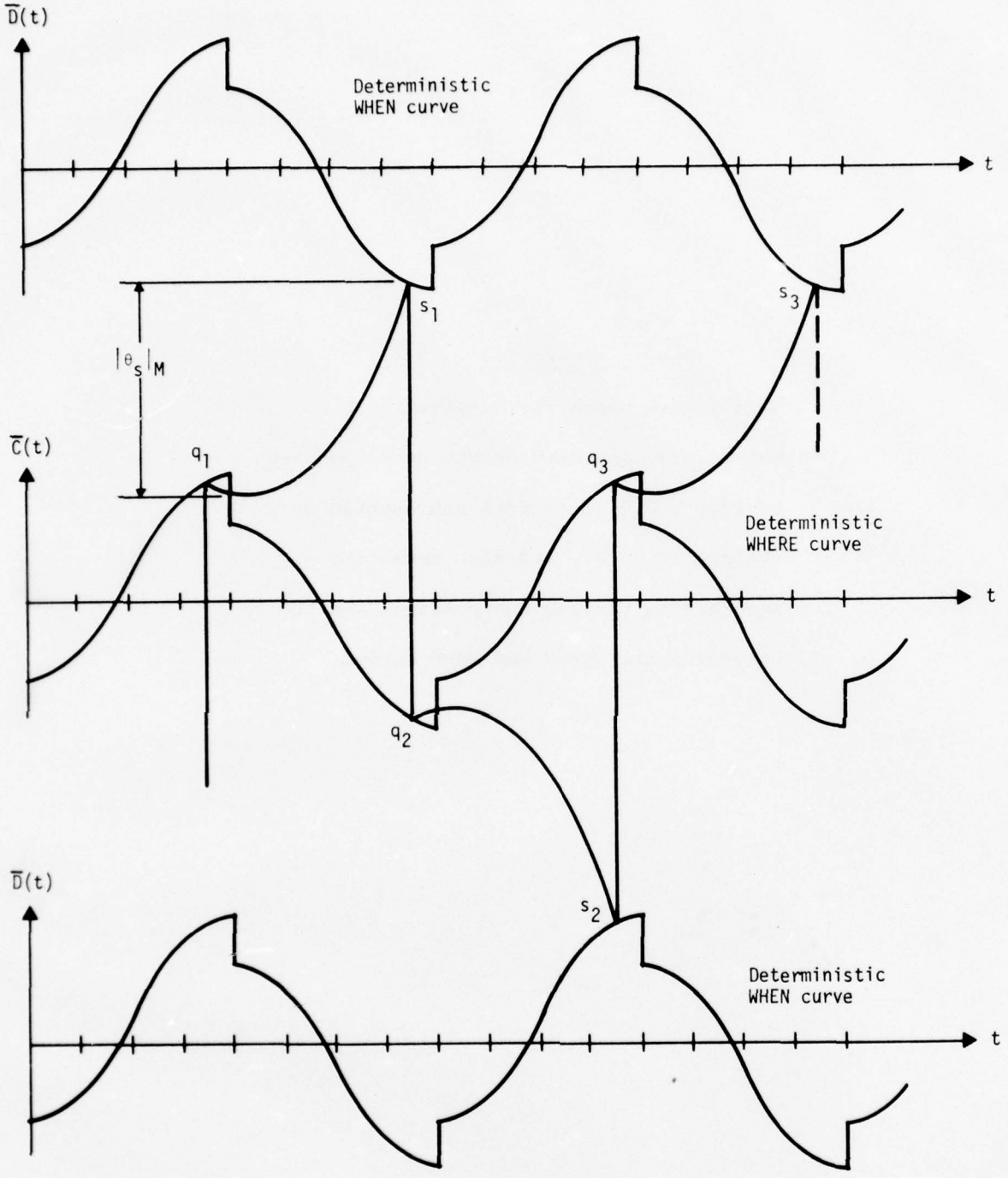

Figure 7.3 Interaction Between Eye Position and WHERE and WHEN curves (corresponds to dotted curve of f(t) in Figure 7.1)

After some trials and errors, we have found that $T_L = 0.6$ gives a good approximation to the shape (ratio $\frac{|\theta_s|_M}{Q}$) of the VOR response for f = 1.2 Hz with A = 30 in (7.3.3). The sinusoidal VOR response is more sensitive to T_L at f = 1.2 Hz because of (7.3.2). At f = 0.25 Hz and f = 0.05 Hz, $|sT_L|$ is not much greater than 1 in (7.3.1) and the nystagmus is relatively independent of T_L. In the step responses, the determination of T_L was based on rough visual inspection of curves such as in Figure 5.4 B-F. This was an uncertain way to estimate T_L. For this reason, the value of T_L is adjusted at 1.2 Hz and $T_L = 0.6$ was adopted for our model.

7.4 The variance of the noise input to the model

Referring to Figure 6.3, we can see that the standard deviations $\sigma(r_1^*)$ and $\sigma(r_2^*)$ depend on $\sigma(W_{x_1})$, $\sigma(W_{x_2})$, $\sigma(W_{z_1})$, and $\sigma(W_{z_2})$. Because of (6.3.39), we note that $\sigma(W_{x_1}) = C\sigma(W_{x_2})$ and $\sigma(W_{z_1}) = C\sigma(W_{z_2})$ in which C is given by (6.3.47). For given (experimentally obtained) $\sigma(r_1^*)$ and $\sigma(r_2^*)$, the values of $\sigma(W_{x_2})$ and $\sigma(W_{z_2})$ are determined by means of (6.4.1) to (6.4.5) along with (6.3.64).

According to the data from our cat's responses for step input head velocities, $\sigma(r_1^*) \simeq 5$ deg and $\sigma(r_2^*) \simeq 2.5$ deg for $|\phi| \gtrsim 22$ deg/sec. That is, the noise on the WHEN curve is about twice as big as the noise on the WHERE curve. This

would naturally make the linear correlation coefficient between each slow-phase magnitude and the subsequent quick-phase magnitude bigger than that between each quick-phase magnitude and subsequent slow-phase magnitude. Indeed, the value of the former is 0.846, while that of the latter is 0.326.

However, when we run our model with the computed values of $\sigma(W_{x_2})$ and $\sigma(W_{z_2})$, we have observed some "backward" quick-phases in the same direction as the ongoing slow-phases in the step responses from our model. Around ϕ = 22 deg/sec, we have observed more than a few of them for each computer run.

The backward quick-phase occurs when the slow-phase eye movement crosses the WHEN curve in the region in which the WHERE curve and the WHEN curve overlap as shown in Figure 7.4. Note that, in our model, whenever the eye crosses the WHEN curve it seeks the WHERE curve regardless of where that curve may be located. The probability of the two curves being overlapped increases as $|\phi|$ falls below 22 deg/sec because of the decreasing value of Q (see Figure 5.9).

Figure 7.4

This figure shows the situation in which the backward quick-phase occurs when the slow-phase eye movement crosses the WHEN curve in the region in which the WHERE curve and the WHEN curve overlap.

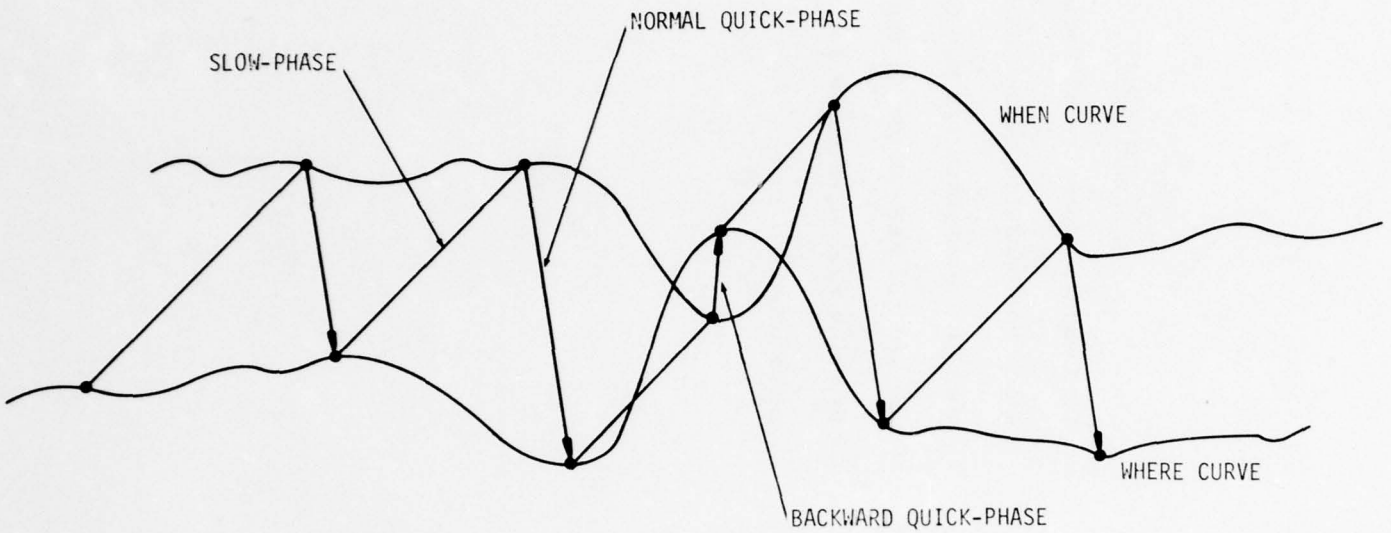

Figure 7.4 Backward Quick-Phase

Because we have not observed any backward quick-phases in our cat's step responses, with several trials for head velocities equal to or over 10 deg/sec, we have decided to eliminate them by controlling the noise generation at its source level, rather than at its output level. That is, we have decided to eliminate them by limiting the magnitude of the four one-dimensional independent Gaussian sequences (with zero mean and variance 1) from which W_x and W_z are generated, until no backward quick-phases are observed in the model output for step input head velocities above 22 deg/sec. We have observed that by limiting the magnitudes of the Gaussian sequence sources to 1.65 times their standard deviations (which are all equal to one), we could eliminate the backward quick-phase for $|\phi| \geq 22$. For a Gaussian distribution, with this limitation, 90% of all possible numbers are still included. Every time this limit is exceeded, the computer brings out another number from the Gaussian distribution until the requirement is met. This results in another distribution which is approximately Gaussian with slightly smaller variance than the original one. This would somewhat decrease the predicted output variances. These variances are subject to a further decrease due to another problem which we call the "shading effect" to be discussed later in this section (see Table 7.3). Due to

the SCC's 12-second time constant, the number of data points in each step response from our cat is limited to not more than about a dozen points. In addition, the platform on which our cat is rotated was not servo-controlled and, therefore, could not maintain a constant velocity within an individual run or several runs intended for the same nominal head velocity. Under these situations, statistics have large variabilities and we have not insisted too much on an exact numerical match between model and experimental statistics.

The probability of the two curves being overlapped increases as $|\phi|$ falls below 22 deg/sec because of the decreasing threshold value Q, as mentioned before. This necessitates decreasing the values of $\sigma(W_{x_2})$ and $\sigma(W_{z_2})$ to prevent backward quick-phases at lower velocities. In addition, for values of ϕ near zero, it was necessary to decrease the values of $\sigma(W_{x_2})$ and $\sigma(W_{z_2})$ for the following additional reason. For a sinusoidal input head velocity of 0.05 Hz (with an amplitude of about 30 deg/sec), the transition region within which the slow-phase of the VOR response goes through zero velocity (t_{TR} in Figure 7.21) is about 2 seconds. Too much noise near zero velocity interrupts this transition region with quick-phases, making the resulting duration t_{TR} much too short.

One problem in this regard is that cats make saccades in the dark. Perhaps the rapid eye movements that occur for very small head velocities, whether in the step responses or in the transition region of low frequency sinusoidal responses, are really saccades and not quick-phases. However, for modeling purposes only, we assume this model, which has no saccadic system, should not make quick-phases for very small head velocities. In practice, when the head is still, the model should produce no rapid eye movements. To do this, it is necessary to greatly reduce the noise when $|\phi| = 0$.

One way to meet these requirements is to reduce $\sigma(x_2)$ and $\sigma(z_2)$ of x_2 and z_2 (see Figure 6.3) for low velocities. It is often the case in neurophysiology that a reduced intensity of a neural signal is accompanied by a reduction in its noise. In the model, $\sigma(x_2)$ and $\sigma(z_2)$ for $|\phi| < 22$ are made to be proportional to $|\phi|^3$ as explained below. We have assumed that $\sigma(x_2)$ and $\sigma(z_2)$ should be monotonically decreasing as $|\phi|$ approaches zero, and should become zero at $|\phi| = 0$, although it does not have to become zero at $|\phi| = 0$. At $|\phi| = 22$, we require that $\sigma(z_2) = \frac{1}{\tau_1}\sigma(r_2^*) = 2.5$ for $\tau_1 = 1$ [see (6.4.2)] and $\sigma(x_2) = \frac{1}{\tau_1}\sqrt{\sigma^2(r_1^*) - \sigma^2(r_2^*)} = \sqrt{5^2 - 2.5^2}$ for $\tau_1 = 1$ [see (6.4.3)] to meet the boundary condition at $|\phi| = 22$. Note that $\sigma(x_2)$ and $\sigma(z_2)$, for $|\phi| > 22$, are constant and have the same values as at $|\phi| = 22$.

The profiles of $\sigma(x_2)$ and $\sigma(z_2)$ are shown in Figure 7.5, in which the values of K_1 and K_2 are determined by the boundary conditions at $|\phi| = 22$. We have used a cubic function of $|\phi|$ because a linear or square function does not reduce the noise level fast enough to meet our requirement for the duration of the transition region t_{TR} at f = 0.05 Hz. This cubic noise condition also eliminates all backward quick-phases for $|\phi| < 22$. The profiles of the variances of $\sigma(x_2)$ and $\sigma(z_2)$ in Figure 7.5 are created in the model by similarly shaping the variances of the noise sources σ_{wx} and σ_{wz}. That is, in the model $\sigma_{wz2} = 0.4058\tau_1\sigma(x_2)$ and $\sigma_{wz2} = 0.4058\tau_1\sigma(z_2)$ based on (6.4.4) and (6.4.5). According to (6.3.64) and (6.3.65), $[F(\tau_1, \tau_2, T)]^{\frac{1}{2}}$ is 0.4058 for $\tau_1 = 1$, $\tau_2 = 0.125$ and T = 0.01.

We recognize that these limitations on noise would cause decreases in $\sigma(r_1^*)$ and $\sigma(r_2^*)$ computed from the model output at low velocities in addition to decreases in $\sigma(r_1^*)$ and $\sigma(r_2^*)$ caused by clipping off the peaks of the one-dimensional Gaussian sources for all velocities. There is still another reason that $\sigma(r_1^*)$ would be further decreased. We call it the "shading effect" (Figure 7.6). As slow-phase velocity becomes smaller, the eye position tends to touch the WHEN curve more often near its lower peaks as shown in Figure 7.6. This would naturally make the sampled WHEN noise less

Figure 7.5

This figure shows the profiles of the standard deviations $\sigma(x_2)$ and $\sigma(z_2)$ of noises $x_2(t)$ and $z_2(t)$ used in our stochastic VOR model.

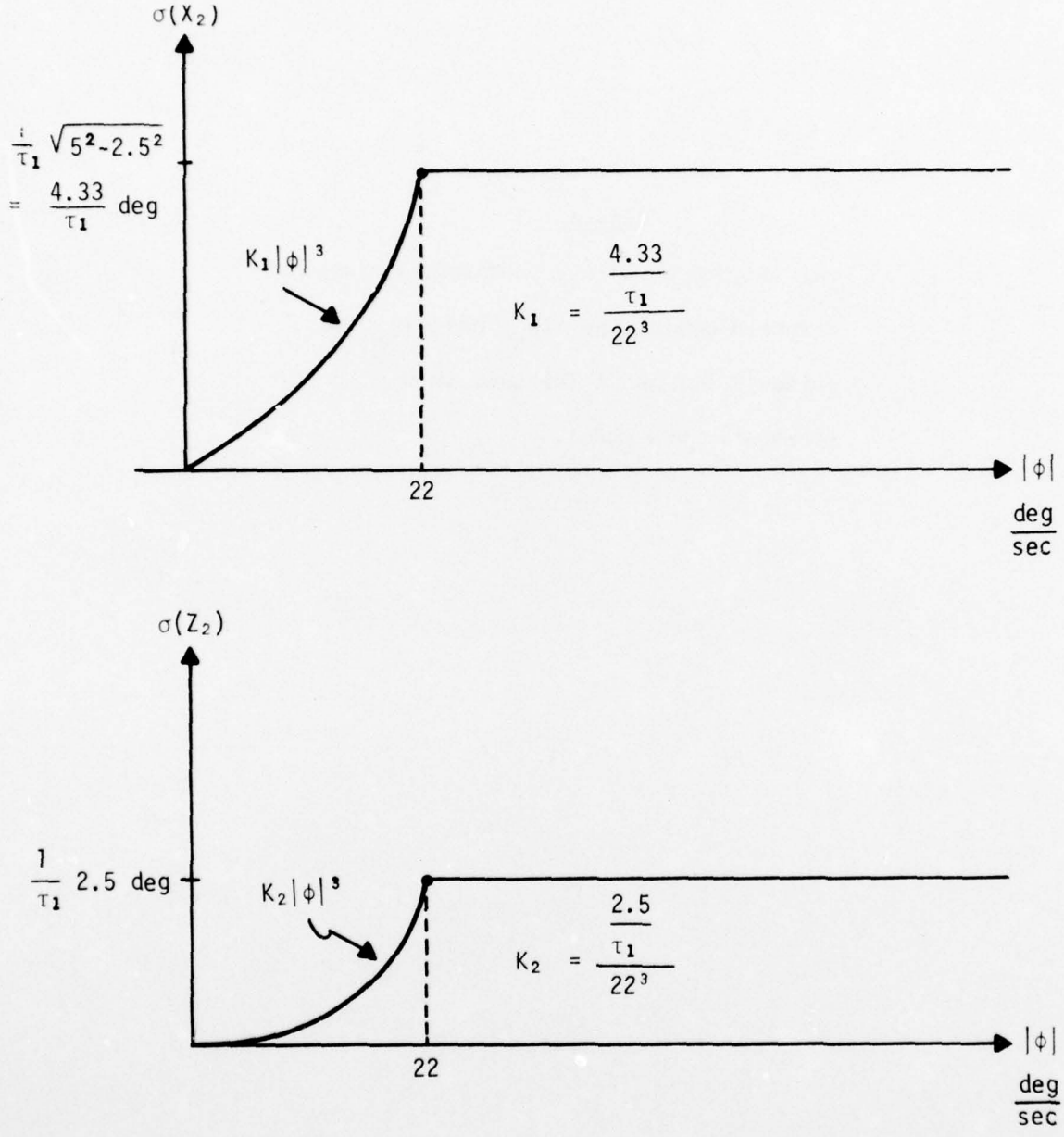

Figure 7.5 Profiles of the Standard Deviations $\sigma(x_2)$ and $\sigma(z_2)$

Figure 7.6

This figure shows what we call "shading effect" in which as slow-phase velocity becomes smaller, the eye position tends to touch the WHEN curve more often near its lower peaks.

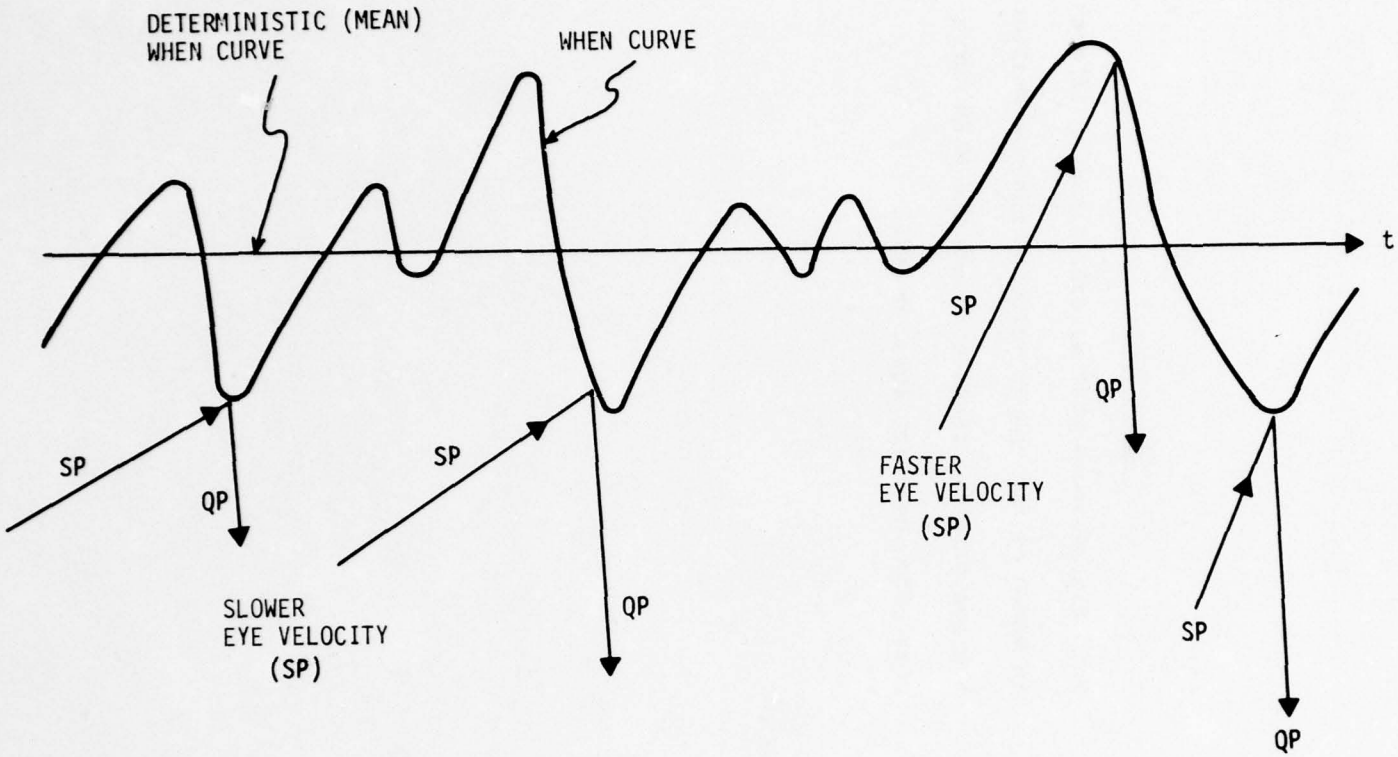

Figure 7.6 Shading Effects

fluctuating, thus making $\sigma(r_1^*)$ smaller. However, as the eye velocity becomes faster, $\sigma(r_1^*)$ would gradually increase approaching the standard deviation $\sigma(r_1)$ of the noise itself. Thus, calculated values of $\sigma(r_1)$ overestimate the actual values of $\sigma(r_1^*)$ produced by the model. The "shading effect" is only a problem for the sampled WHEN curve, and not the sampled WHERE curve.

Before closing this section, we want to make a comment on the refractory period of 50 msec for quick-phases instead of 200 msec. Originally we started with a 200 msec refractory period in our model because we assumed at first that the refractory period for quick-phases must be similar to that for saccades which is recognized as about 200 msec. However, with a 200 msec refractory period the linear correlation coefficient R_{12} (6.4.6) from the model was much too low compared with those obtained from the cat's data. The reason was that when the noise demanded a short duration SP (e.g., 6 deg in size at a velocity of 40 deg/sec which takes only 0.15 sec) the refractory period would not allow it. This causes $\Delta\theta$ to cross the WHEN curve and the quick-phase occurred later at an eye position that was not on the WHEN curve, and which was consequently uncorrelated with the WHERE curve. With this in mind, we have carefully re-examined the cat's analogue data, and found that the refractory period for our cat is actually only 50 msec instead of 200 msec, contrary to our previous assumption. After we have changed the refractory period to the new value of

50 msec, the values of R_{12} increased, giving acceptable results compared with that from our cat as shown in Table 7.3.

7.5 Results

The final results are obtained with parameter values and noise models determined as previously described. In what follows, the results obtained from the VOR model output for various step input head velocities are shown in subsection (A), and the results for sinusoidal input head velocities are shown in subsection (B). The discussion of the results and other comments are given in section 7.6 and section 7.7.

(A) Results - step input head velocity

The typical step responses from our cat are shown in Figures 7.7, 7.8, 7.9, and 7.10. The corresponding step responses from the stochastic (with noise) VOR model for similar input head velocities are shown in Figures 7.11, 7.12, 7.13, and 7.14.

The numerical results from our cat and from our VOR model for various step input head velocities are shown in Table 7.3, in which various symbols have the following meanings:

$\dot{\theta}_s$: slow-phase eye velocity in deg/sec

σ_{WN}: standard deviation of the sampled noisy WHEN signal in deg

σ_{WR}: standard deviation of the sampled noisy WHERE signal in deg

R_{12}: linear correlation coefficient between the WHEN and WHERE signal [same as R_{12} of (6.4.6)]

Table 7.3. Step Responses

$\dot{\theta}_s$ (deg/sec)	σ_{WN} cat (deg)	σ_{WN} model (deg)	σ_{WR} cat (deg)	σ_{WR} model (deg)	R_{12} cat	R_{12} model
8.9	3.8	0.5	2.5	0.4	0.46	0.67
21.0	5.0	3.0	2.7	1.6	0.34	0.32
30.8	4.7	3.4	2.1	1.8	0.30	0.30
46.5	4.9	3.5	2.8	1.7	0.27	0.16

Figure 7.7, 7.8, 7.9, and 7.10

These figures show the responses from our cat for various step input head velocities.

AD-A042 342 NAVAL SURFACE WEAPONS CENTER DAHLGREN LAB VA F/G 6/4
MATHEMATICAL MODEL OF THE VESTIBULOOCULAR REFLEX.(U)
JUN 77 K S CHUN
UNCLASSIFIED NSWC/DL-TR-3669 NL

3 OF 3
AD
A042342

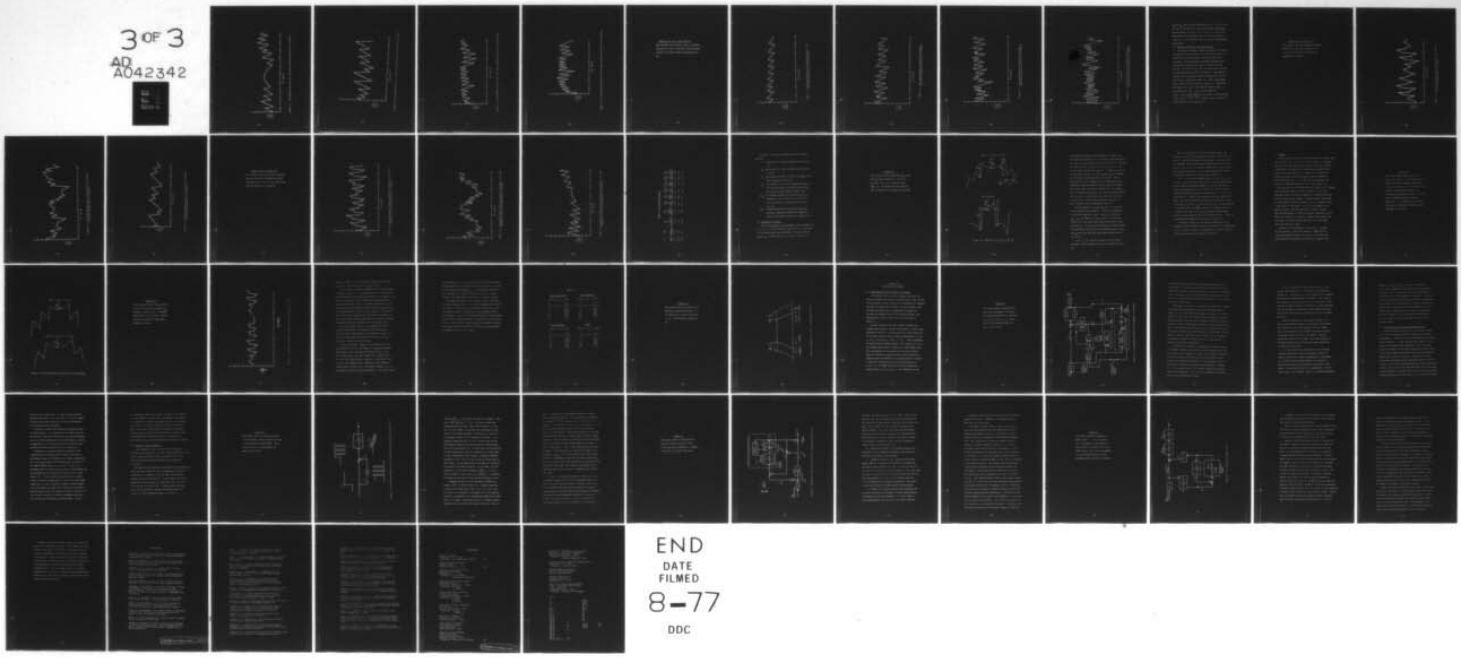

END
DATE
FILMED
8-77
DDC

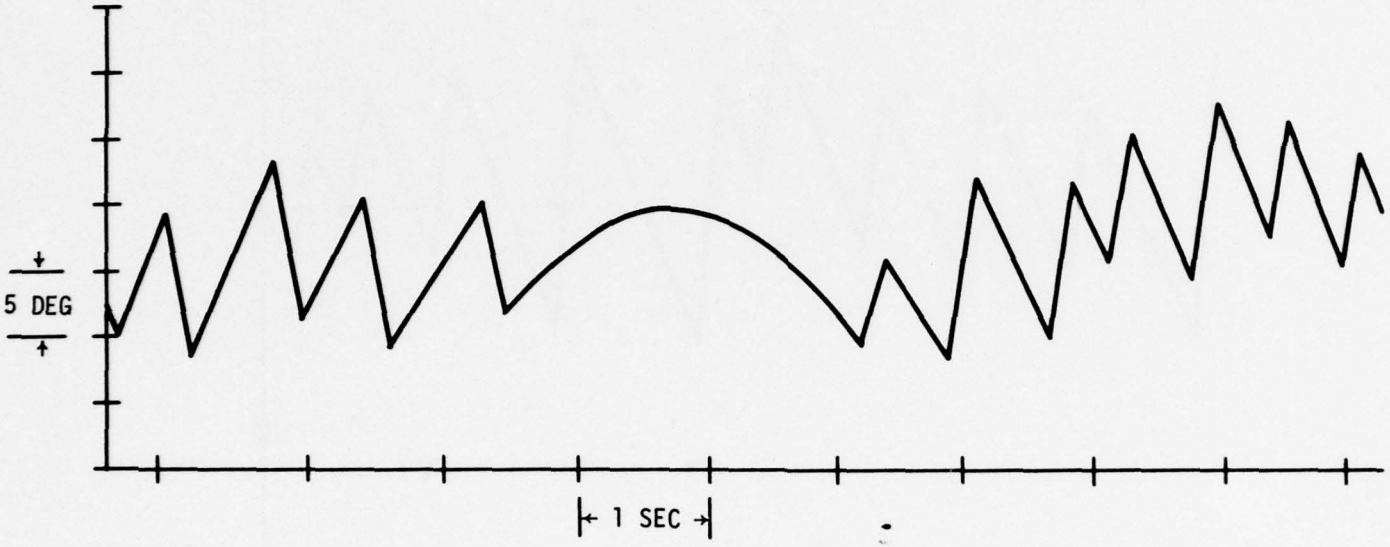

Figure 7.7 Step Response from Our Cat (with mean slow-phase velocity of 8.9 deg/sec)

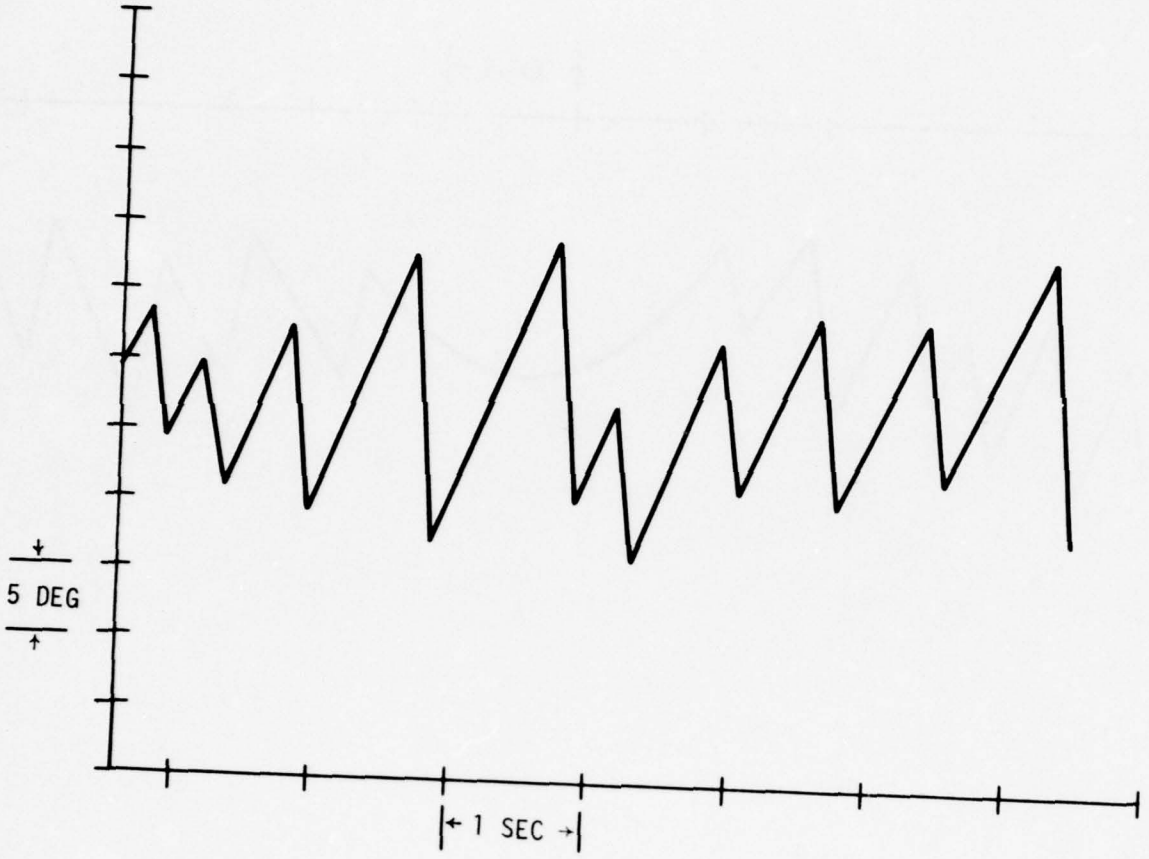

Figure 7.8 Step Response from Our Cat (with mean slow-phase velocity of 21.0 deg/sec)

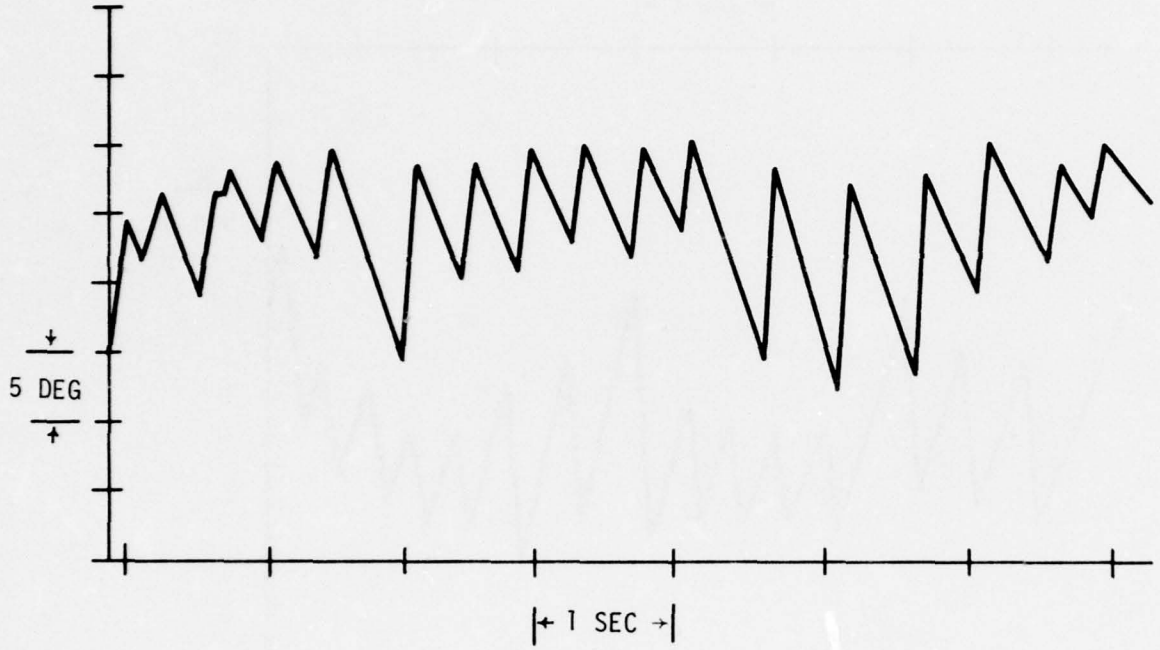

Figure 7.9 Step Response from Our Cat (with mean slow-phase velocity of 30.8 deg/sec)

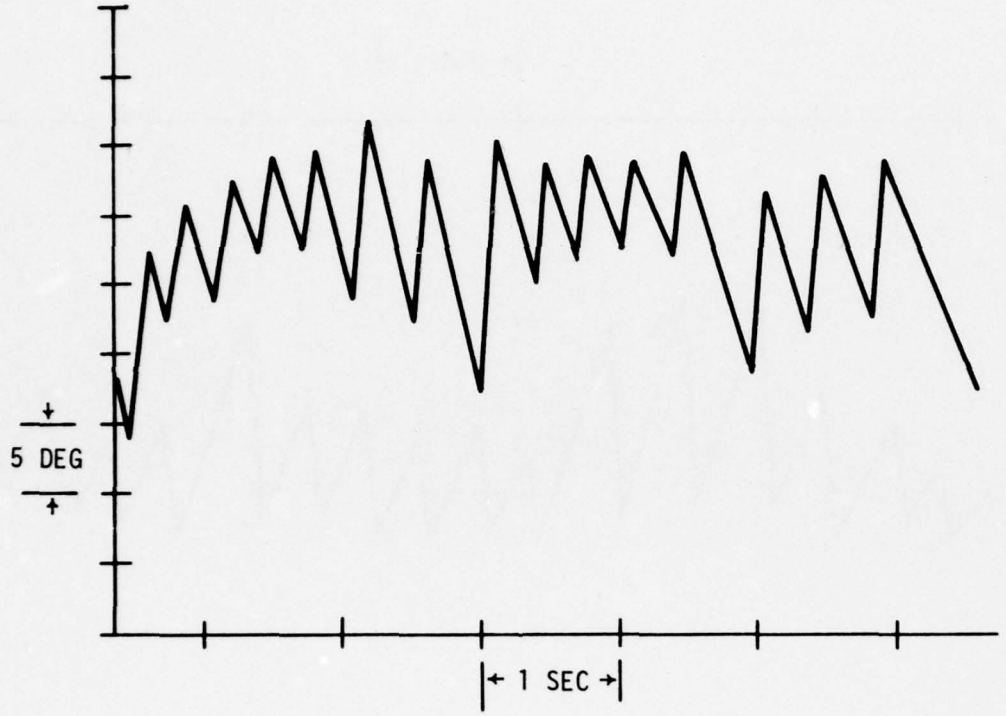

Figure 7.10 Step Response from Our Cat (with mean slow-phase velocity of 46.5 deg/sec)

Figures 7.11, 7.12, 17.13, and 7.14

These figures show responses from our stochastic VOR model for various step input head velocities similar to the input velocities applied to our cat.

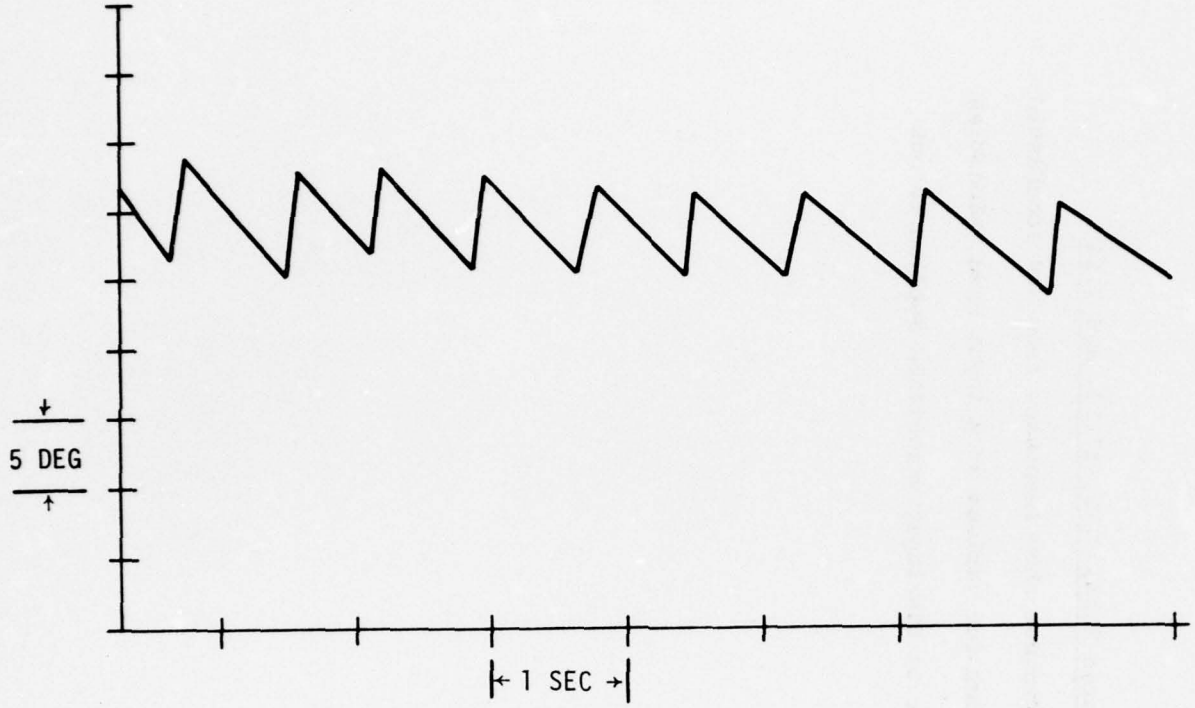

Figure 7.11 Step Response from Our Stochastic VOR Model (with mean slow-phase velocity of 8.9 deg/sec)

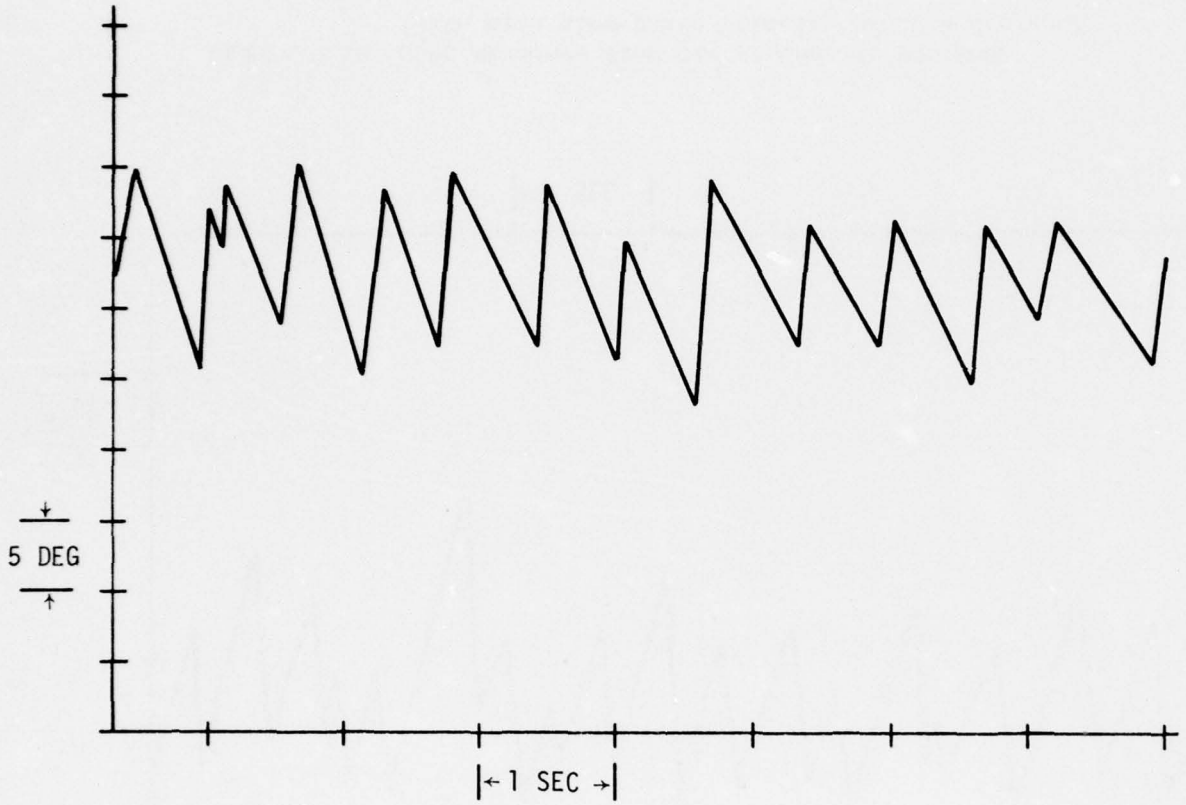

Figure 7.12 Step Response from Our Stochastic VOR Model
(with mean slow-phase velocity of 21.0 deg/sec)

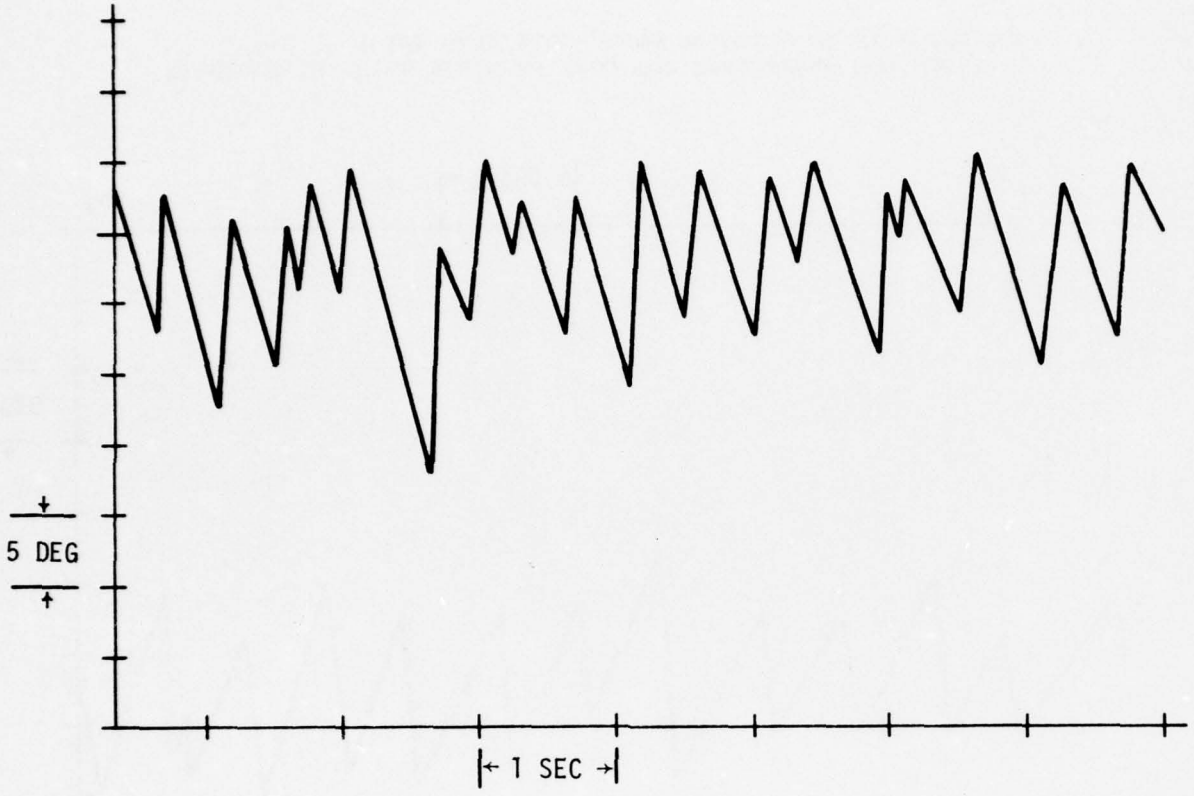

Figure 7.13 Step Response from Our Stochastic VOR Model
(with mean slow-phase velocity of 30.8 deg/sec)

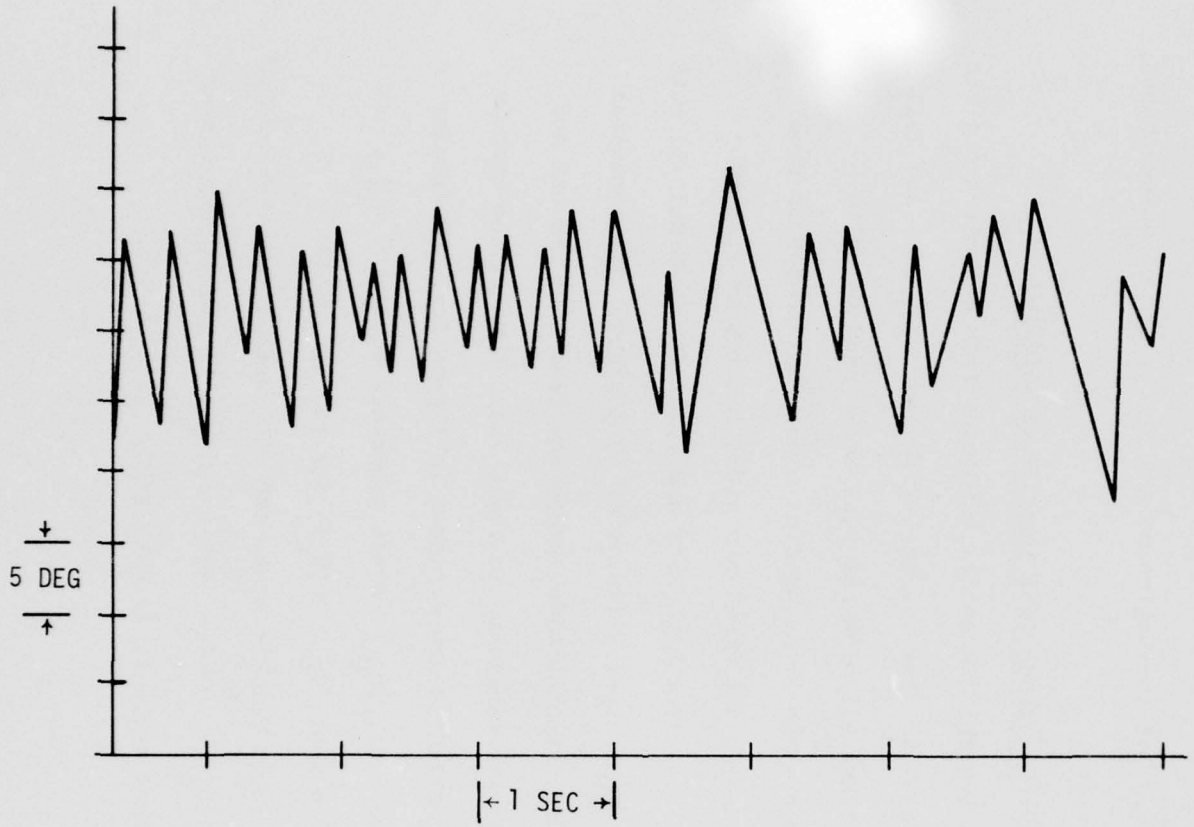

Figure 7.14 Step Response from Our Stochastic VOR Model
(with mean slow-phase velocity of 46.5 deg/sec)

σ_{WN} and σ_{WR} from the model correspond to $\sigma(r_1^*)$ and $\sigma(r_2^*)$ of r_1^* and r_2^* in Figure 6.3. More specifically, σ_{WN} and σ_{WR} from the model are computed by the computer (using running means) based on the efference copy of the eye position θ' (Figure 6.2) at the beginning and at the end of quick-phases, respectively.

(B) Results - sinusoidal input head velocity

The typical sinusoidal responses from our cat are given in Figures 7.15 (for 1.2 Hz), 7.16 (for 0.25 Hz), and 7.17 (for 0.05 Hz) all with the peak input head velocity of 30 deg/sec. The corresponding sinusoidal responses from our stochastic VOR model are given in Figures 7.18 (for 1.2 Hz), 7.19 (for 0.25 Hz), and 7.20 (for 0.05 Hz) all with the same peak input velocity of 30 deg/sec. The numerical results of the sinusoidal responses from both the cat and the model are tabulated in Table 7.4. Some of the symbols used in Table 7.4 are depicted in Figure 7.21. Referring to Figure 7.21, $|\theta_{Q_1}|$ is not generally equal to $|\theta_Q|_2$. It may happen that $|\theta_Q|_1 > |\theta_Q|_2$ for the cat while $|\theta_Q|_1 < |\theta_Q|_2$ for the model and vice versa. We have defined $|\bar{\theta}_Q|$ by $|\bar{\theta}_Q| = \frac{|\theta_Q|_1 + |\theta_Q|_2}{2}$ simply to get an estimate of Q when head velocity is near zero.

Figures 7.15, 7.16, and 7.17

These figures show the sinusoidal responses from our cat with input frequencies of 1.2 Hz, 0.25 Hz, and 0.05 Hz, and with amplitude of 30 deg/sec.

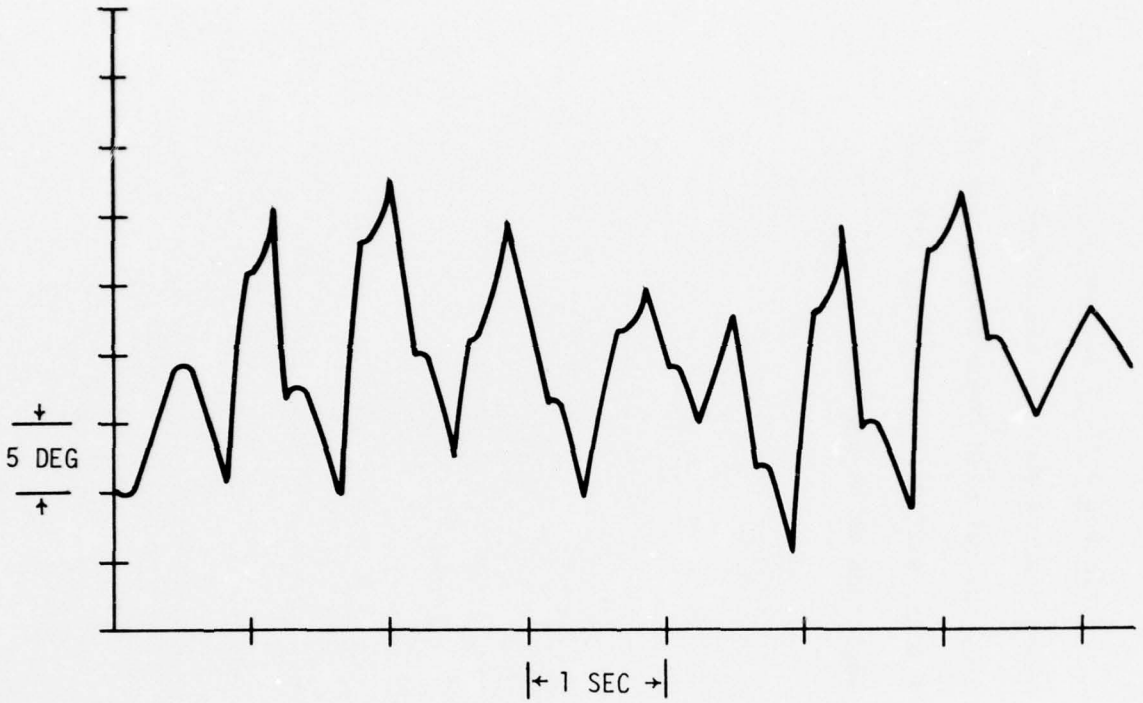

Figure 7.15 Sinusoidal Response from Our Cat (with input frequency of 1.2 Hz and amplitude of 30 deg/sec)

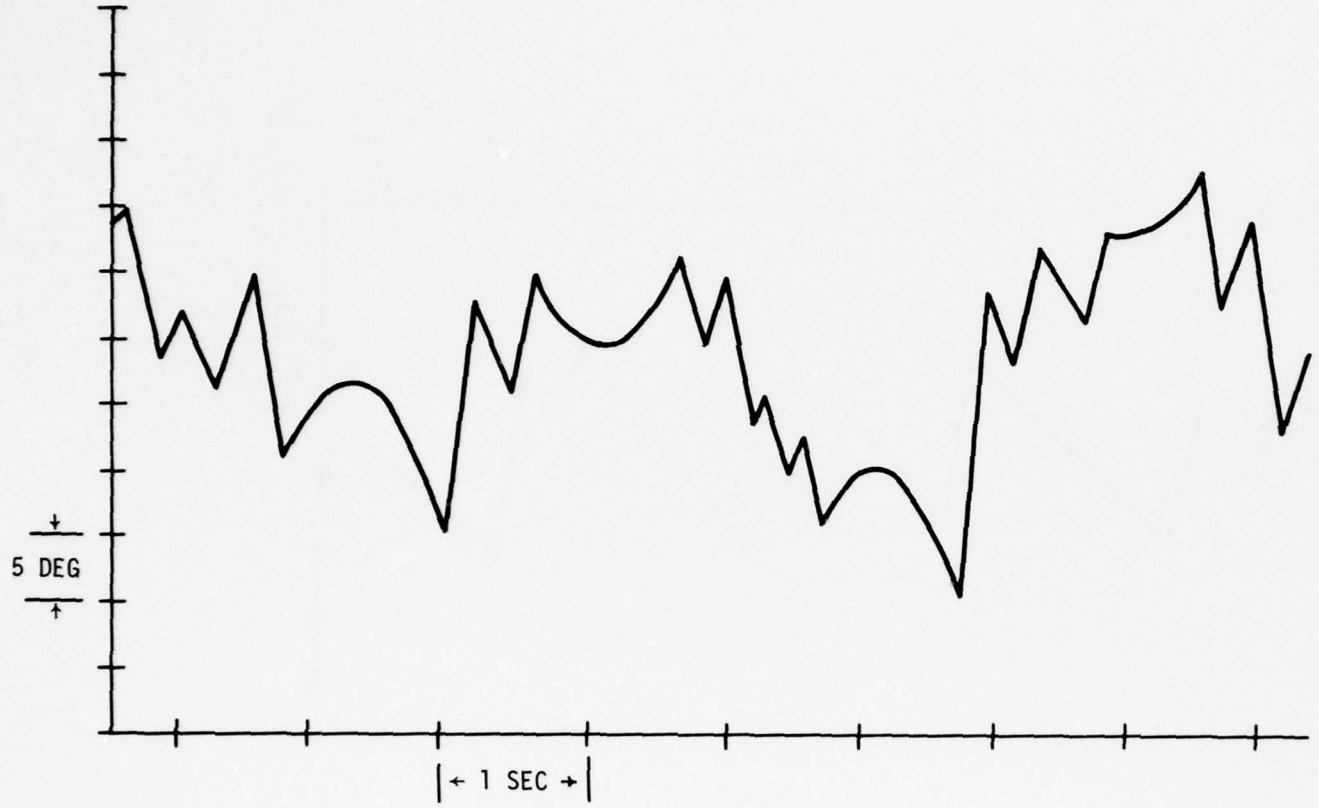

Figure 7.16 Sinusoidal Response from Our Cat (with input frequency of 0.25 Hz and amplitude of 30 deg/sec)

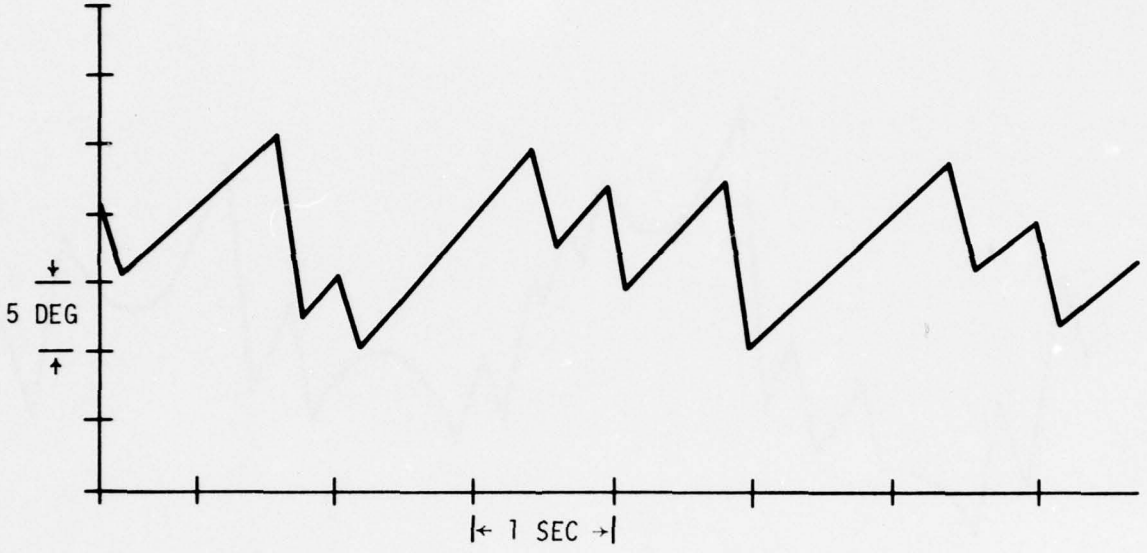

Figure 7.17 Sinusoidal Response from Our Cat (with input frequency of 0.05 Hz and amplitude of 30 deg/sec)

Figures 7.18, 7.19, and 7.20

These figures show the sinusoidal responses from our stochastic VOR model with input frequencies of 1.2 Hz, 0.25 Hz, and 0.05 Hz, and with amplitude of 30 deg/sec.

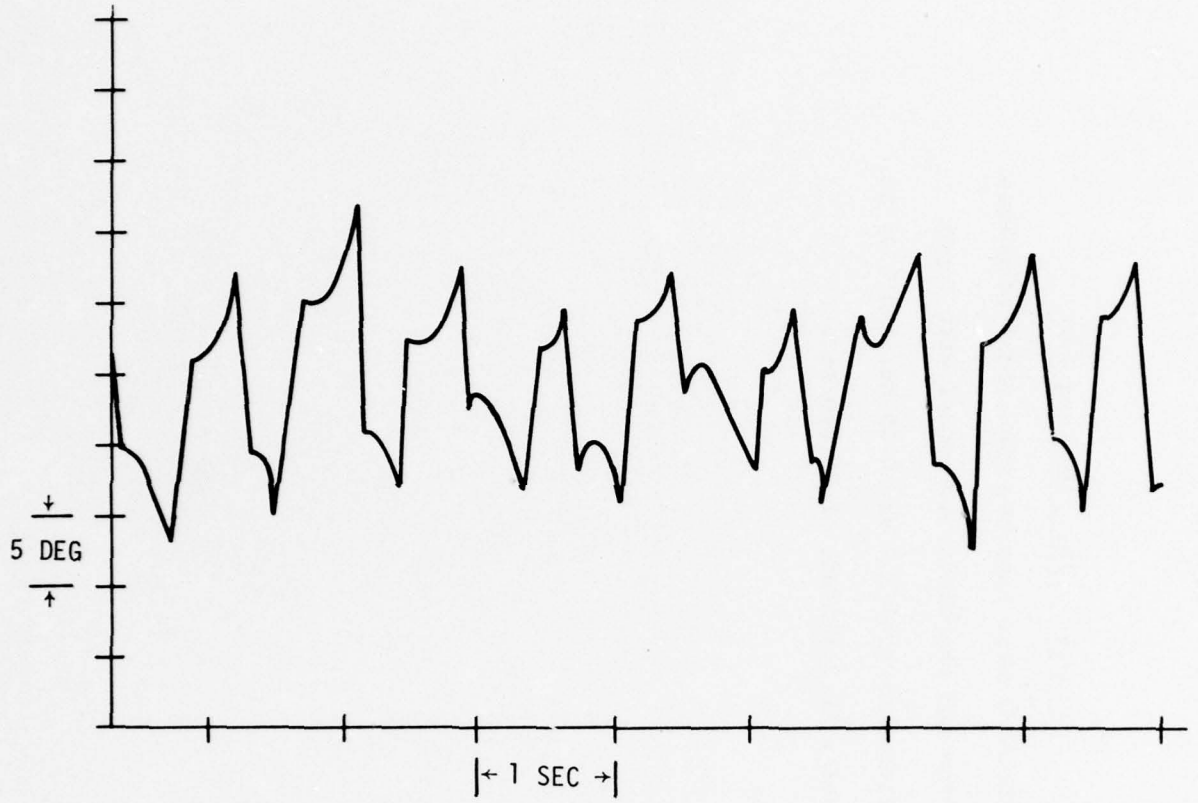

Figure 7.18 Sinusoidal Response from Our Stochastic VOR Model (with input frequency of 1.2 Hz and amplitude of 30 deg/sec)

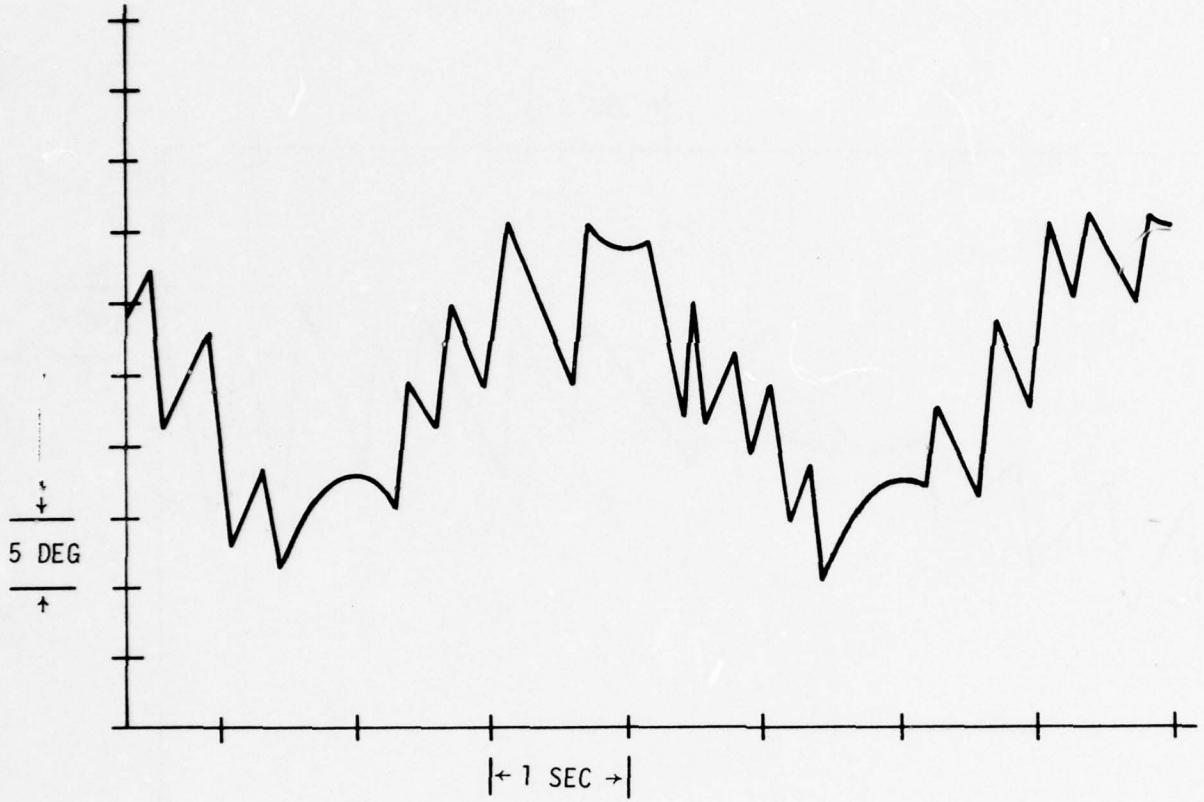

Figure 7.19 Sinusoidal Response from Our Stochastic VOR Model (with input frequency of 0.25 Hz and amplitude of 30 deg/sec)

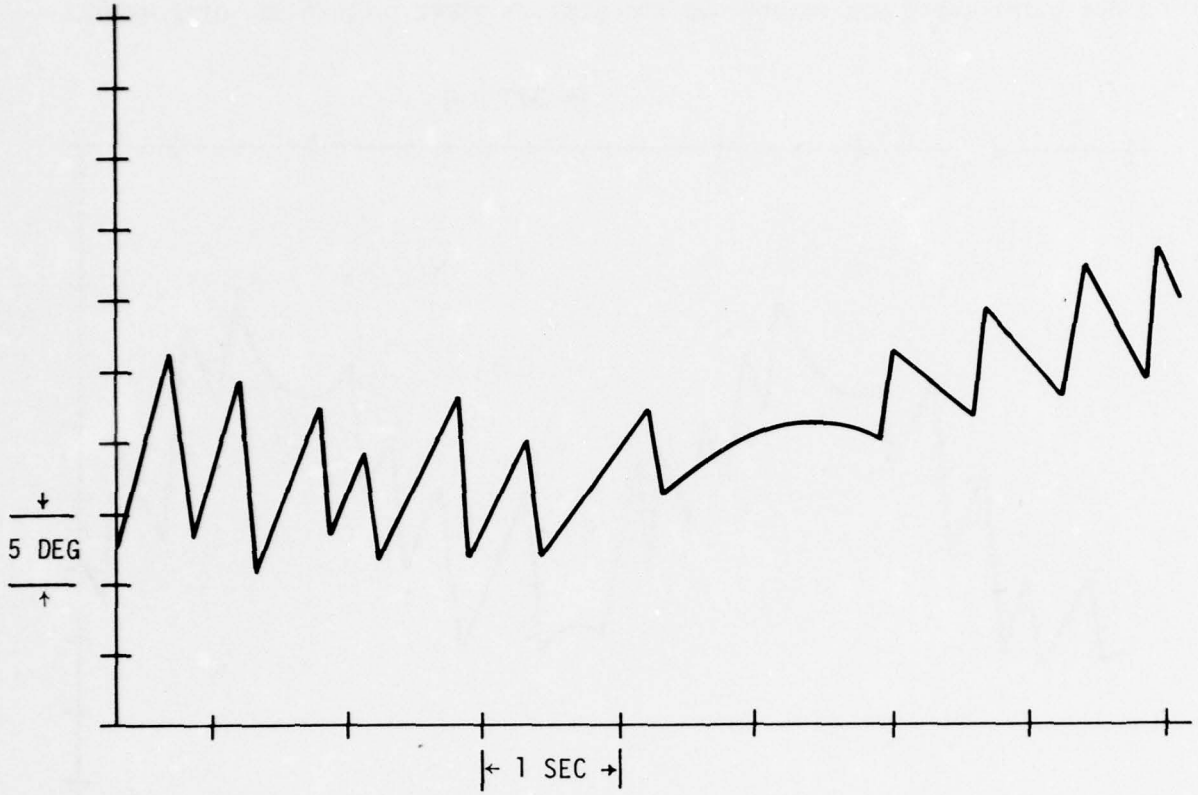

Figure 7.20 Sinusoidal Response from Our Stochastic VOR Model (with input frequency of 0.05 Hz and amplitude of 30 deg/sec)

Table 7.4 Sinusoidal Responses

f	$\dot{H}_M$	f'_{θ}	f'_{θ}	t_{TR}	t_{TR}	$\lvert\theta_s\rvert_M$	$\lvert\theta_s\rvert_M$	$\lvert\bar{\theta}_{\theta}\rvert$	$\lvert\bar{\theta}_{\theta}\rvert$
		cat	model	cat	model	cat	model	cat	model
(Hz)	(deg/sec)	($cycle^{-1}$)	($cycle^{-1}$)	(sec)	(sec)	(deg)	(deg)	(deg)	(deg)
1.2	30	1.1	2.0	0.30	0.30	5.0	4.8	17.5	14.2
0.25	30	6.6	7.9	1.1	0.39	6.4	2.0	11.5	8.8
0.05	30	23.0	24.0	2.7	2.5	9.0	9.7	8.8	7.3

In Table 7.4, the various symbols have the following meanings:

f: frequency of the input sinusoidal head velocity in Hz

$\dot{H}_M$: amplitude of the input sinusoidal head velocity in deg/sec

f_Q': quick-phase frequency (in beats) per cycle of the input frequency (not per sec)

t_{TR}: time duration in sec of the transition region in which the slow-phase eye velocity goes through zero without an interruption (Figure 7.21)

$|\theta_s|_M$: the maximum magnitude of the eye position displacement (*trough to peak*) in the transition region caused by the slow-phase in deg (Figure 7.21)

$|\bar{\theta}_Q|$: average magnitude of the two quick-phase displacements immediately before and immediately after the transition region in deg (Figure 7.21)

7.6 Discussion of results

First we consider the step responses (refer to Table 7.3). For $\dot{\theta}_s = 8.9$, the differences in σ_{WN} and those in σ_{WR} between the cat and the model are significant. The low values of σ_{WN} and σ_{WR} from the model at $\dot{\theta}_s = 8.9$ are caused by the

Figure 7.21

This figure depicts schematically t_{TR}, $|\theta_s|$, and $|\theta_Q|$ used in Table 7.4. These are defined in the text in connection with Table 7.4. Two frequencies are shown one low, one high, but the symbols are the same.

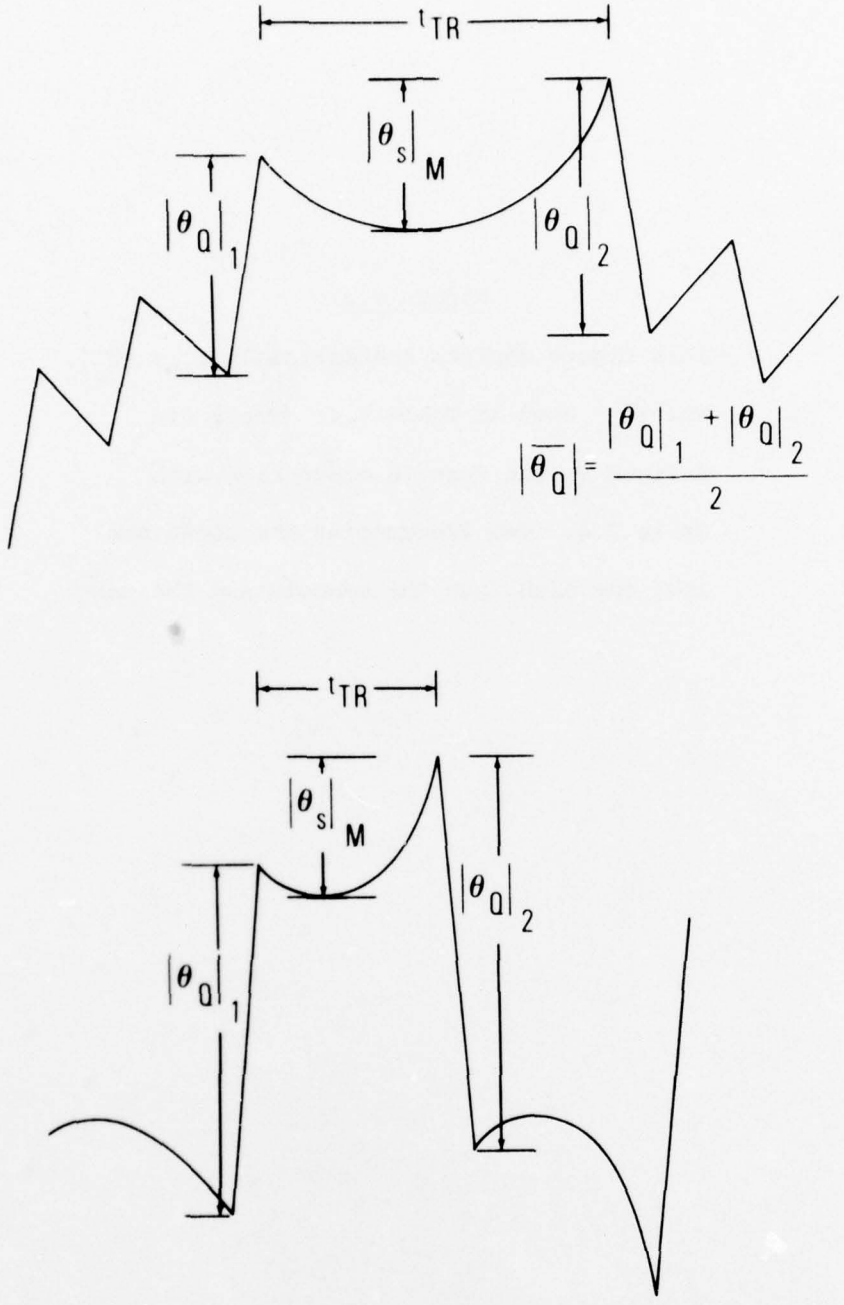

Figure 7.21 Depiction of t_{TR}, $|\theta_s|$, and $|\theta_Q|$

particular noise models we have adopted (see Figure 7.5). As discussed in section 7.4, if the noise is not decreased in this region, many backward quick-phases would occur. How the cat manages to have a σ_{WN} of 3.8 deg and a σ_{WR} of 2.5 deg without making backward quick-phases is a problem unresolved in this study. For $\dot{\theta}_s \geq 22$, both σ_{WN} and σ_{WR} for the model are consistently lower than those for the cat. This is partially due to the limitations of the magnitudes of the independent Gaussian numbers (with zero mean and variance one) to the value of 1.65 (see section 7.4). For example, in one simulation run with $\dot{\theta}_s = 46.5$ with this noise limitation, σ_{WN} was 3.4 deg, while without the noise limitation it was 3.9 deg. With the noise limitation σ_{WR} was 1.7, while without the noise limitation it was 2.6.

The discrepancies in σ_{WR} and σ_{WN} for $\dot{\theta} > 22$ deg/sec could probably be eliminated by: successive readjustment of the noise bandwidth τ_1 and τ_2; the noise intensities σ_{wx_2}, σ_{wz_2}; the shapes of $\sigma(|\phi|)$ (Figure 7.5) and $Q(|\phi|)$ (Figure 5.9); and using skewed rather than Gaussian noise distributions. This was not done because the limited amount of physiological data keeps the experimental values of σ_{WR} and σ_{WN} from being much more than rough estimates of the true values.

As for R_{12}, we consider the match to be reasonable considering limited samples from both the computer and the cat.

Next, we consider the sinusoidal responses (Table 7.4). Overall, in view of limited samples from our cat (only one or two runs at a particular frequency and amplitude), we consider that the responses from the model compare reasonably with those from the cat. For f = 1.2 Hz, the match between the cat and the model is reasonable except for f_Q'. A possible explanation for this discrepancy is hysteresis as discussed in section 7.7.

For f = 0.25 Hz, the mismatch both in t_{TR} and $|\theta_s|_M$ is significant. This is partially the result of our modeling approach. We have adjusted the model parameters (Q and T_L) and noises to meet the requirements for f = 1.2 Hz and f = 0.05 Hz, the two frequency extremes, and hoped for good luck at f = 0.25 Hz. We did not get it. However, the hysteresis effect may again be to blame. This will be described in the next section, but briefly, the values of t_{TR} and $|\theta_s|_M$ are sensitive to $\dot{H}_M$. We have observed in the model that, for example, when $\dot{H}_M$ is decreased from 30 to 20 deg/sec, the value of t_{TR} and $|\theta_s|_M$ jumps discontinuously becuse one quick-phase may drop out of each half cycle. This can increase these parameters by as much as a factor of 2.

Referring to Table 7.4, we regard the comparison in $|\bar{\theta}_Q|$ between the cat and model as rough justification for the dependence of Q on ϕ shown in Figure 5.9, especially at low head velocities which occur near the zero crossings at 0.05 Hz.

7.7 Comments

First, we will discuss the so-called "hysteresis effect" (Figures 7.22 and 7.23). For f = 1.2 Hz, for example, as the amplitude $\dot{H}_M$ of the peak head velocity gradually increases, suddenly a quick-phase is initiated at a certain amplitude $\dot{H}_M'$ and then occurs in all subsequent cycles. However, as the amplitude gradually decreases, the quick-phases suddenly disappear at another amplitude, $\dot{H}_M''$. It is always the case that $\dot{H}_M' > \dot{H}_M''$, similar to a magnetic hysteresis loop. In our model, (at 1.2 Hz) $\dot{H}_M'$ occurs at 14.75 deg/sec while $\dot{H}_M''$ occurs at 7.77 deg/sec for the noise-free model as shown in Figure 7.22. For the stochastic model, the values of $\dot{H}_M'$ and $\dot{H}_M''$ fluctuate from trial to trial. $\dot{H}_M'$ fluctuates about $\pm$ 3 deg/sec around a mean value of 14.75 deg/sec, while $\dot{H}_M''$ fluctuates about $\pm$ 1 deg/sec around a mean value of 7.96 deg/sec. For our cat, $\dot{H}_M'$ appears to be about 10 deg/sec, while $\dot{H}_M''$ appears to be about 7 deg/sec. When the experimental cat data was obtained, hysteresis was not explicitly looked at so the data is limited and $\dot{H}_M'$ and $\dot{H}_M''$ are very rough. The match between model and cat is thus maybe better than one might expect.

Because of this phenomenon, if t_{TR}, $|\theta_s|_M$ or f_Q' were plotted against $\dot{H}_M$, they would change by a jump each time a new quick-phase was added to the output. This means that these measures of performance are sensitive to $\dot{H}_M$ and could

Figure 7.22

This figure depicts what we call the "hysteresis effect". As the magnitude of the input head velocity gradually increases, suddenly a quick-phase is initiated and then occurs in all subsequent cycles. As the magnitude gradually decreases, the quick-phases suddenly disappear at another magnitude. It is always the case that the magnitude of the former is greater than the magnitude of the latter.

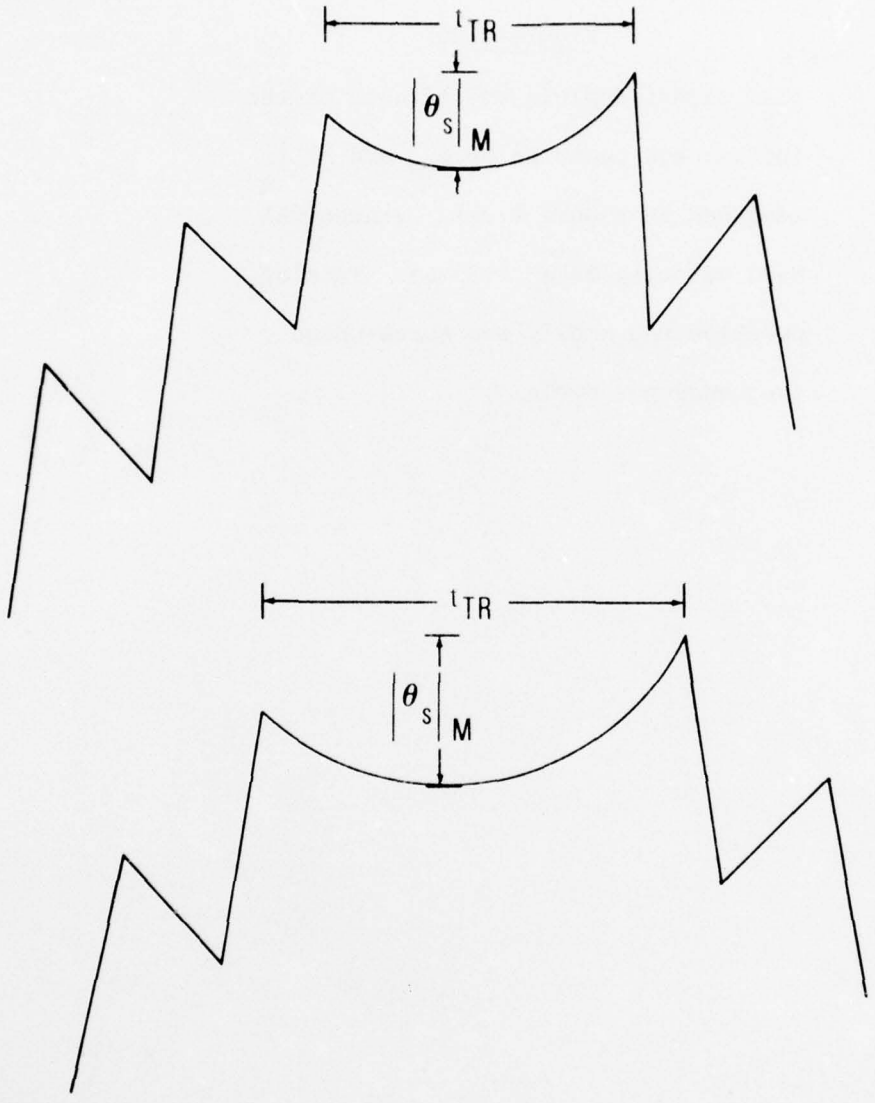

Figure 7.22 Hysteresis Effect Demonstrated on the VOR Model

Figure 7.23

This figure depicts the effects of the initial eye position on t_{TR} and $|\theta_s|_M$ (defined in Figure 7.21). Sinusoidal head velocity is at 0.25 Hz. Initial position can modify the quick-phase frequency per cycle.

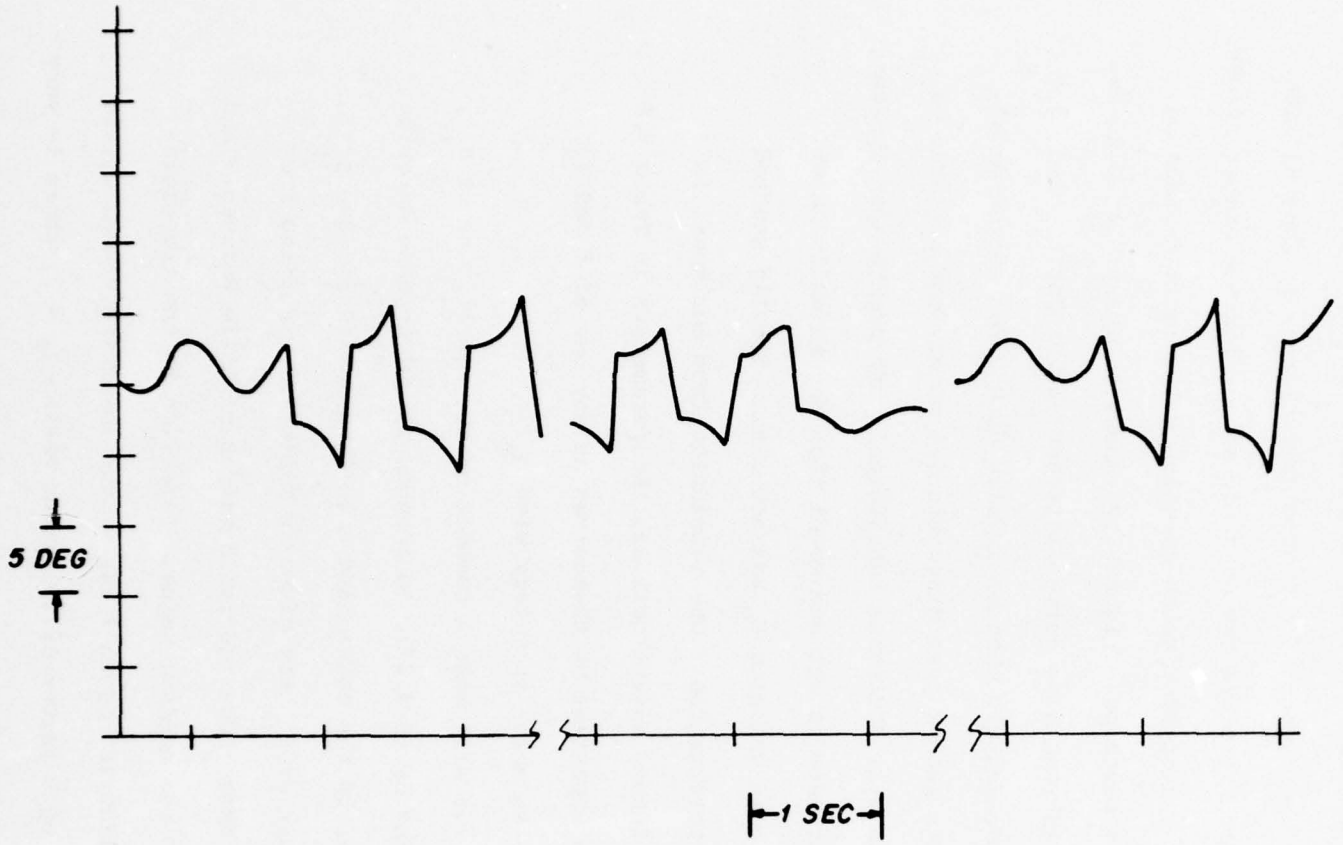

Figure 7.23 Effects of Initial Eye Position on t_{TR} and $|\theta_s|_M$ at f = 0.25

explain in (Table 7.4) the differences between cat and model in f_Q' at 1.2 Hz, and in t_{TR} and $|\theta_s|_M$ at 0.25 Hz.

As usual with a hysteresis phenomenon, the behavior depends on ititial position. If a sinusoidal stimulus is applied with $\dot{H}_M$ such that there are two possible values for the number of QPs, because of hysteresis, which solution will result depends on initial eye position. Figure 7.23 shows an example at 0.25 Hz. The two solutions have quite different values for t_{TR} and $|\theta_s|_M$. If one unfortunately chooses a value of $\dot{H}_M$, for cat or model, that is near such a jump discontinuity point, the measures we have chosen will fluctuate considerably and create more apparent discrepancy between cat and model that may actually exist.

Peak head velocity $\dot{H}_M$ was not systematically studied in this investigation. One conclusion from our model is that, for future investigations, the parameters in Table 7.4 are not so important by themselves at any one of f and H_M as the way in which they vary with $\dot{H}_M$.

Next, we will make a comment on the sensitivity of R_{12}, approximated by (6.4.17), to changes in quick-phase duration and changes in the noise band edge frequencies $\frac{1}{\tau_1}$ and $\frac{1}{\tau_2}$. These values of R_{12} are given in Table 7.5. Judging from our cat's data, most realistic values of L lie between 5 and 20 with 10 the nominal value. Referring to the trapezoid-shaped filter in Figure 7.24, if the lower frequency, w_1, is decreased by a factor of two, thus making $\tau_1 = 2$, there is very

little change in R_{12}. This is not surprising. The correlation should depend more on high rather than low frequencies. In fact, if the higher break-frequency, w_2, is increased by a factor of two, thus making $\tau_2 = \frac{1}{16}$, the value of R_{12} for L = 10 drops sharply. This means that the choice of τ_2 is fairly critical.

Note that the values of R_{12} in Table 7.5 (e.g., the value 0.19 in the nominal case for L = 10) are determined from (6.4.17) with $\sigma(r_1) = 5.0$ and $\sigma(r_2) = 2.5$, while the values of R_{12} (for the model) in Table 7.3 (typically 0.3) are computed based on the simulation output of our stochastic model with its associated effects and its noise limitations. Consequently, the main value of 6.4.17 is to provide a rough quantitative estimate of experimental data and, more important, to show how R_{12} should depend on parameters like τ_1, τ_2, T, and L.

Table 7.5

Nominal Bandwidth

(for $\tau_1 = 1$, $\tau_2 = 1/8$)

L	R_{12}
0	0.50
1	0.46
5	0.31
10	0.19
15	0.11
20	0.06

High Frequencies

(for $\tau_1 = 1$, $\tau_2 = 1/16$)

L	R_{12}
0	0.50
1	0.42
5	0.21
10	0.08
15	0.02
20	~0

Low Frequencies

(for $\tau_1 = 2$, $\tau_2 = 1/8$)

L	R_{12}
0	0.50
1	0.46
5	0.32
10	0.21
15	0.13
20	0.08

Both

(for $\tau_1 = 2$, $\tau_2 = 1/16$)

L	R_{12}
0	0.6
1	0.42
5	0.22
10	0.09
15	0.03
20	~0

Figure 7.24

This figure depicts the effect of the band-pass characteristic when $\tau_1 = 1$ is increased by a factor of two and $\tau_2 = \frac{1}{8}$ is decreased by a factor of two.

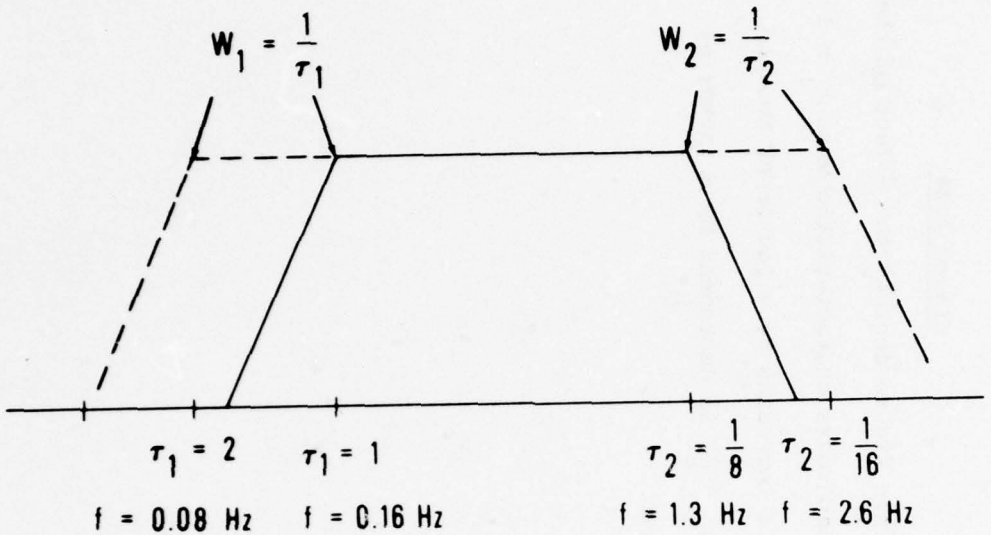

Figure 7.24 Effect of τ_1 and τ_2 on the Band-Pass Filter

CHAPTER VIII

DISCUSSIONS AND COMMENTS

8.1 Modification of the VOR model for saccades

In evolution, when the fovea developed along with the need for saccades, the saccadic system appears to have utilized the quick-phase circuits because the two movements are identical and share the same neural circuits. For this reason, a good VOR model should be able to accommodate the signals for saccadic eye movements without too much modification. The modifications in our VOR model to do this are shown in Figure 8.1.

We want our model to be able to make a saccadic eye movement when perceptual systems have selected a visual target. Referring to Figure 8.1, the selection of a visual target and the decision to make a saccade requires moving switch S_3 from s_{31} to s_{32}, and switch S_4 from s_{41} to s_{42}. These arrangements are made for the following reasons. For a saccade, the vestibular WHERE signal must be replaced by a visual WHERE signal which corresponds to the position of the target in space. Since the decision to acquire a visual target dictates an immediate rapid eye movement to the target position, provided it meets the refractory period of 200 milliseconds (see section 5.1), the WHEN function must also be bypassed by setting switch S_3 to s_{32} from s_{31}. The difference in the

Figure 8.1

This figure shows the modified VOR model with arrangement for saccades. The switch-positions for the VOR mode are S_3 at s_{31} and S_4 at s_{41}, while those for the saccadic mode are S_3 at s_{32} and S_4 at s_{42}.

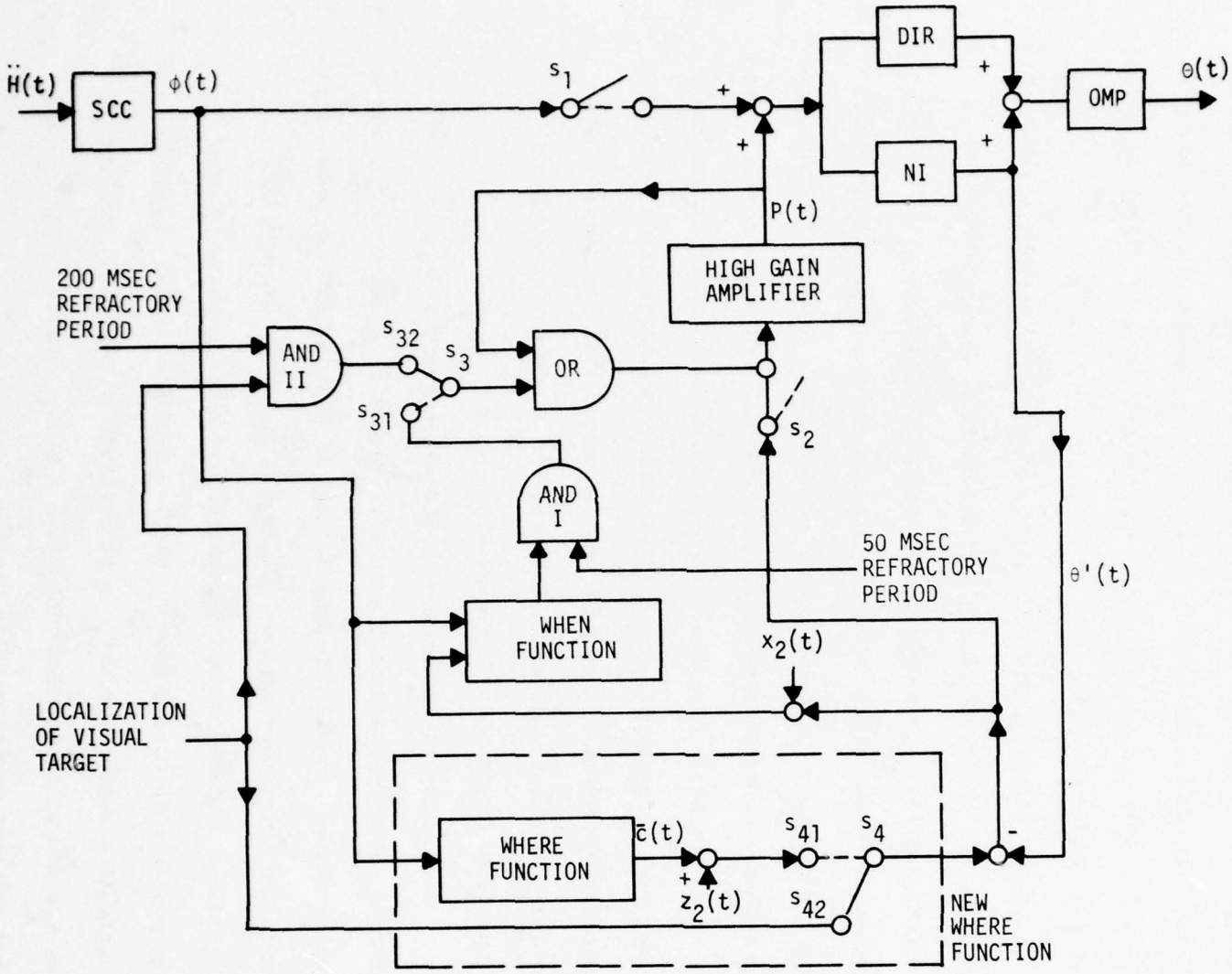

Figure 8.1 Our Modified VOR Model with Arrangement for Saccades

refractory periods between the saccades and quick-phases may be attributable to the signal processing time required by the visual system which separates saccades by 200 msec. This might be bypassed by the vestibular system for large fast head movements when the demand for a second quick-phase overrides the value of visual analysis at the end of the first.

Essentially, in Figure 8.1, the basic motor machinery is shared by saccades and quick-phases but the control signals, WHEN and WHERE, are just taken over by one system or the other. In foveate animals, in the light, the saccadic system is usually in control. During rotation in the dark, the VOR system is usually in control. But there are many intermediate situations in which they might compete. This means that the switches are an oversimplification and they really represent some sort of nonlinear, multi-input, decision process. However, there have been no studies of how saccades and quick-phases interact with each other so it is not possible to improve on the scheme in Figure 8.1.

A new AND-gate II assures a 200-millisecond refractory period for saccades, instead of the 50-millisecond refractory period for quick-phases used in AND-gate I. Again, this artificial separation into two refractory periods points out lack of knowledge about saccade and quick-phase interaction. If a quick-phase occurs, is it possible to make a saccade within 50 milliseconds? Probably not. If a saccade occurs, is it possible to make a quick-phase within 200 milliseconds? This is not known because the situation has not been experimentally studied.

As for the locations of noises, that of $x_2(t)$ is not altered, while that of $z_2(t)$ is shifted to a new location (Figure 8.1). The noise $x_2(t)$ is not involved in the saccadic mode because the WHEN function is bypassed. Since saccades are accurate, not noisy, the noise $z_2(t)$ is shifted to a new location as shown in Figure 8.1 so that it is associated only with the VOR mode. Conceptually, we may regard the portion enclosed by the dotted lines in Figure 8.1 as the "New WHERE Function."

A basic problem that is made clear by Figure 8.1 is: What is the difference between a saccade and a quick-phase? Is it possible to say with certainty, this is a saccade, that is a quick-phase? Four possible situations for rapid eye movements seem to exist in this regard. They are: active head rotation in the light; active head rotation in the dark; passive head rotation in the light; and passive head rotation in the dark.

It is our opinion that, regardless of the light-dark condition under which a rapid eye movement is made, the criteria (for whether a rapid eye movement is a quick-phase or a saccade) should indicate whether it is caused by a passive head rotation or by the active acquisition of the target. For the former case, it is a quick-phase. For the latter case, it is a saccade. Thus, in a coordinated head-eye

movement to a seen target in the light or an auditory, felt, or even remembered target in the dark, the movement is a saccade. It is a saccade whether the eye moves before or during the active head movement. Conversely, if the head is passively rotated, the rapid eye movement is a quick-phase. In the dark that is by definition, but even in the light we suggest that if there were no conscious attempt to acquire a target, then the movement should be called a quick-phase. This idea underlies Figure 8.1, because only when higher perceptual levels are trying to acquire a target are the switches thrown.

8.2 Discussion on head velocity around zero value.

For head velocities near zero (e.g., less than 10 deg/sec), we do not know much about the behavior of our cat's eye movements. First of all, we do not know what the threshold value Q should be. In fact, when the head velocity is zero, the question becomes almost meaningless. Also, we do not know how to handle the noise level around zero velocity since it can cause backward "quick-phases" when the noisy WHEN and WHERE curves intersect each other. Here again, the terms quick-phase and backward become meaningless when the velocity is zero. In the absence of supporting data, we have arbitrarily picked a value for Q (6 deg) and allowed the level of the noise at low velocities to approach zero to try and fit the sinusoidal behavior particularly in the region, at f = 0.05 Hz, where head

velocity passes through zero. The main problem there was backward quick-phases. For this reason, if we are to extend the research, we would investigate the cat's VOR behavior at low velocities more thoroughly.

Our model is clearly not designed for operation around zero head velocity. One alternative is to suggest that the VOR system is simply disconnected when the head is stationary; that is, in some neighborhood of zero head velocity. One way to implement this is to always throw the switches into the saccadic mode below some level of $\dot{\phi}(t)$ in Figure 8.1.

Although it is poorly designed for operation in the neighborhood of zero head velocity because of the lack of physiological data, our VOR model, as it stands, would behave for a zero canal signal in the following way. The noise on the WHEN and WHERE curves is zero (refer to Figure 7.5). The WHERE curve is located at zero (section 5.3 and Figure 5.8), and the WHEN curves are located at $\pm$6 deg (section 5.4 and Figure 5.9). If the initial position of the eye is within $\pm$6 deg, the eye will remain there as long as the canal signal remains zero. If the cat makes a saccade to a point beyond the $\pm$6 deg boundary and then loses "interest" in this real or imagined target so that the switches in Figure 8.1 return to the VOR mode, the eye will return to the WHERE curve (zero), in this case by a quick-phase, and remain there. This is

not unreasonable behavior but, again, we come to the problem of what distinguishes a saccade from a quick-phase. The former is "voluntary" or "active" and assumes the cat is "interested," all of which are subjective terms and hard to deal with in a model. Thus, even if more data were available, eye movement records at very low head velocities would be filled with rapid eye movements and it would be difficult or impossible to decide which ones were saccades and which ones were quick-phases.

8.3 Comments on other VOR models.

To our knowledge, there exist three other VOR models concerned with quick-phases. They are by Sugie and Melvill Jones (1971), Schmid and Lardini (1976), and Barnes (1977). The latter two models were published while this research was in progress.

The model by Sugie and Melvill Jones was the first published model that drew attention to the anti-compensatory nature of quick-phases. To compare it with our model, its essential features are shown in Figure 8.2. In this figure, our present nomenclature has been used; the canal output $\phi(t)$, the pulse $P(t)$, and the eye position $\theta(t)$. It uses periodic sampling every 200 milliseconds to initiate quick-phases which, of course, is a bad oversimplification. The transfer

Figure 8.2

This figure shows the essential features of the VOR model by Sugie and Melvill Jones (1971) with associated waveforms. For a step input $\phi(t)$, it would produce the output $\theta(t)$ as shown.

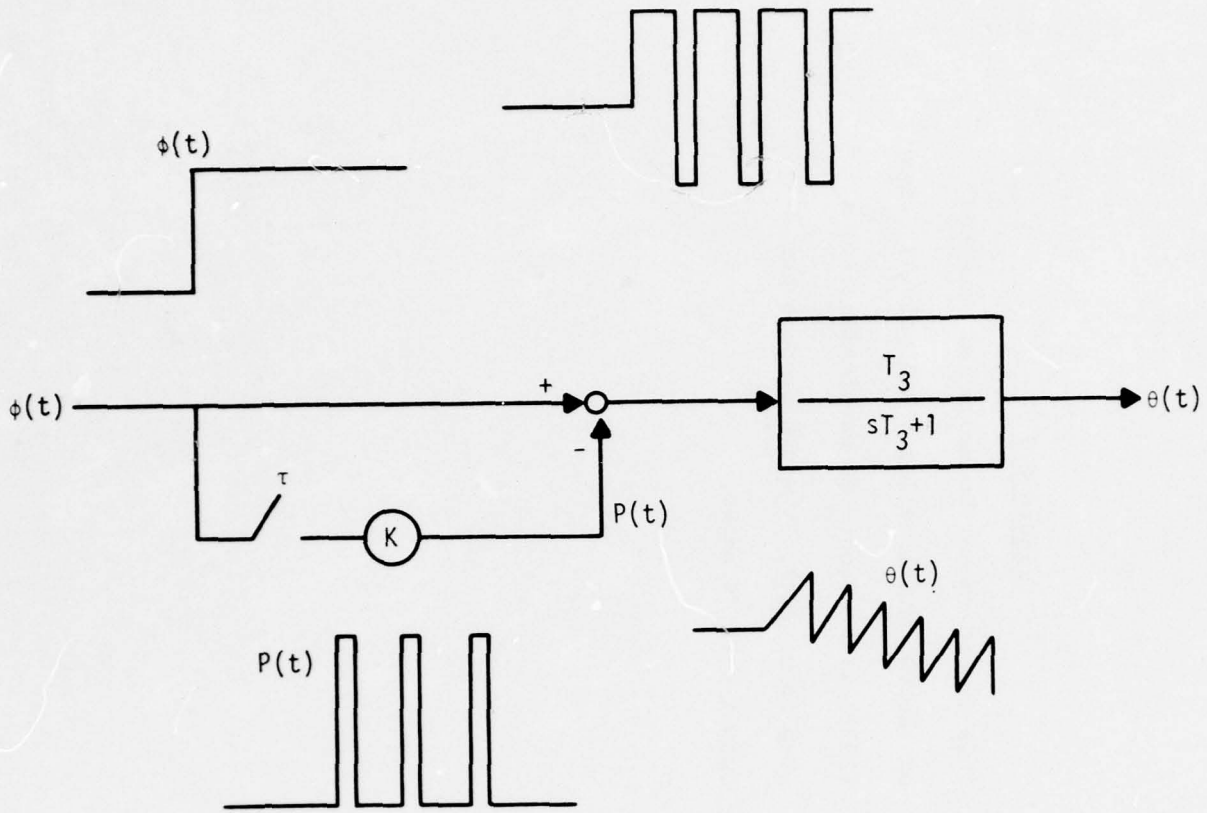

Figure 8.2 The Essential Features of the VOR Model by Sugie and Melvill Jones (1971)

function $\frac{T_3}{sT_3 + 1}$ corresponds to our neural integrator. They used a time constant T_3 = 1 sec. This time constant was determined from cats under light ether anesthesia. In Figure 5.12, the element in our model most susceptible to anesthesia is the neural integrator. Anesthesia, or even loss of alertness, causes its time constant to decrease. It is generally agreed now that 1 sec is a correct value for the anesthetized situation, but does not apply to alert animals. This short time constant of 1 sec would cause the eye position to decay exponentially after the completion of a quick-phase so that a quick-phase itself creates a slow-phase component unrelated to $\phi(t)$. This, in fact, became the whole point of their model. It now appears that it was based on a situation that applies only under anesthesia. In our model, the time constant T_n of the neural integrator, $\frac{T_n}{sT_n + 1}$, is 25 sec. Thus in essence, it acts like a pure integrator. In addition, this model did not deal with the stochastic behavior of VOR.

A simplified version of the VOR model by Schmid and Lardini (1976) is shown in Figure 8.3. Variables analogous to those in our model such as $\phi(t)$, $C(t)$, $\theta(t)$, $\Delta\theta(t)$, and $P(t)$ have been so labelled. The output $C(t)$ of the transfer function σ corresponds to our deterministic WHERE curve except that σ is a scalar. This means that $C(t)$ is linearly proportional to $\phi(t)$ and it does not saturate like ours. This, of

course, contradicts with experimental observations because it does saturate in reality. If $\Delta\theta$ exceeds $\pm Q$, a quick-phase is triggered. $\frac{e^{-\tau s}}{s}$ is a separate neural integrator with a delay of $\tau = 0.2$ sec for a refractory period although it can be as low as 50 milliseconds, which is not a trivial matter. Figure 8.3 is misleading. What actually happens in the quick-phase mechanism, when $|\Delta\theta|$ is bigger than Q, is that a sample is taken. Then, the sampler is inhibited for 200 milliseconds. Then, it is enabled, so that another sample can be taken if $|\Delta\theta|$ is bigger than Q. That is what Schmid and Lardini meant to depict. This integrator is in addition to another neural integrator, $\frac{T_5}{sT_5 + 1}$, for the slow-phase with a time constant of 150 sec. Although this model has two neural integrators, there are several reasons both theoretical and neurophysiological why both quick-phase and slow-phase eye movements must share the same neural integrator as summarized below (Robinson, 1975):

A. This is a theoretical argument. There is no reason to suppose a saccade differs from a quick-phase (Ron et al., 1972). The best evidence for this is that all neurons seen so far throughout the brain which discharge in a saccade-correlated way do the same thing for quick-phases in the dark. Now, during rotatory nystagmus in the dark, if there were separate integrators, then (see θ_r and θ_s in Figure 8.3) one would accumulate all the slow-phases in one direction,

Figure 8.3

This figure shows the simplified VOR model by Schmid and Lardini (1976). It has two neural integrators. Comments on this fact are given in the text.

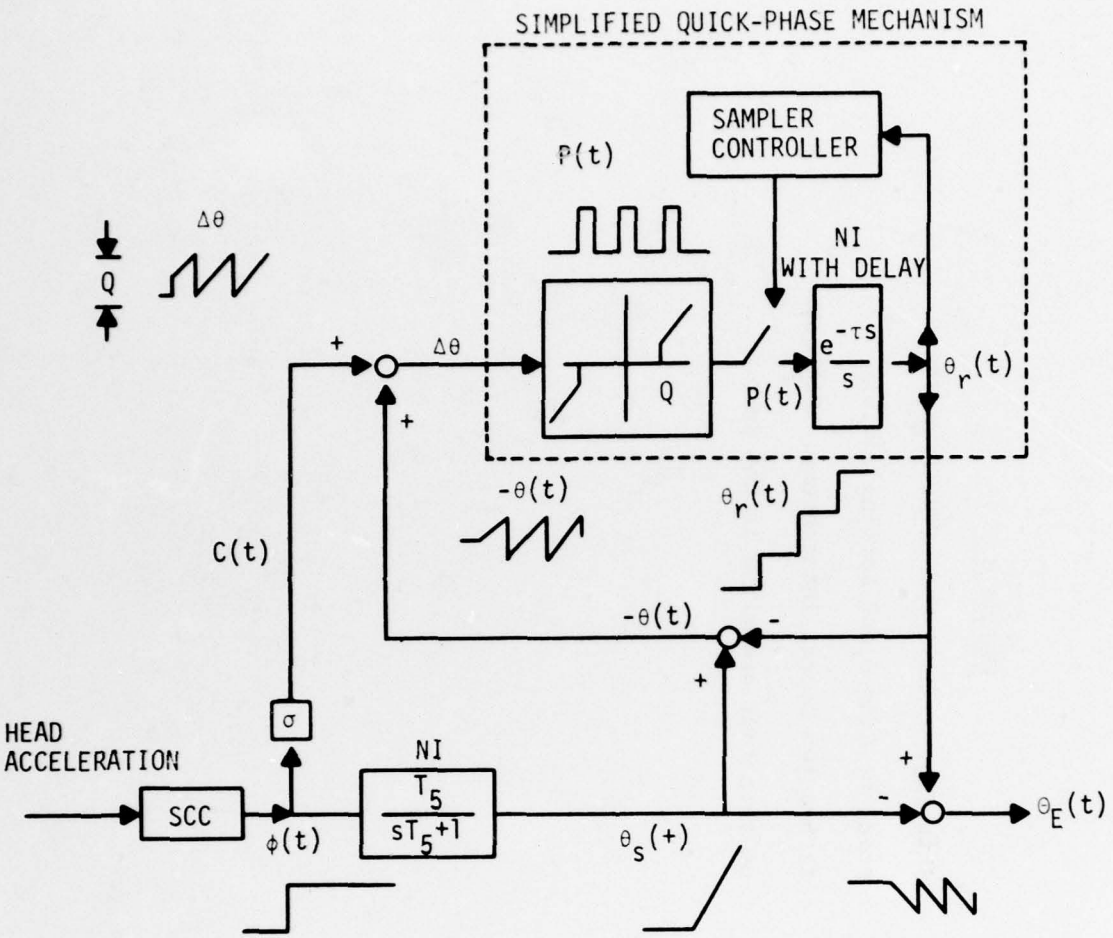

Figure 8.3 Simplified Version of the VOR Model by Schmid and Lardini (1976)

the other, all the quick-phases in the other. After a short period of time, each integrator would have stored within it the equivalent of many complete revolutions of the eye in the head. This unlikely idea can be dismissed simply on conceptual grounds. It is quite clear that each quick-phase pulse must reset the neural integrator to a discharge rate proportional to the new eye position. But that, of course, is equivalent to putting the pulse into the integrator as shown in Figure 4.1 and Figure 5.12.

B. Neurons which behave in the unlikely fashion just described (the two integrator hypothesis) have never been observed in the brains of alert monkeys.

C. *Cerebellar lesions in cat* (as well as in man and monkey) make the eye position at the end of a saccade slip back with a time constant of 1.3 sec. It turns out that for the same cat the slow-phase of the nystagmus is also leaky (does not have a constant velocity) and velocity falls off with the same time constant of 1.3 sec. It is unlikely that this is a coincidence and the simplest explanation is that there is only one integrator now made leaky by cerebellectomy.

D. Finally, if a single integrator was responsible for creating all version eye movements, a lesion that destroyed it would abolish all such movements. It is well known in neuro-ophthalmology that the pprf is just such a location.

In addition, this model does not deal with the stochastic behavior of the VOR. A comment on the sampling system is given later in this section.

A VOR model by Barnes (1977) is shown in Figure 8.4. Again, we have substituted our own terminology to help in comparing this model to our own. The output C(t) of the transfer function A corresponds to our deterministic WHERE curve. But, unlike ours, it does not saturate, which is contrary to observed behavior. Since $|C(t) - \theta''(t)|$ is the input to the threshold device T, the quantity θ'' more or less corresponds to our efference copy of the eye position (θ' in Figure 5.12), while the transfer function F seems to convert velocity to position (more or less), and so corresponds to our neural integrator. The transfer function B provides a phase-lead to compensate for the phase-lag caused by the eye dynamics. This could easily be traded off to a direct path around the neural integrator as in Figure 3.1 and Figure 5.12. The discharge pattern similar to the output signals P(t) and $\theta''(t)$ from B and F are not observable among a variety of brainstem neurons (see, for example, Figure 5 of Robinson, 1975), while in our model all internal signals are consistent with the neurophysiological observations. This model has two neural integrators if we view F as an integrator. In this case both are reset by quick-phases. Thus, one can only object to two integrators on the grounds of parsimony. In addition, this model does not deal with the stochastic behavior of the VOR.

Figure 8.4

This figure shows the VOR model by Barnes (1977). $\theta''(t)$, the output of F, corresponds to the efference copy of the eye position $\theta'(t)$ in our model (Figure 5.12), and T corresponds to our high-gain amplifier in the bang-bang control system of our model.

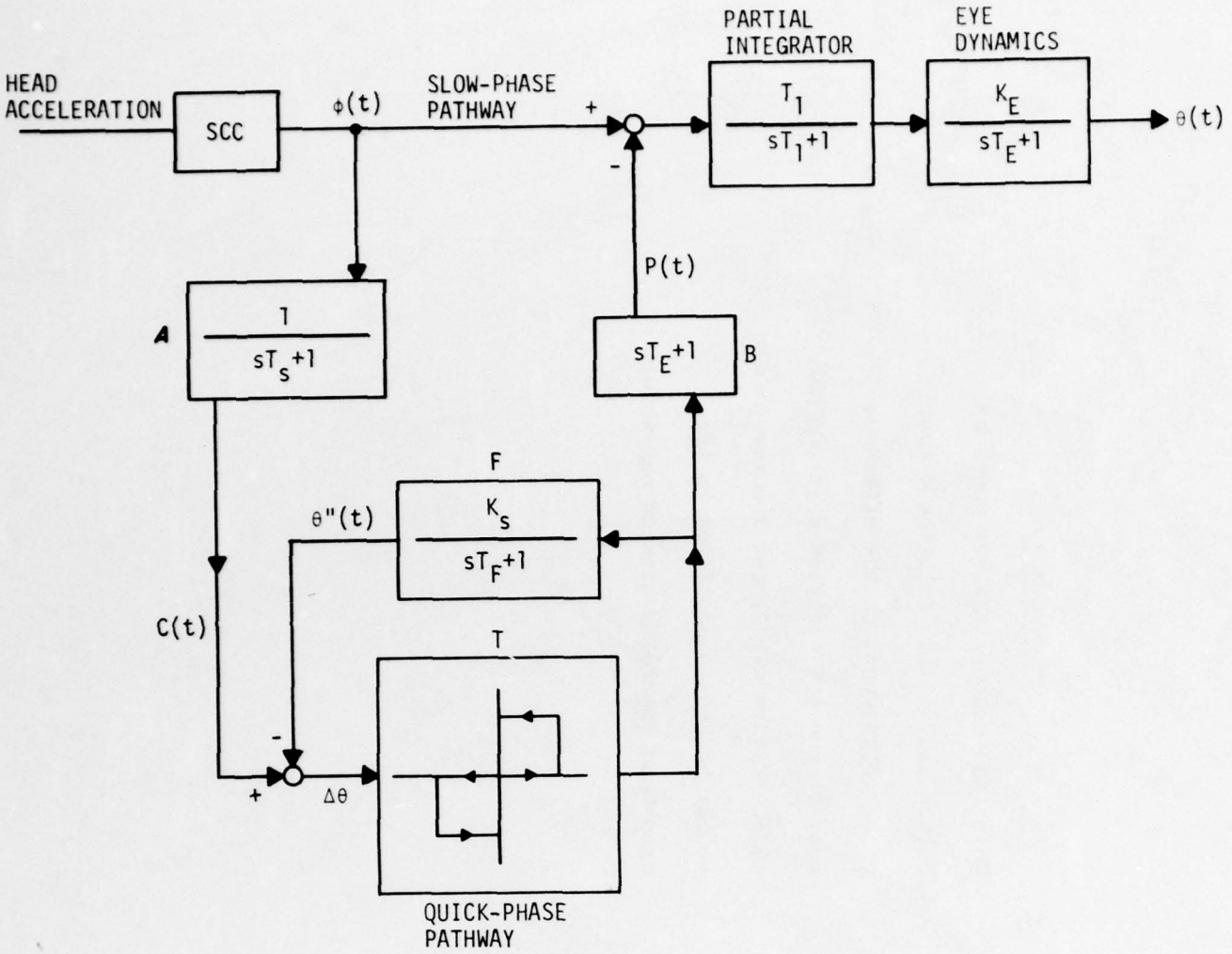

Figure 8.4 The VOR Model by Barnes (1977)

In summary, if the goal of the VOR model is to represent real neurophysiology, we believe our model is more realistic than others for the following reasons.

First, our model deals with the stochastic behavior of the VOR, while the other three models do not. This is important simply because the cat's real data is noisy, and the noise statistics are an important part of the data base.

However, a really significant criteria of the merit of the model is whether the internal signals of the model are similar to the neural discharge patterns observed in the brain. The internal signals in our model do correspond to discharge patterns of neurons in the brainstem. In other models, this is not the case as explained before in connection, for example, with P(t) and $\theta''(t)$ in Figure 8.4. The model by Schmid and Lardini (Figure 8.3) and the model by Barnes (Figure 8.4) both have two neural integrators, which is not correct for reasons given before. The model by Sugie and Melvill Jones (Figure 8.2) and the model by Schmid and Lardini (Figure 8.3) both use a sampler which is an open-loop, ballistic pulse generator, instead of a closed-loop bang-bang controller (pulse generator) as in our model. We have explained in Chapter 4 why we chose the latter over the former. Furthermore, the sampling system has inherent problems associated with it because, being open-loop and ballistic, it has to

specify the amplitude of the sampler output so that the end point of quick-phase reaches the predetermined goal. If one now adds noise in the system, in particular to the threshold device, it becomes complicated and a little unnatural as to how to realize a sampler with neurons that will respond to the noise in an approximate manner. The closed-loop continuous controller avoids these problems.

Of course, there are similarities between our model and the other models. It is generally accepted that quick-phases are made by a pulse, which therefore necessitates an integrator. The pulse must be triggered, so some form of threshold device is needed (save for the Sugie and Melvill Jones model) into which some time varying signal must go. Almost any model would of necessity have such elements. All modelers since 1971 have recognized the fact that quick-phases carry the eye in the anti-compensatory half of the motor field and all have used a signal from the canals [C(t)] to effect this. Such elements are fairly basic and it is not surprising that they are common to all models in one form or another.

However, the model presented here does differ in other ways than just circuit details. The approach has been teleological. The question has always been what was nature trying to accomplish in designing the system, and then, what is the simplest neural circuit to achieve that goal? This approach is subjective and disliked by some but to us it has more appeal than simply wiring together black boxes to fit a data base.

Probably the largest difference between this study and others is the quantitative testing. Other modelers are often content to show one or two pictures of nystagmus created by the model and comment on how similar they looked to physiological records. While our data base was not as large as we realized later it should have been, the analysis of both cat and model behavior is much more extensive than anything attempted before. Thus, this model, despite its obvious imperfections, is much closer quantitatively to physiological behavior over a wide range of vestibular stimuli than is the case for other models so far.

BIBLIOGRAPHY

Barnes, G. R. (1977) *The Generation of Saccadic Eye Movements in Vestibular Nystagmus*, RAF Institute of Aviation Medicine, Great Britain (in press).

Becker, W. and Klein, H. M. (1973) *Accuracy of Saccadic Eye Movements and Maintenance of Eccentric Eye Positions in the Dark*, Vision Res. 13, 1021-1034.

Bryson, A. E., Jr. and Ho, Y. C. (1975) *Applied Optimal Control*, John Wiley & Sons, New York, NY.

Cheng, M. (1972) *Point Process Analysis in the Physiological Study of Human Nystagmus*, Ph.D. Thesis, McGill University, Montreal, Canada.

Cohen, B. and Henn, V. (1972) *The Origin of Quick-Phases of Nystagmus in the Horizontal Plane*, Bibl. Ophthal. 82, 36-55.

Fernandez, C. and Goldberg, J. M. (1971) *Physiology of Peripheral Neurons Innervating Semicircular Canals of the Squirrel Monkey: II Response to Sinusoidal Stimulation and Dynamics of Peripheral Vestibular System*, J. Neurophysiology 34, 661-684.

Fuchs, A. F. and Kimm, J. (1975) *Horizontal Angular Acceleration and Eye Movement*, J. Neurophysiology 38, 1140-1161.

Fuchs, A. F. and Luschei, E. S. (1970) *Firing Patterns of Abducens Neurons of Alert Monkeys in Relationship to Horizontal Eye Movement*, J. Neurophysiology 33, 382-392.

Fuchs, A. F. and Robinson, D. A. (1966) *A Method for Measuring Horizontal and Vertical Eye Movement Chronically in the Monkey*, J. Appl. Physiology 21, 1068-1070.

Hallet, P. E. and Lightstone, A. D. (1976) *Saccade to Flashed Targets*, Vision Res. 16, 107-114.

Jürgens, R. and Becker, W. (1975) *Is There a Linear Addition of Saccades on Pursuit Movement?* Basic Mechanisms of Ocular Motility and Their Clinical Implications, Pergamon Press, Oxford and New York.

Keller, E. L. (1974) *Participation of the Medial Pontine Reticular Formation in Eye Movement Generation in Monkey*, J. Neurophysiology 37, 316-332.

Keller, E. L. and Robinson, D. A. (1971) *Absence of a Stretch Reflex in Extraocular Muscles of Monkey*, J. Neurophysiology 34, 908-919.

Melvill Jones, G. (1964) *Predominance of Anti-Compensatory Oculomotor Response During Rapid Head Rotation*, Aerospace Medicine 35, 965-968.

Melvill Jones, G. and Milsum, J. H. (1965) *Spatial and Dynamic Aspects of Visual Fixation*, IEEE Trans. Bio-med. Eng. BME 12(2), 54-62.

Melvill Jones, G. and Milsum, J. H. (1971) *Frequency - Response Analysis of Central Vestibular Unit Activity Resulting from Rotational Stimulation of the Semicircular Canals*, J. Physiology 218, 1-25.

Morasso, P. (1973) *Adjustment of Saccade Characteristics During Head Movements*, Experimental Brain Research 16, 492-500.

Outerbridge, J. S. (1969) *Experimental and Theoretical Investigation of Vestibular-Driven Head and Eye Movement*, Ph.D. Thesis, McGill University, Montreal, Canada.

Papoulis, A. (1965) *Probability, Random Variables, and Stochastic Processes*, McGraw-Hill Book Company, New York, NY.

Robinson, D. A. (1963) *A Method of Measuring Eye Movement Using a Scleral Search Coil in a Magnetic Field*, IEEE Transaction on Bio-medical Electronics 10, 137-145.

Robinson, D. A. (1970) *Oculomotor Unit Behavior in the Monkey*, J. Neurophysiology 33, 393-404.

Robinson, D. A. (1973) *Models of the Saccadic Eye Movement Control System*, Kybernetic 14, 71-83.

Robinson, D. A. (1975) *Oculomotor Control Signals*, Basic Mechanism of Ocular Motility and Their Clinical Implications, Pergamon Press, Oxford and New York.

Robinson, D. A. (1976) *Adaptive Gain Control of Vestibuloocular Reflex by the Cerebellum*, J. Neurophysiology 39,954-969.

Robinson, D. A. and Keller, E. L. (1972) *The Behavior of Eye Movement Motoneuron in the Alert Monkey*, Bibl. Ophthal. 82, 7-16.

Ron, S., Robinson, D. A. , and Skavenski, A. A. (1972) *Saccades and the Quick Phase of Nystagmus*, Vision Res. 12, 2018-2022.

Scheuer, E. M. and Stoller, D. S. (1962) *On the Generation of Normal Random Vectors*, Technometrics 4, 278-281.

Schmid, R. and Lardini, F. (1976) *On the Predominance of Anti-Compensatory Eye Movements in Vestibular Nystagmus*, Biol. Cybernetics 25, 135-148.

Shimazu, H. and Precht, W. (1966) *Inhibition of Central Vestibular Neurons from the Contralateral Labyrinth and Its Mediating Pathway*, J. Neurophysiology 29, 467-492.

Skavenski, A. A., Haddad, G., and Steinman, R. M. (1972) *The Extraretinal Signal for the Visual Perception of Direction*, Perception and Psychophysics 11, 287-290.

Skavenski, A. A. and Robinson, D. A. (1973) *Role of Abducens Neurons in the Vestibuloocular Reflex*, J. Neurophysiology 36, 724-738.

Sparks, L. L. and Travis, R. P., Jr. (1971) *Firing Patterns of Reticular Formation Neurons During Horizontal Eye Movements*, Brain Res. 33, 477-481.

Sugie, N. and Melvill Jones, G. (1971) *A Method of Eye Movements Induced by Head Rotation*, IEEE Transactions on Systems, Man, and Cybernetics, Vol. SMC 1(3), 251-260.

Young, L. R. (1969) *The Current Status of Vestibular System Models*, Automatica 5, 369-383.

Young, L. R. and Stark, L. (1963) *Variable Feedback Experiments Testing a Sample Data Model for Eye Tracking Movements*, IEEE Trans of the Prof. Tech. Grp. on Human Factors in Elect. HFE 4, 38-51.

Zee, D. S. Optican, L. M., Cook, J. D., Robinson, D. A., and Engel, W. K. (1976) *Slow Saccades in Spinocerebellar Degeneration*, Archives of Neurology 33, 243-251.

DISTRIBUTION

Library of Congress
Washington, D. C. 20540
Attention: Gift and Exchange Division (4)

Defense Documentation Center
Cameron Station
Alexandria, Virginia 22314 (12)

Strategic Systems Project Office
Department of the Navy
Washington, D. C. 20360
Attention: D. Gold (SP-230)
LCDR Ferriter (SP-23110)

General Electric Ordnance Systems
100 Plastics Avenue
Pittsfield, Massachusetts 01201
Attention: B. Flood
P. Schubert

Charles Stark Draper Laboratory
555 Technology Square
Cambridge, Massachusetts 02139
Attention: P. Howard
C. Hrbek
K. Vincent

The Analytic Sciences Corporation
Six Jacob Way
Reading, Massachusetts 01867
Attention: J. Bortz
J. Kasper, Jr.

Chief of Naval Research
Department of the Navy
Arlington, Virginia 22217

Applied Physics Laboratory
Johns Hopkins University
Johns Hopkins Road
Laurel, Maryland 20810

Department of Ophthalmology
School of Medicine
Johns Hopkins University
Baltimore, Maryland 21205
Attention: Professor D. A. Robinson (9)

Department of Aeronautics and Astronautics
Massachusetts Institute of Technology
Cambridge, Massachusetts 02139
Attention: Professor Yao Tzu Li
Professor Laurence R. Young

National Aeronautics and Space Administration
Washington, D. C. 20547
Attention: Technical Library

National Research Institute
National Naval Medical Center
Bethesda, Maryland 20014

Defense Printing Service
Washington Navy Yard
Washington, D. C. 20374

Department of Electrical Engineering
Virginia Polytechnic Institute and
State University
Blacksburg, Virginia 24061
Attention: Professor Van Landingham

Local:

CC		DK-56	
CD		DK-60	
DD		DK-70	
		DK-71	
DF		DN	
DF-30		DN-23	
DG		DT	
DG-40		WD	
DK		WA	
DK-01		WE	
DK-02		WR	
DK-05		WU	
DK-10	(2)		
DK-20		DX-21	(2)
DK-30	(2)	DX-222	(6)
DK-40		DX-40	
DK-50	(3)		
DK-51			
DK-53			
DK-54			
DK-55			
DK-55 (Chun)	(35)		